

**RESTRICTED**  
**CONFIDENTIAL**

*Paul G. Fournier*

**AUTHOR'S PERSONAL COPY**

**NACA**

# RESEARCH MEMORANDUM

LONGITUDINAL STABILITY AND CONTROL CHARACTERISTICS OF AN  
AIRPLANE MODEL HAVING A 42.8° SWEEPBACK CIRCULAR-ARC  
WING WITH ASPECT RATIO 4.00, TAPER RATIO 0.50, AND  
SWEEPBACK TAIL SURFACES

By

Joseph Weil, Paul Comisarow, and Kenneth W. Goodson

Langley Memorial Aeronautical Laboratory  
Langley Field, Va.

CLASSIFIED DOCUMENT

This document contains classified information affecting the National Defense of the United States within the meaning of the Espionage Act, USC 50:31 and 32. Its transmission or the revelation of its contents in any manner to an unauthorized person is prohibited by law. Information so classified may be imparted only to persons in the military and naval services of the United States, appropriate civilian officers and employees of the Federal Government who have a legitimate interest therein, and to United States citizens of known loyalty and discretion who of necessity must be informed thereof.

CLASSIFICATION CHANGED TO UNCLASSIFIED  
AUTHORITY: NACA RESEARCH ABSTRACT NO. 128  
DATE: JUNE 24, 1959

CLASSIFICATION CHANGED TO  
CONFIDENTIAL  
AUTHORITY CROWLEY CHANGE #2145  
DATE 12-1-75

## NATIONAL ADVISORY COMMITTEE FOR AERONAUTICS

WASHINGTON

October 17, 1947

**RESTRICTED**



## NATIONAL ADVISORY COMMITTEE FOR AERONAUTICS

## RESEARCH MEMORANDUM

LONGITUDINAL STABILITY AND CONTROL CHARACTERISTICS OF AN  
AIRPLANE MODEL HAVING A  $42.8^\circ$  SWEEPBACK CIRCULAR-ARC  
WING WITH ASPECT RATIO 4.00, TAPER RATIO 0.50, AND  
SWEEPBACK TAIL SURFACES

By Joseph Weil, Paul Comisarow, and Kenneth W. Goodson

## SUMMARY

Tests were made in the Langley 300 MPH 7- by 10-foot tunnel of an airplane model having a  $42.8^\circ$  sweptback wing with aspect ratio 4.00, taper ratio 0.50, with a  $42.8^\circ$  sweptback horizontal tail, and a  $40.3^\circ$  sweptback vertical tail to determine its low-speed longitudinal stability and control characteristics. This investigation includes data on the effect of vertical-wing location, fuselage size, horizontal-tail location, and stall-control vanes on the wing.

For the flaps-neutral condition (cruising configuration), the model tested either as a low-wing or semihigh-wing airplane became unstable at moderate lift coefficients. In the flaps-deflected condition (landing configuration), the low-wing model had a positive static margin which became marginal at high lift coefficients; whereas, the semihigh wing model became markedly unstable at moderate lift coefficients. Small stall-control vanes located at the leading edge of the low-wing version removed the longitudinal instability present below the stall for the neutral-flap configuration. It was necessary to raise the horizontal tail 9 inches on the model vertical tail to effect a considerable improvement in the flap-neutral stability in the high lift range.

Nose-flap deflection extended the longitudinal stability over a larger lift range for both flap configurations. Nose-flap deflection also increased the maximum lift coefficient.

## INTRODUCTION

Much thought is currently being given to the design of supersonic airplanes. Many of the proposed designs incorporate radical changes

characterized by complex fields of air flow both in the low- and high-speed flight ranges. Low-speed wind-tunnel tests are therefore necessary to predict adequately the low-speed aerodynamic characteristics, especially for the landing configuration.

This paper presents the results of an investigation made to insure acceptable low-speed stability characteristics for a specific supersonic design. Much of the data obtained, however, have general application. Data pertaining to the longitudinal stability and control for various modifications, stall characteristics, and the effect of the presence of a ground board on the model are presented. The model incorporates a  $42.8^\circ$  sweptback circular-arc wing of aspect ratio 4.0 and taper ratio 0.50. Lateral stability and control data for this model are presented in reference 1.

A previously published paper dealt with the stability characteristics of a related supersonic model which had a  $45.1^\circ$  sweptback wing of aspect ratio 2.5 and taper ratio 0.49 (reference 2). The airfoil section of this wing was of the NACA 65 series.

#### COEFFICIENTS AND SYMBOLS

The results of the tests are presented as standard NACA coefficients of forces and moments. Pitching-moment coefficients are given about the center-of-gravity location shown in figures 1(a) and 1(b) (26.0 percent of the mean aerodynamic chord). The data are referred to the stability axes, which are a system of axes having their origin at the center of gravity and in which the Z-axis is in the plane of symmetry and perpendicular to the relative wind, the X-axis is in the plane of symmetry and perpendicular to the Z-axis, and the Y-axis is perpendicular to the plane of symmetry. The positive directions of the stability axes, of angular displacement, of the airplane and control surfaces are shown in figure 2.

The coefficients and symbols are defined as follows:

$C_L$	lift coefficient	$\left(\frac{\text{Lift}}{qS}\right)$
$C_X$	longitudinal-force coefficient	$\left(\frac{X}{qS}\right)$
$C_m$	pitching-moment coefficient	$\left(\frac{M}{qS c'}\right)$

Lift = -Z

$\left. \begin{array}{l} X \\ Z \end{array} \right\}$	forces along axes, pounds
M	moment about axis, pound-feet
q	free-stream dynamic pressure, pounds per square foot $\left( \frac{\rho V^2}{2} \right)$
q <sub>t</sub>	effective dynamic pressure at tail, pounds per square foot
S	wing area (12.70 sq ft)
c	airfoil section chord
c'	wing mean aerodynamic chord (M.A.C.) (1.85 ft)
b	wing span (7.12 ft)
V	air velocity, feet per second
V <sub>S</sub>	sinking speed, feet per minute
ρ	mass density of air, slugs per cubic foot
α	angle of attack of fuselage center line, degrees
ψ	angle of yaw, degrees
ε	angle of downwash, degrees
i <sub>t</sub>	angle of stabilizer with respect to fuselage center line, degrees; positive when trailing edge is down
δ	control-surface deflection, measured perpendicular to reference line, degrees
δ <sub>e</sub>	elevator deflection measured perpendicular to horizontal- tail reference line, degrees
Γ	geometric dihedral angle, degrees
n <sub>p</sub>	neutral-point location, percent of wing mean aerodynamic chord (center-of-gravity location for neutral stability in trimmed flight)

A	aspect ratio $\left(\frac{b^2}{S}\right)$
$\Lambda$	angle of sweepback measured to leading edge, degrees
$\lambda$	taper ratio $\left(\frac{\text{Tip chord}}{\text{Root chord}}\right)$
$M_o$	free-stream Mach number in tunnel
W	weight, pounds
$\gamma$	glide-path angle, degrees
$C_{L\alpha}$	total derivative of lift coefficient with respect to angle of attack

## Subscripts:

$f_s$	split flap
$f_p$	plain flap
$f_n$	nose flap (wing leading edge)

## Abbreviations:

c.g.	center of gravity
H.T.	horizontal tail

## DESIGNATION

It is convenient to specify a method of designating wing and tail plan forms. For the present paper, a numerical designation is adopted to indicate in order the sweepback, aspect ratio, and taper ratio of the wing and tail surfaces. For example, in a wing designation of the form

$$42.8 - 4.00 - 0.50$$

the number preceding the first dash (42.8) gives the angle of sweepback  $\Lambda$  in degrees measured with respect to the leading edge, the number following the first dash (4.00) gives the aspect ratio A,

and the number following the second dash (0.50) gives the taper ratio  $\lambda$ . This notation was previously used in reference 2.

### MODELS AND APPARATUS

Three-view drawings of the models are presented as figure 1 and the physical characteristics of the models are presented in table I. The models are shown mounted for testing in the Langley 300 MPH 7- by 10-foot tunnel in figure 3.

The wing was tested in a low and semihigh position (fig. 1(a)). Two fuselages were tested. The original fuselage had a fineness ratio of 7.89, whereas the smaller revised fuselage had a fineness ratio of 9.46. (See fig. 1(a).)

Variations of the vertical location of the horizontal tail tested are shown in figure 4. In order to facilitate the installation of the horizontal tail in the raised positions, a  $\frac{5}{16}$ -inch-thick steel plate of the same plan form as the vertical tail was used for this series of tests. The small fuselage of the model was also extended 12 inches with a constant-diameter cylinder inserted at station 80.16 to obtain the effect of increased tail length of the horizontal tail.

Details of various stall-control vane configurations tested are presented in figure 5. Construction lines of the round leading-edge modification of the circular-arc wing are shown in figure 6. The fillet of the wing-fuselage juncture is shown in figure 7.

The effective Reynolds number for some tests was increased by using a turbulence net (fig. 3(a)). The turbulence net was a standard fish net made of  $\frac{3}{16}$ -inch-diameter cotton twine with a square mesh of  $1\frac{1}{4}$  inches on a side, and was located 97 inches upstream of the center line of the balance frame.

Flow was observed by means of tufts on the right wing for various flap conditions to determine the stalling characteristics of the model. The behavior of the tufts, besides being observed visually, was also recorded with a motion-picture camera.

For the ground-board tests, the model was mounted in the tunnel above a ground board which completely spanned the tunnel and extended

about 58 inches forward and 66 inches rearward of the center-of-gravity location of the model (fig. 8). The ground board was located 14.1 or 24.1 inches below the reference center of gravity at zero angle of attack for testing at two ground heights. Figure 9 shows the model in the landing attitude ( $15^\circ$ ) in the tunnel with the ground board 14.1 inches below the reference center of gravity.

The elevator and rudder were 20-percent-chord plain flaps and were flat sided from the hinge line to the trailing edge. For the large fuselage, the wing had a 20-percent-chord split flap and a 15-percent-chord nose flap at the leading edge (fig. 10). For the small fuselage, however, the wing had a 20-percent-chord plain flap for the ailerons and flaps and a 15-percent-chord nose flap.

## TESTS AND RESULTS

### Test Conditions

Tests were made at a dynamic pressure of 40.0 pounds per square foot ( $M_o = 0.16$ ). The corresponding Reynolds number (based on the M.A.C. of 1.85 ft) was 2,150,000. The Reynolds number was computed using a turbulence factor of unity. The degree of turbulence of the tunnel is not known quantitatively but is believed to be small because of the high contraction ratio (14:1).

A few tests were made with a turbulence net in place. The turbulence factor for these tests was 2.24, which corresponds to an effective Reynolds number of 4,820,000.

### Corrections

Tare corrections were not applied since they are considered negligible. Jet-boundary corrections were computed from reference 3 and an unpublished analysis shows this to be in good agreement for sweptback wings up to  $45^\circ$  sweep. Corrections applied were as follows:

$$\alpha = \alpha_M + 1.42C_{T_M}$$

$$C_X = C_{X_M} - 0.0203C_{T_M}^2$$

$$C_m = C_{m_M} + 0.010C_{T_M} \quad (\text{for tail on})$$

where subscript M denotes measured value.

Jet-boundary corrections were not applied to the ground-board tests because they have been shown to be negligible (reference 4).

All forces and moments were corrected for blocking, which was computed by a method given in reference 5.

An increment in longitudinal force coefficient of 0.0015 has been applied to account for the horizontal buoyancy.

### Presentation of Results

A table of the figures presenting the results is given below:

	Figure No.
I. Longitudinal stability and control	
A. Wing-alone data . . . . .	11
B. Effect of wing position <sup>L</sup> . . . . .	12 to 15
C. Effect of vertical location of horizontal tail <sup>S</sup> . . . . .	16 to 19
D. Effect of extended fuselage <sup>S</sup> . . . . .	20
E. Effect of stall-control vanes <sup>S</sup> . . . . .	21 to 25
F. Effect of stall-control vanes with round leading edge <sup>S</sup> . . . . .	26
G. Effect of round leading edge <sup>S</sup> . . . . .	27 to 29
H. Effect of wing fillet <sup>L</sup> . . . . .	30
I. Nose-flap deflection <sup>L</sup> . . . . .	31
J. Various split-flap and nose-flap combinations <sup>L</sup> . . . . .	32
K. Elevator effectiveness <sup>L</sup> . . . . .	33
L. Effect of Reynolds number <sup>L</sup> . . . . .	34
M. Sinking speed and glide-path angle <sup>S</sup> . . . . .	35
II. Stalling characteristics <sup>L</sup> . . . . .	36
III. Effect of ground board <sup>S</sup> . . . . .	37 to 38
L large fuselage	
S small fuselage	

### DISCUSSION

#### Longitudinal Stability and Control

Wing-alone aerodynamic characteristics.— The aerodynamic characteristics of the wing alone (flaps neutral) are presented in figure 11.

The pitching-moment curve had a progressively destabilizing trend at moderately high lift coefficients, which was probably caused by premature tip stalling. The lift-curve slope,  $C_{L\alpha}$  for the wing alone (at low angles of attack) was 0.061.

Effect of wing position.— Stabilizer data are presented for the low wing position ( $\Gamma = 5.7^\circ$ ) and the semihigh wing position ( $\Gamma = 0^\circ$ ) in figures 12 and 13, respectively. The elevator-fixed neutral points were computed from these data and are presented in figure 14.

For the flaps-neutral condition the model data indicate instability above lift coefficients of 0.44 and 0.32 for the low and semihigh wing positions, respectively, at the 0.26 mean aerodynamic chord reference center of gravity. At higher lift coefficients marked instability is indicated.

With the flaps deflected ( $\delta_{f_s} = 55^\circ$ ;  $\delta_{f_n} = 30^\circ - 60$  percent span), the semihigh-wing configuration shows marked instability above a lift coefficient of 0.55. (See fig. 13(b).) However, with the low-wing version ( $\delta_{f_s} = 55^\circ$ ;  $\delta_{f_n} = 30^\circ - 100$  percent span), neutral stability is indicated at about  $C_L = 0.60$ , and at higher lift coefficients only marginal instability is shown up to the stall where a marked instability is indicated. (See figs. 12(b) and 14.) The principal reason for the higher stability with the low-wing version is attributable to a substantially lower value of  $\partial\epsilon/\partial\alpha$  (fig. 15). Note that for the low wing position, nose flaps, when used, are 100-percent span, while for the semihigh wing, nose flaps were used only on the outboard 60-percent span. Data for the low wing position indicate the 100-percent-span nose flaps had somewhat higher stability than the 60-percent-span nose flaps at moderate lift coefficients. (See figs. 31 and 32.) For stability reasons, the low wing position was adopted for all future models.

The  $C_{L_{\max}}$  (trimmed) for the low-wing model was 0.85 with flaps neutral and 1.20 with flaps deflected. For the semihigh-wing model, the  $C_{L_{\max}}$  (trimmed) was 0.94 with flaps neutral and 1.35 with flaps deflected. (See figs. 12 and 13.) The largest part of  $\Delta C_L$ , due to flap deflection, was attributable to the effect of nose-flap deflection on a circular-arc wing. (See fig. 32.)

Effect of smaller fuselage.— Stabilizer data for the revised fuselage are presented in figure 16. (Horizontal-tail location number 1 is normal position.) The neutral points presented in figure 18 indicate a decreasing stability with increased  $C_L$  about

the 0.26 mean aerodynamic chord center of gravity with instability indicated above  $C_L = 0.5$ . This is again attributable to a large increase in  $\partial\epsilon/\partial\alpha$  (fig. 19). The use of the smaller fuselage increased the stability approximately 3-percent mean aerodynamic chord (compare figs. 14 and 18) as compared to a theoretical increase of 3.8 percent mean aerodynamic chord (reference 4).

For the landing condition  $\delta_{fp} = 50^\circ$ ,  $\delta_{fn} = 15^\circ$  (40-percent span) the model was stable through the lift range except between lift coefficients of 0.60 to 0.80 where slight instability exists (fig. 18). In this instance also the values of  $\partial\epsilon/\partial\alpha$  (fig. 19) remained close to 1 at high angles of attack, but the tail-off aerodynamic center moved rearward at high lift coefficients (fig. 16(b)) which resulted in a corresponding stable neutral-point shift. No direct comparison can be made with the original fuselage condition because of the changed flap configuration.

Effect of vertical location of the horizontal tail.— An effort was made to improve static longitudinal stability by locating the horizontal tail in a region of more favorable downwash. It was therefore decided to investigate several vertical positions of the horizontal tail (fig. 5). Neutral points were computed from the stabilizer data of figures 16 and 17 and are presented in figure 18. When the horizontal tail was raised to the highest position tested, a considerable improvement was obtained in the flap-neutral stability in the higher lift range; however, the static margin about the reference center of gravity was still marginally negative in this lift range (fig. 18). The improvement shown results mainly from the decrease in  $\partial\epsilon/\partial\alpha$  (fig. 19(a)). Although the primary purpose in relocating the tail was to improve the flap-neutral stability, it also increased the flap-down. ( $\delta_{fp} = 0^\circ$ ;  $\delta_{fn} = 15 - 40$  percent span) stability, resulting in a positive static margin about 26-percent center of gravity throughout the lift range (fig. 18).

With the horizontal tail in the low position, the stability was generally less at low  $C_L$  compared to the higher tail locations primarily because of a loss in effective dynamic pressure at the tail. (See figs. 18 and 19.) However, near stall there is a gain in stability caused by the large reduction in  $\partial\epsilon/\partial\alpha$ .

Effect of extended fuselage.— Stabilizer data for the extended fuselage are presented in figure 20 for the flaps-neutral configuration. The extended fuselage showed very little improvement in the stability over that realized with the normal-tail location. (Compare figs. 20 and 16(a).)

Effect of stall-control vanes.— Tuft studies (fig. 37) had shown a strong cross flow to be present, especially in the region of the leading edge of the wing, which apparently contributed to the separation over the outboard wing panel. It was felt that if this flow could be alleviated, a beneficial rearward movement of the wing-fuselage aerodynamic center might be realized. Consequently, it was decided to investigate a series of thin longitudinal vanes herein referred to as stall-control vanes. All of the vane configurations shown in figure 5 were tested; however, only pertinent results are presented and discussed. The initial vane tests were made with the flaps neutral using vanes 1, 2, and 3 (fig. 5). With the vane located at  $0.45\frac{b}{2}$  from the center section, the pitching-moment curve was stable throughout the lift range except for a "pip" at maximum lift, and vane locations at  $0.30\frac{b}{2}$  and  $0.60\frac{b}{2}$  gave similar results but with slightly less improvement in the pitching-moment curve. (See fig. 21.)

It was thought that the stalling tendency shown at  $C_{L_{max}}$ , while surely not desirable, will nevertheless not be unduly dangerous, for there should be little possibility of inadvertently pulling a dangerous overload. The flat-top lift curve should be a help inasmuch as a few degrees above the angle at which the stalling moment is experienced a stabilizing moment is encountered. (See fig. 21.) It should also be remembered that many airplanes experience lateral or longitudinal trim changes at stall and unless these changes occur close to the ground or are particularly violent they should be tolerable.

Using the best spanwise location found with the rectangular vane, the effect of vane size was investigated. A large reduction in size made little difference in the improvement obtained, providing the vane was at the leading edge of the wing (fig. 22).

Stabilizer data with vane 13 are presented in figure 23 for the flaps neutral and deflected ( $\delta_{fp} = 50^\circ$ ;  $\delta_{fn} = 15^\circ - 40$  percent span) from which neutral points were obtained (fig. 24). This vane provided at least neutral stability up to the stall, followed by the aforementioned pip in the  $C_m$ -curve.

In the flaps-up condition, practically all of the increase in stability is provided by the rearward shift of the wing-fuselage aerodynamic center with the vane on. (See figs. 23(a) and 25.) For the flaps-down configuration, the stability is affected only slightly by the vane. (See figs. 23(b), 24 and 25.)

Stall-control vanes tested with a 100-percent-span round leading edge had little effect on the longitudinal-stability characteristics. (See fig. 26.) The small vane (vane 13) had no effect on the pitching-moment slope, but the large vane showed some slight improvement near the stall. Other tests have indicated that with the round leading edge the critical cross flow present at the leading edge of the circular-arc wing is alleviated, and as a result the need for the leading-edge vane ceases.

Effect of rounded wing leading-edge modifications.-- Because of the poor stability characteristics at moderate and high lift coefficients with the sharp leading-edge wing, a series of tests were made with the leading edge rounded as shown in figure 6. The 100-percent-span round leading edge apparently showed a definite improvement in the longitudinal stability for the flaps-neutral condition (fig. 27) with stability occurring up to about  $C_L = 0.7$  after which instability was indicated. (See fig. 28.) However, at low lift coefficients the gain in stability can be almost completely attributed to the 0.075 rearward movement of the wing mean aerodynamic chord affected by the nature of the modification. (See fig. 6.) At a moderate lift coefficient (about 0.6) a larger increase in stability is realized, mainly because of the delayed tip stall associated with the round leading edge. (Compare tail-off curves, figs. 27 and 16(a).) The raised horizontal tail (position 2) further increases the stability only slightly (fig. 28).

No change in stability was noted when only the outboard 40 percent of the wing span was rounded (fig. 29).

Effect of wing fillet.-- The effect of wing fillet (fig. 8) on the tail-off aerodynamic characteristics was slight. (See fig. 30.)

Effect of nose-flap deflection.-- Nose-flap deflection resulted in an improvement in the aerodynamic characteristics which resulted from a delayed stall (fig. 31). Deflecting the nose flap extended the stable pitching-moment variation with lift coefficient to a larger lift range for both flap configurations:

Lift characteristics obtained from figure 31 are summarized in the following table:

	$\delta_{f_s} = 0^\circ$ $\delta_{f_n} = 0^\circ$	$\delta_{f_s} = 55^\circ$ $\delta_{f_n} = 0^\circ$	$\delta_{f_s} = 0^\circ$ $\delta_{f_n} = 30^\circ$ (100 percent b)	$\delta_{f_s} = 55^\circ$ $\delta_{f_n} = 30^\circ$ (100 percent b)
$C_{L_{max}}$ (trim)	0.85	0.93	1.10	1.20
$\Delta C_{L_{max}}$ (due to $\delta_{f_n}$ )	--	--	0.25	0.27
$\Delta C_{L_{max}}$ (due to $\delta_{f_s}$ )	--	0.08	--	0.10

Deflecting the nose flap also increased the angle of attack for maximum lift coefficient, especially for the split-flap neutral condition, primarily by alleviating the negative pressure peaks that cause leading-edge separation near maximum lift.

It is also interesting to note the decrease in the drag coefficient with nose-flap deflection at a given lift coefficient. (See fig. 31.) With airfoils having sharp leading edges, the drag coefficient increases fairly rapidly as the angle of attack departs from zero. Nose-flap deflection has the favorable effect of a large leading-edge radius, which tends to improve the air-flow conditions around the leading edge at high lift coefficients and thus improves the aerodynamic characteristics.

Various split-flap and nose-flap combinations.— The effects of various split-flap and nose-flap combinations are presented in figure 32. For split flaps neutral and 60-percent outboard span nose flaps deflected  $30^\circ$ , the pitching-moment curve is unstable over a greater  $C_L$  range than for full-span nose-flap deflection. (Compare figs. 31(a) and 32(a).) It should be noted that trimmed  $C_{L_{max}}$  is about the same for the reduced-span nose flaps as with full-span nose flaps

(fig. 31(a)). Similarly, for the  $\delta_{F_S} = 55^\circ$  condition (fig. 32(b)), the stability is unfavorable over a greater  $C_L$ -range with the 60-percent-span nose flaps than with the 100-percent-span nose flap deflected (compare figs. 31(b) and 32(b)), but the trimmed  $C_{L_{max}}$  is actually higher with the smaller-span-nose flaps.

Elevator effectiveness.— Elevator-effectiveness tests, which were made with the large fuselage and the wing in the semihigh position ( $\Gamma = 0^\circ$ ), are presented in figure 33. The average elevator effectiveness  $\partial C_m / \partial \delta_e$  through the low lift range for the flaps-neutral configuration was  $-0.0048$ .

Effect of Reynolds number.— The results of pitch tests of figure 34 ( $\psi = 5^\circ$ ) with the turbulence net installed showed that for the complete model a slight decrease in maximum lift coefficient and slope of the lift curve was experienced with an increase in effective Reynolds number. The longitudinal stability was practically unaffected by the effective Reynolds number difference (except near stall with flaps deflected). Circular-arc sections in two-dimensional flow have indicated negligible effect on sectional characteristics between Reynolds numbers of 3 to 9 million (reference 6).

Sinking speed and glide-path angle.— The sinking speed was estimated for a full-scale airplane assuming a  $\frac{W}{S} = 33.3$  at sea level. The effects of flap deflection on the estimated sinking speeds of a full-scale airplane are presented in figure 35. Above approximately 142 miles per hour lower sinking speeds are associated with flaps neutral.

The high sinking velocities shown in figure 35 (generally conceded sinking speed limit—1800 ft/min) indicate that the airplane cannot be flown into ground contact but will have to be "flared" to reduce the landing-gear loads at contact or that power will be required to land. For a more heavily loaded airplane, the sinking speed and the velocities shown in figure 35 increase as the square root of the weight ratio, and landing without power will almost be precluded.

#### Stall Characteristics

The model for these tests was with the large fuselage and the wing in the low position.

$\delta_{F_S} = 0^\circ$ ;  $\delta_{F_N} = 0^\circ$ .— Tuft studies of the flaps-neutral condition (fig. 36(a)) showed that the stall started at the tip of the wing with

an outboard flow along the leading edge ( $\alpha = 2.5^\circ$ ). With increasing angle of attack, the stall area moved inboard.

$\delta_{f_s} = 55^\circ$ ;  $\delta_{f_n} = 0^\circ$ .— For the split-flap-deflected- $55^\circ$  condition, the tuft studies showed an outboard flow along the leading edge. (See fig. 36(b).) As the angle of attack was increased the tip area developed an outboard flow, finally stalling, and the stall area moved inboard with higher angles of attack.

$\delta_{f_s} = 55^\circ$ ;  $\delta_{f_n} = 30^\circ$  (60-percent span).— With the split flap deflected  $55^\circ$  and the 60-percent-span nose flaps deflected  $30^\circ$ , the tip stall was delayed to a considerably higher angle of attack (compare figs. 36(b) and 36(c)) than without nose-flap deflection. At an angle of attack of  $9.3^\circ$ , stall appeared slightly outboard of the root section with an outboard flow on the outer wing panel. As the angle of attack increased, the tip stalls and the inboard stall area is increased. Finally ( $\alpha = 13.6^\circ$ ) the stall area enveloped most of the wing except near the wing-fuselage juncture.

$\delta_{f_s} = 55^\circ$ ;  $\delta_{f_n} = 30^\circ$  (100-percent span).— With nose-flap deflection extended to 100-percent span, the inboard stall area present with 60-percent-span nose flaps was eliminated. Otherwise, the increased nose-flap span appears to cause little change in the stall trend. (Compare figs. 36(c) and 36(d).)

#### Ground Effects

Stabilizer data are presented in figures 37 and 38 for the model (stall-control vane 13) in the presence of a ground board 14.1 inches and 24.1 inches below the center of gravity, respectively. The ground board extended the stable pitching-moment variation with lift coefficient for both flap configurations to higher lift coefficients than were obtained without the ground board.

There is a pronounced pip evident in the pitching-moment curves for both flap-neutral and flap-deflected conditions near  $C_{l_{max}}$  when the ground-board height is 14.1 inches below the center of gravity. The pip is less pronounced (flaps down) with the model farther away from the ground board. (Compare figs. 37(a) and 38.)

## CONCLUSIONS

The following conclusions are based on tests of an airplane model having a  $42.8^\circ$  sweptback wing with aspect ratio 4.00 and taper ratio 0.50 with a  $42.8^\circ$  sweptback horizontal tail and a  $40.3^\circ$  sweptback vertical tail:

1. In the flaps-neutral condition the model tested either as a low-wing or semihigh-wing airplane became unstable at moderate lift coefficients. In the flaps-deflected condition, however, the low-wing model had a positive static margin which became marginal at the high lift coefficients; whereas, the semihigh-wing model became markedly unstable at moderate lift coefficients.

2. Small stall-control vanes located at the leading edge of the low-wing version removed the longitudinal instability present below the stall in the flaps-neutral condition.

3. It was necessary to raise the horizontal tail about 9 inches on the model vertical tail to effect a considerable improvement in the flap-neutral stability in the high lift range.

4. Nose-flap deflection extended the longitudinal stability over a larger lift range for both flap conditions. Nose-flap deflection also increased the maximum lift coefficient and reduced the drag values.

Langley Memorial Aeronautical Laboratory  
National Advisory Committee for Aeronautics  
Langley Field, Va.

## REFERENCES

1. Goodson, Kenneth W., and Comisarow, Paul: Lateral Stability and Control Characteristics of an Airplane Model Having a  $42.8^\circ$  Sweptback Circular-Arc Wing with Aspect Ratio 4.00, Taper Ratio 0.50, and Sweptback Tail Surfaces. NACA RM No. L7G31, 1947.
2. Schuldenfrei, Marvin, Comisarow, Paul, and Goodson, Kenneth W.: Stability and Control Characteristics of an Airplane Model Having a  $45.1^\circ$  Swept-Back Wing with Aspect Ratio 2.50 and Taper Ratio 0.42 and  $42.8^\circ$  Swept-Back Horizontal Tail with Aspect Ratio 3.87 and Taper Ratio 0.49. NACA RM No. L7B25, 1947.
3. Gillis, Clarence L., Polhamus, Edward C., and Gray, Joseph L., Jr.: Charts for Determining Jet-Boundary Corrections for Complete Models in 7- by 10-Foot Closed Rectangular Wind Tunnels. NACA AER No. L5G31, 1945.
4. Recant, Isidore G.: Wind-Tunnel Investigation of Ground Effect on Wings with Flaps. NACA TN No. 705, 1939.
5. Thom, A.: Blockage Corrections in a Closed High-Speed Tunnel. R. & M. No. 2033, British A.R.C., 1943.
6. Underwood, William J., and Nuber, Robert J.: Two-Dimensional Wind-Tunnel Investigation at High Reynolds Numbers of Two Symmetrical Circular-Arc Airfoil Sections with High-Lift Devices. NACA RM No. L6K22, 1947.

TABLE I.— PHYSICAL CHARACTERISTICS OF A MODEL WITH A

42.8 - 4.00 - 0.50 WING

	Wing	Horizontal Tail	Vertical Tail	
			Small (a)	Large (b)
Area, sq ft	12.70	2.06	1.54	2.08
Span, in.	85.50	34.00	16.70	20.08
Sweepback, deg	42.8	42.8	40.3	40.3
Aspect ratio	4.00	3.87	1.26	1.35
Taper ratio	0.50	0.49	0.31	0.35
Dihedral, deg				
Semihigh wing, large fuselage	0	0		
Low wing, large fuselage	5°51'	0		
Low wing, small fuselage	3	0		
Angle of incidence	3°			
Mean aerodynamic chord, in.	22.15			
Root chord, in.	28.50	11.75	20.80	22.14
Theoretical tip chord, in.	14.25	5.75	6.40	7.74
Root airfoil section	NACA 28-(50)(05)-(50)(05)	NACA 65-008	NACA 27-010	NACA 27-010
Tip airfoil section	NACA 28-(50)(05)-(50)(05)	NACA 65-008	NACA 27-010	NACA 27-008

<sup>a</sup>with large fuselage  
<sup>b</sup>with small fuselage

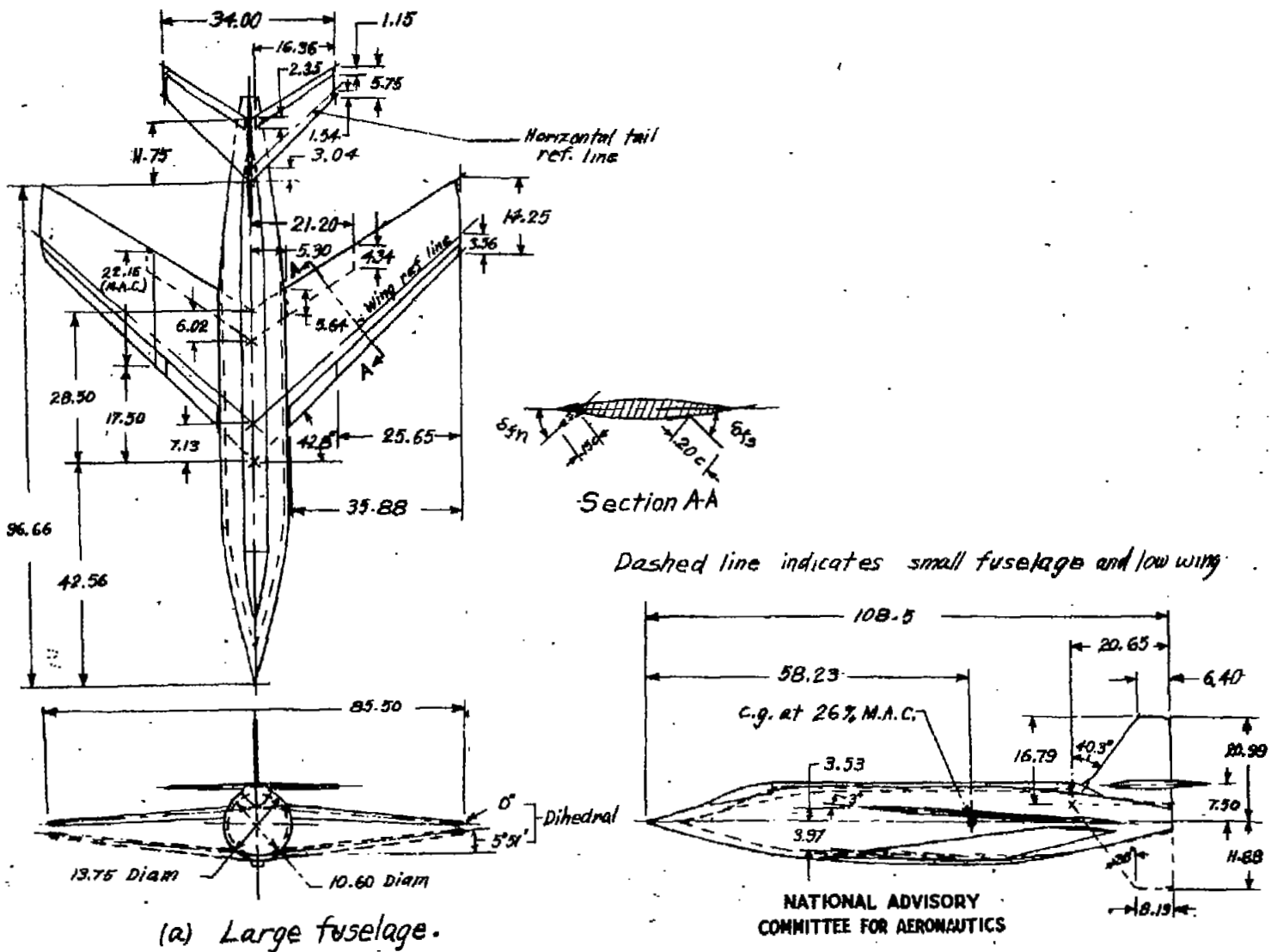


Figure 1. - Three-view drawing of a model with a 42.8 - 4.00 - 0.50 wing.  
All dimensions in inches.

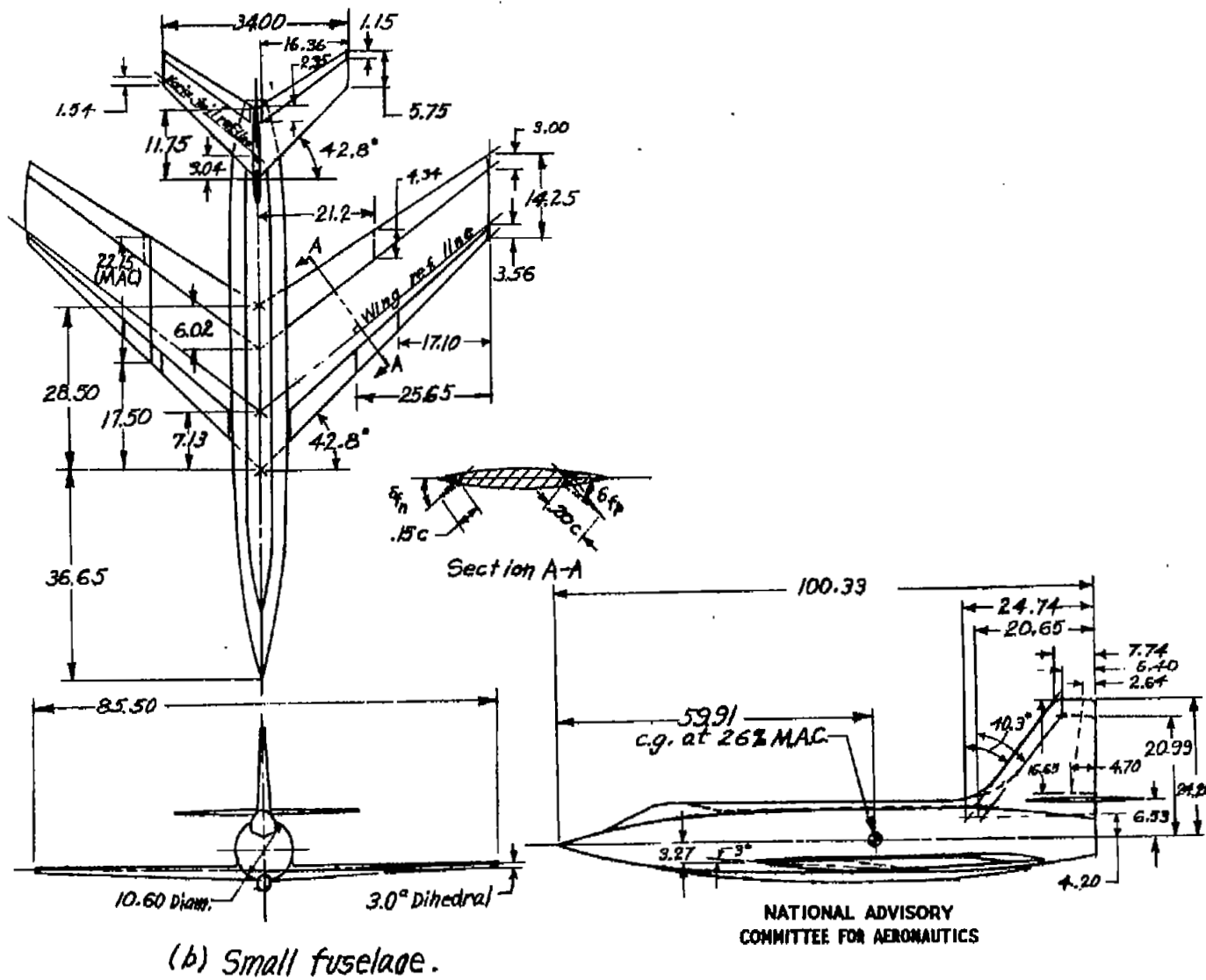


Figure 1.- Concluded.

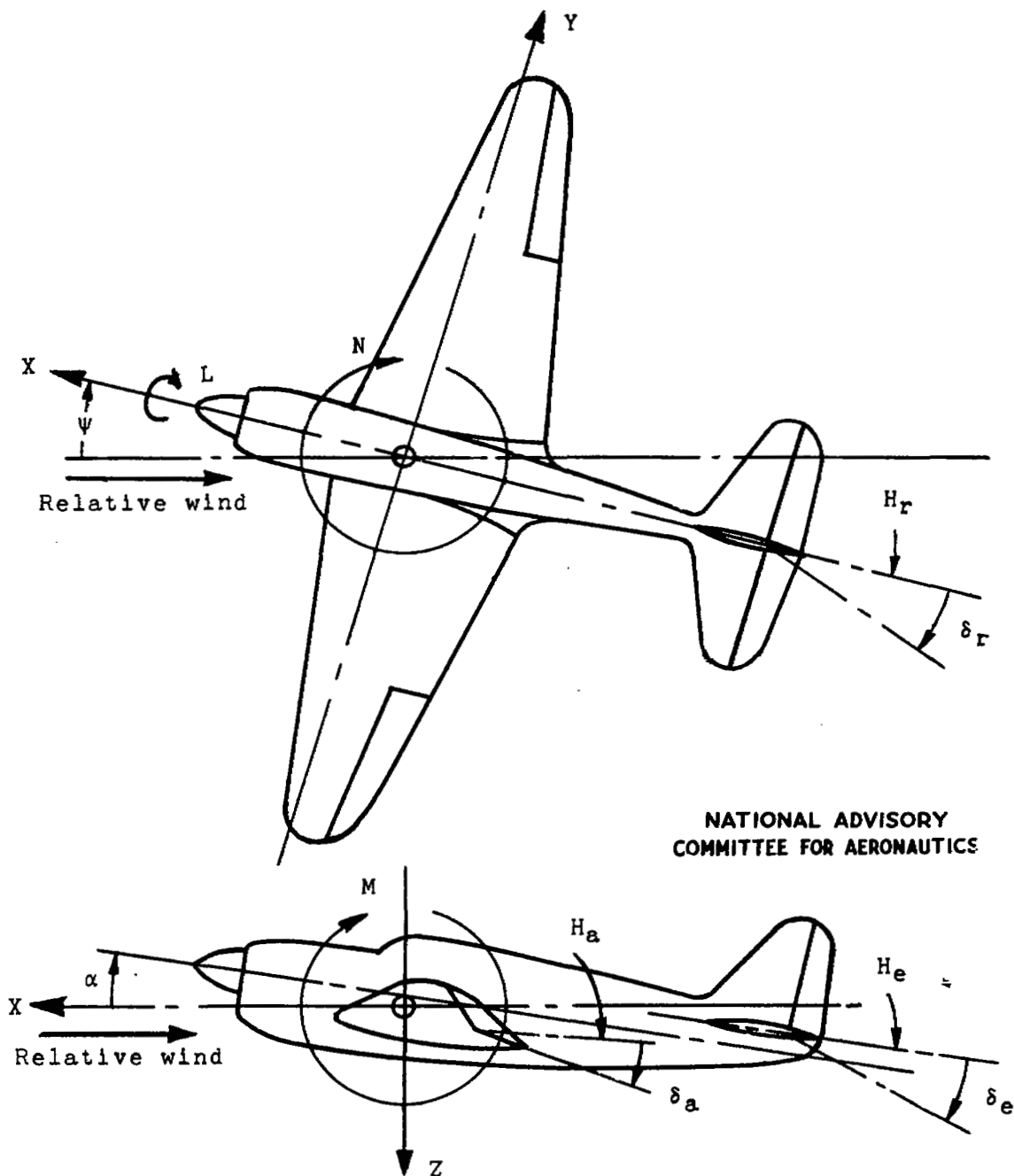


Figure 2.- System of axes and control-surface hinge moments and deflections. Positive values of forces, moments, and angles are indicated by arrows. Positive values of tab hinge moments and deflections are in the same directions as the positive values for the control surfaces to which the tabs are attached.

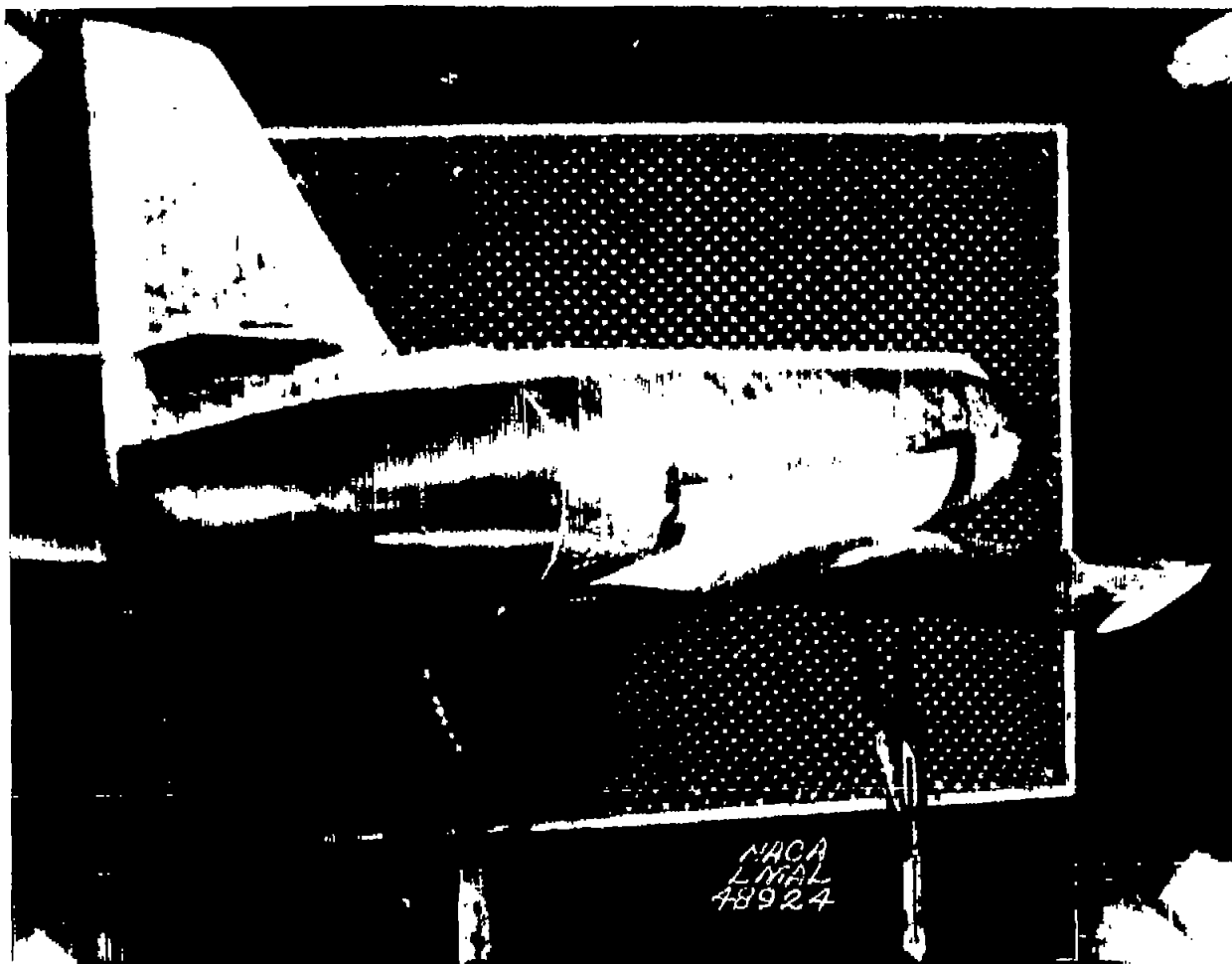


Figure 3(a).- Three-quarter rear view of the model with a 42.8 - 4.00 - 0.50 wing mounted in the Langley 300 MPH 7- by 10-foot tunnel; large fuselage;  $\delta_{f_s} = 0^\circ$ ;  $\delta_{f_n} = 0^\circ$ .



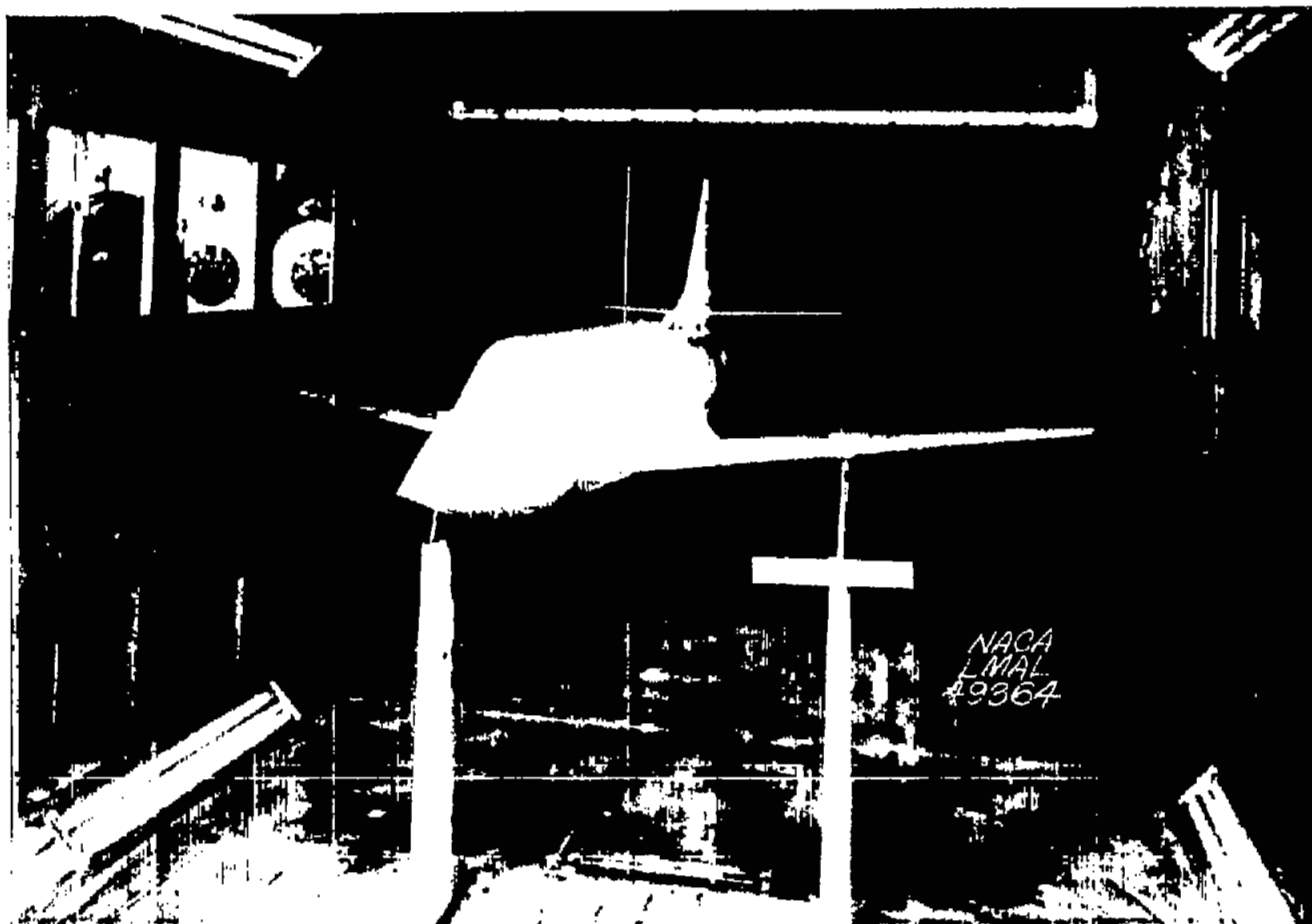


Figure 3(b).- Three-quarter front view of the model with a 42.8 - 4.00 - 0.50 wing mounted in the Langley 300 MPH 7- by 10-foot tunnel; small fuselage;  $\delta_{f_p} = 0^\circ$ ;  $\delta_{f_n} = 0^\circ$ .



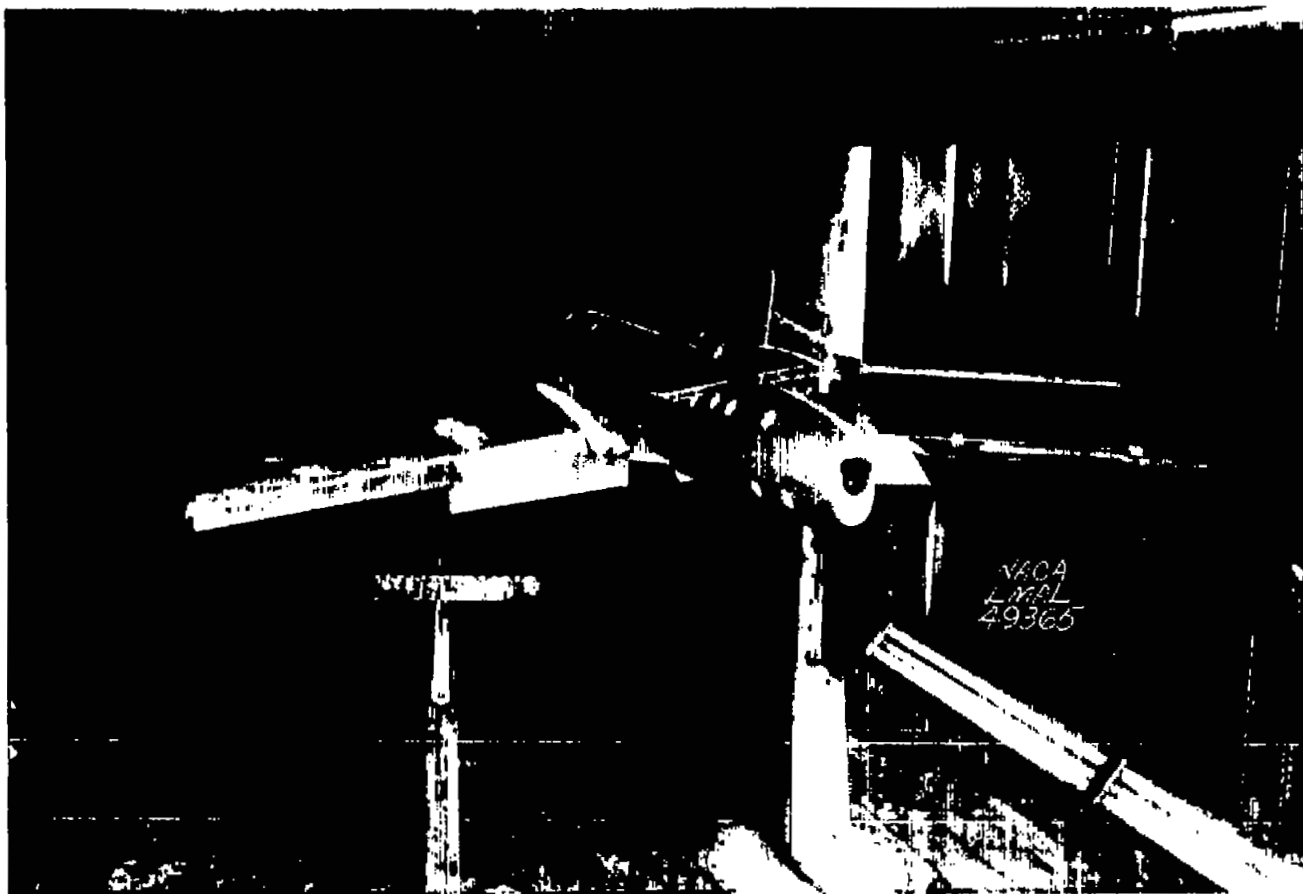


Figure 3(c).- Three-quarter rear view of the model with a 42.8 - 4.00 - 0.50 wing mounted in the Langley 300 MPH 7- by 10-foot tunnel; small fuselage;  $\delta_{fp} = 50^\circ$ ;  $\delta_{fn} = 15^\circ$  (40-percent span).



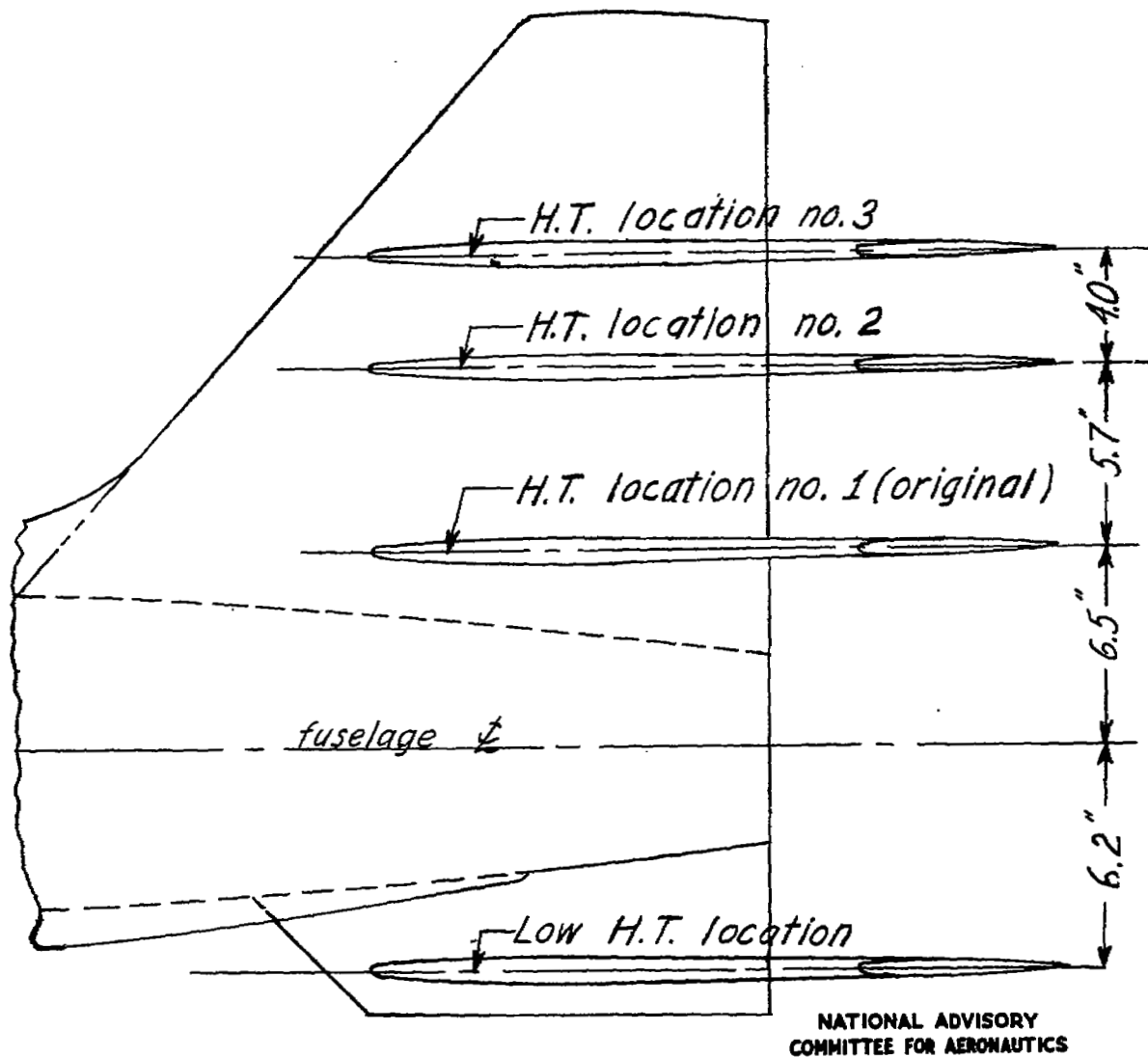


Figure 4.- Horizontal-tail locations as tested on the model with a 42.8 - 4.00 - 0.50 wing.

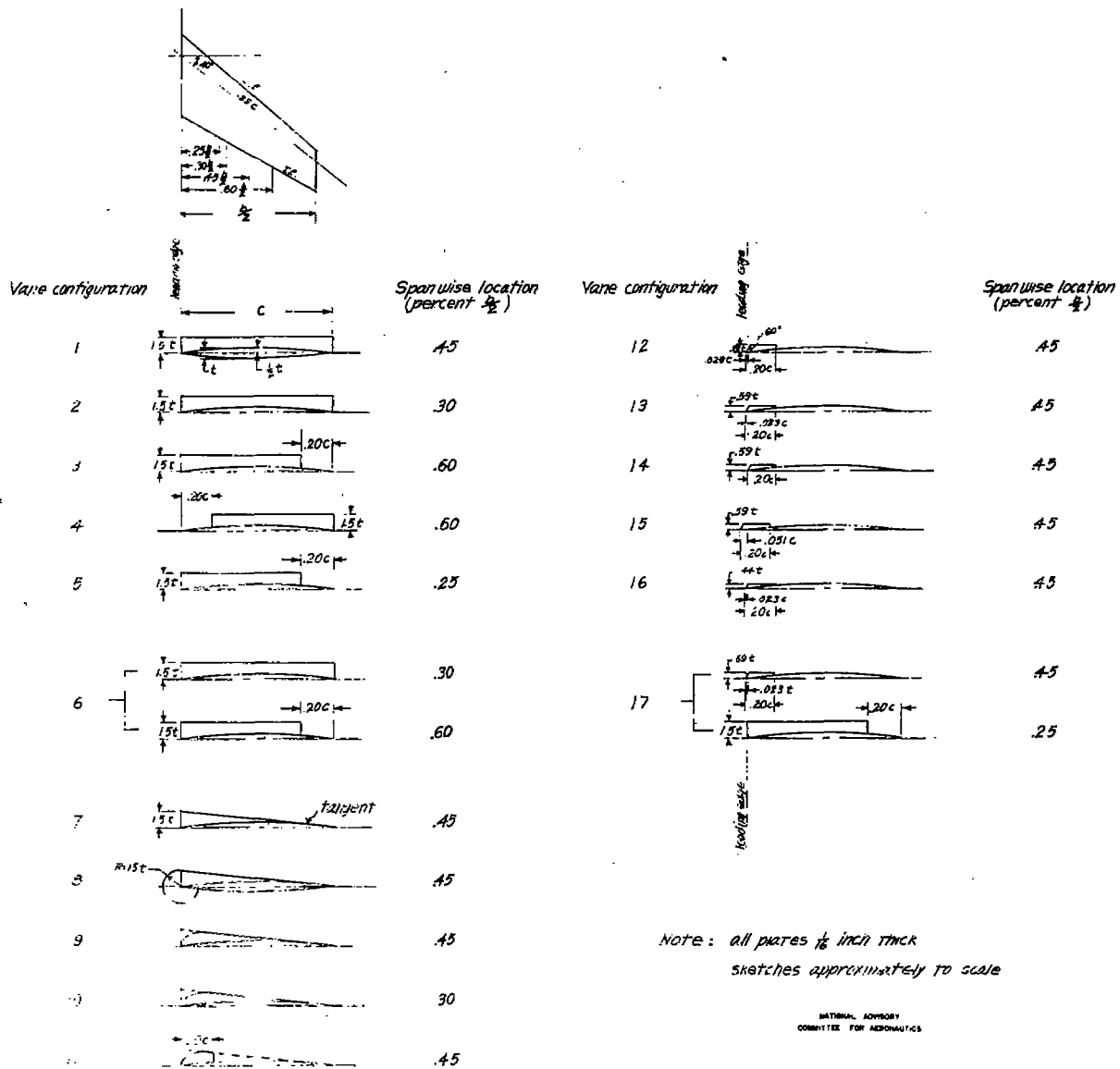


Figure 5.- Details of stall-vane configurations tested on a model with a 42.8 - 4.00 - 0.50 wing.

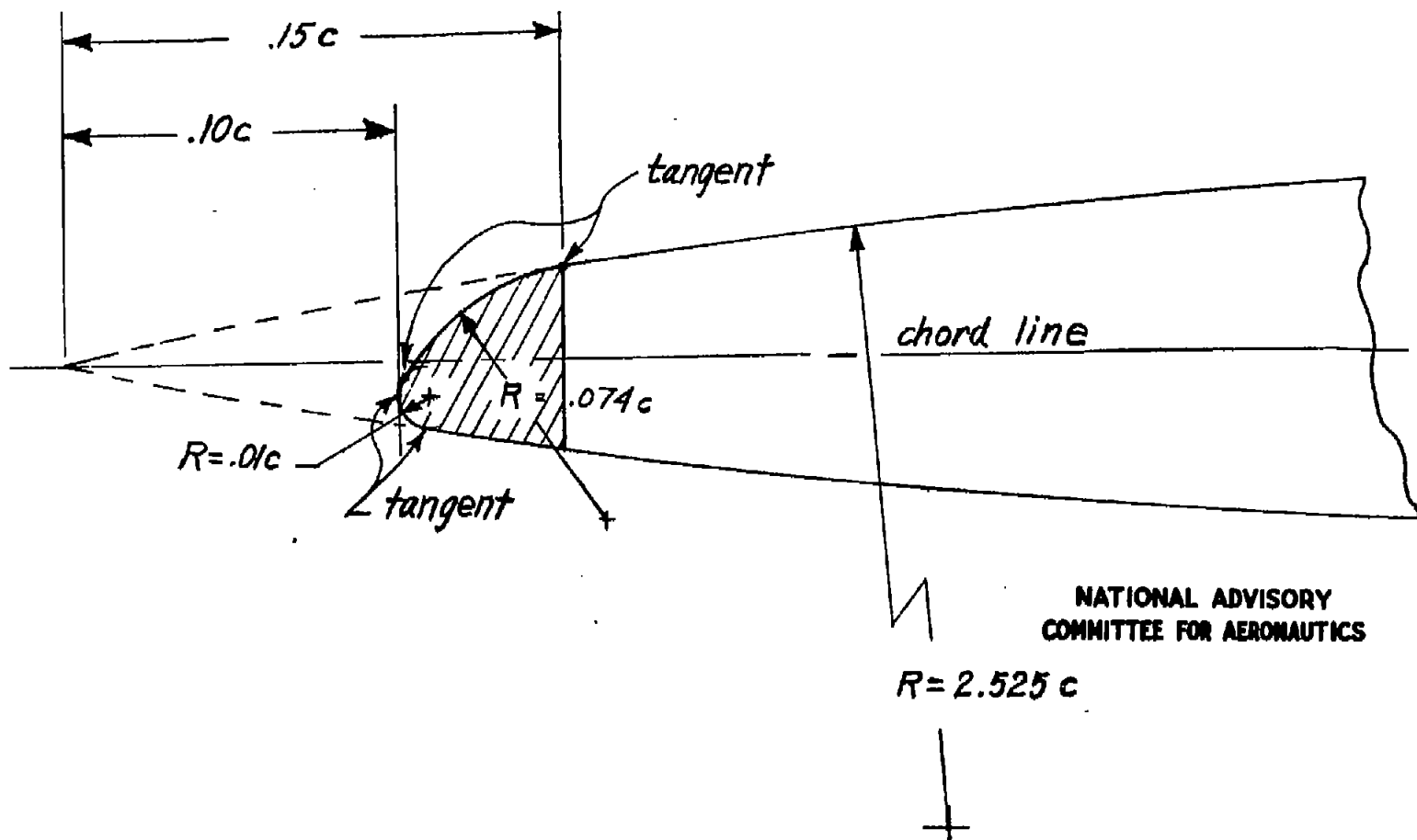


Figure 6.- Construction lines of the round leading-edge modification for the circular-arc wing of the model with a 42.8 - 4.00 - 0.50 wing.



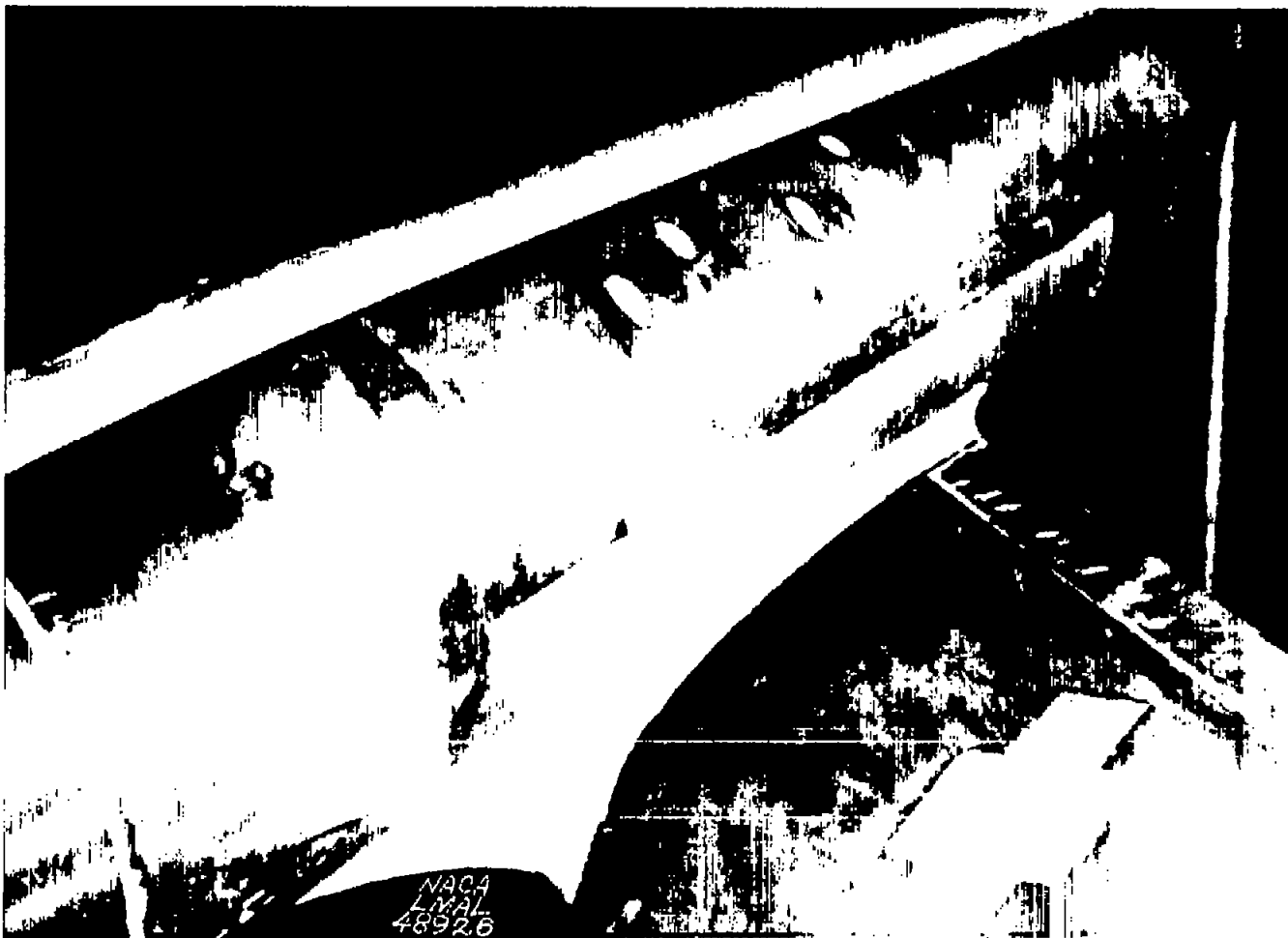
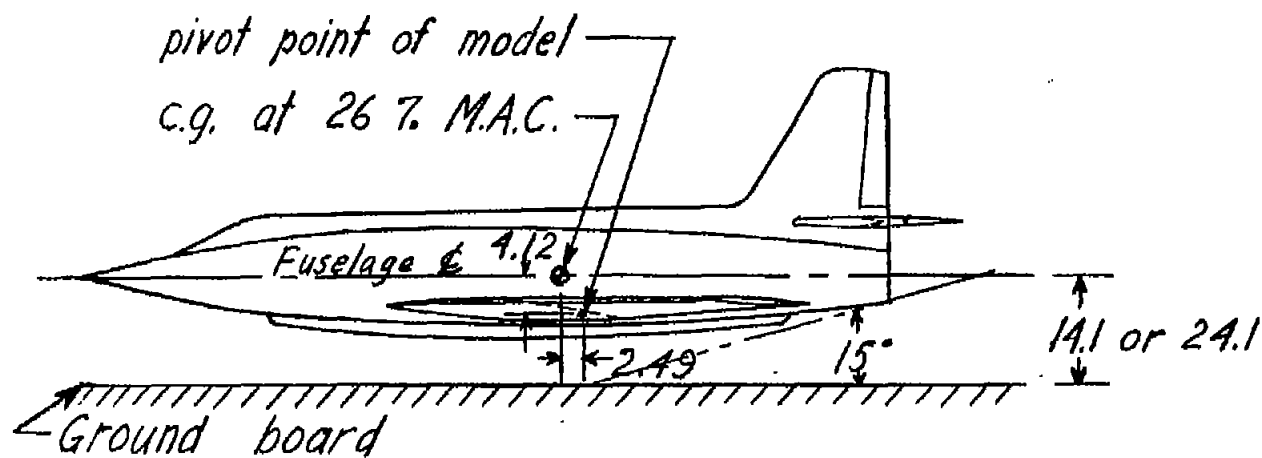


Figure 7.- The fillet of the wing-fuselage juncture of the model with a 42.8 - 4.00 - 0.50 wing.





NATIONAL ADVISORY  
 COMMITTEE FOR AERONAUTICS

Figure 8.- Position of the model with a 42.8 - 4.00 - 0.50 wing and the ground board in the wind tunnel.  $\alpha = 0^\circ$ . All dimensions in inches.

•

•

•

•

•

•

•

•

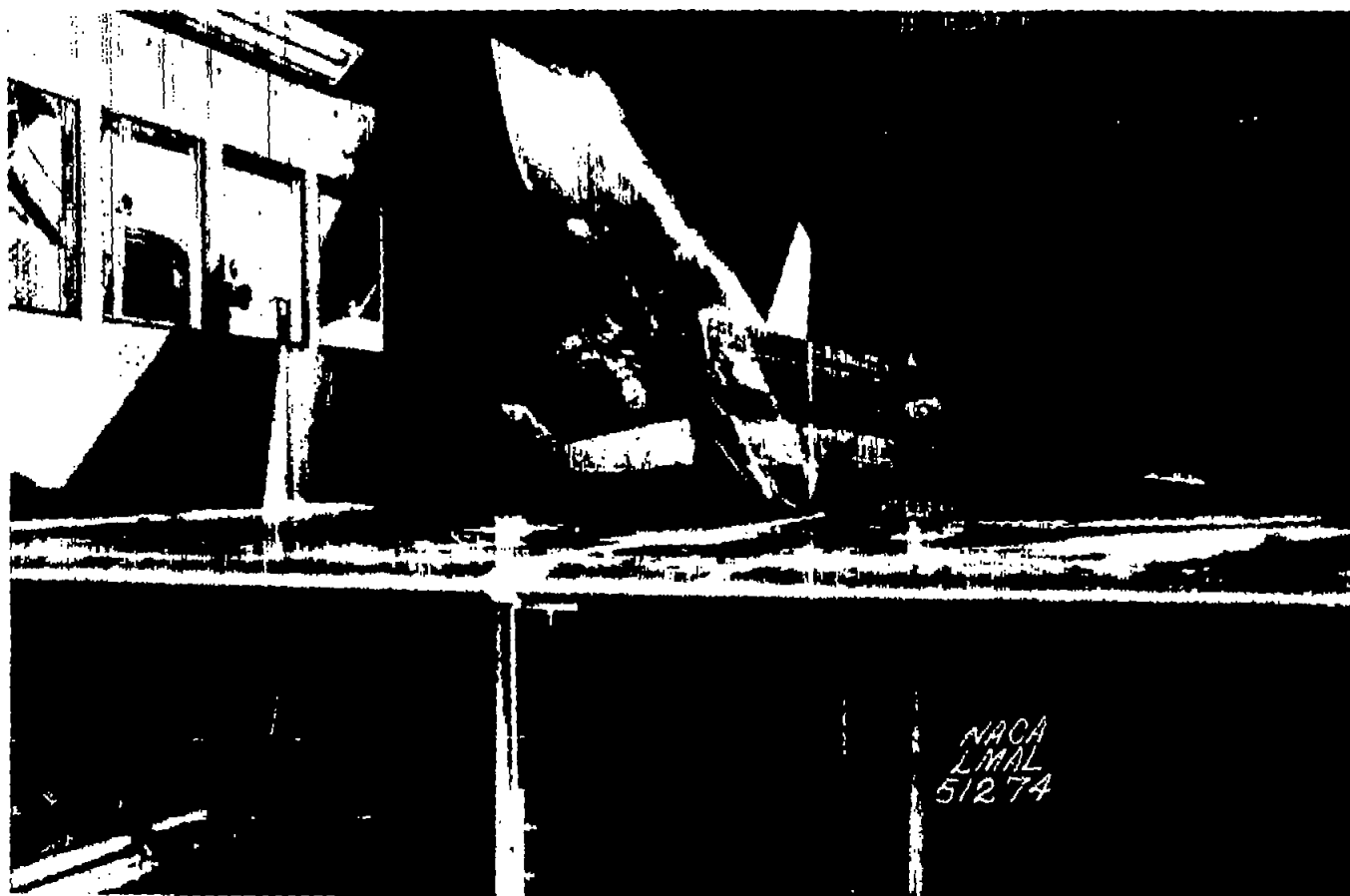
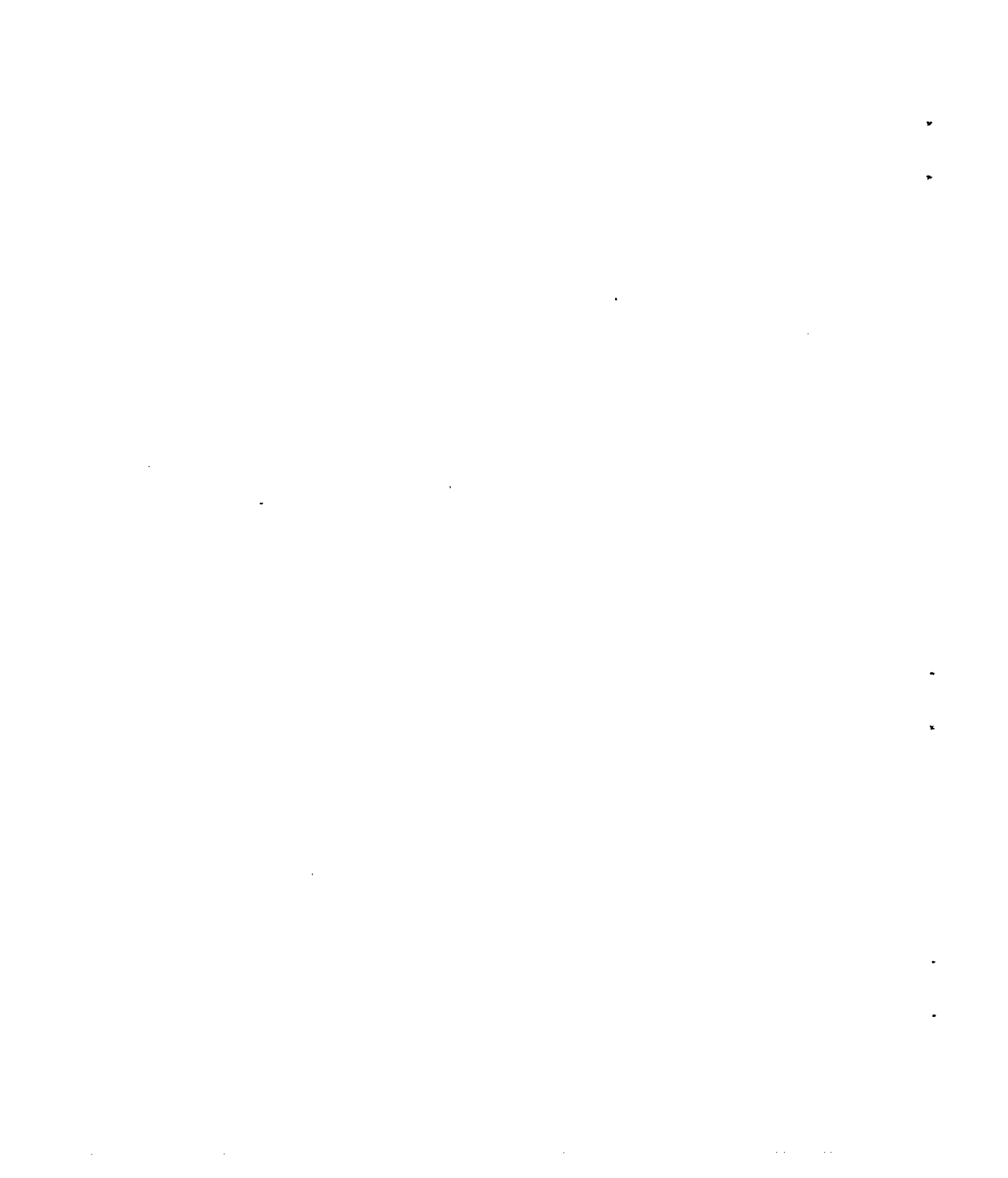


Figure 9.- A model with a 42.8 - 4.00 - 0.50 wing in the landing attitude ( $15^\circ$ ) in the presence of a ground board as tested in the Langley 300 MPH 7- by 10-foot tunnel;  $\delta_{fp} = 50^\circ$ ;  $\delta_{fn} = 15^\circ$

(40-percent span).



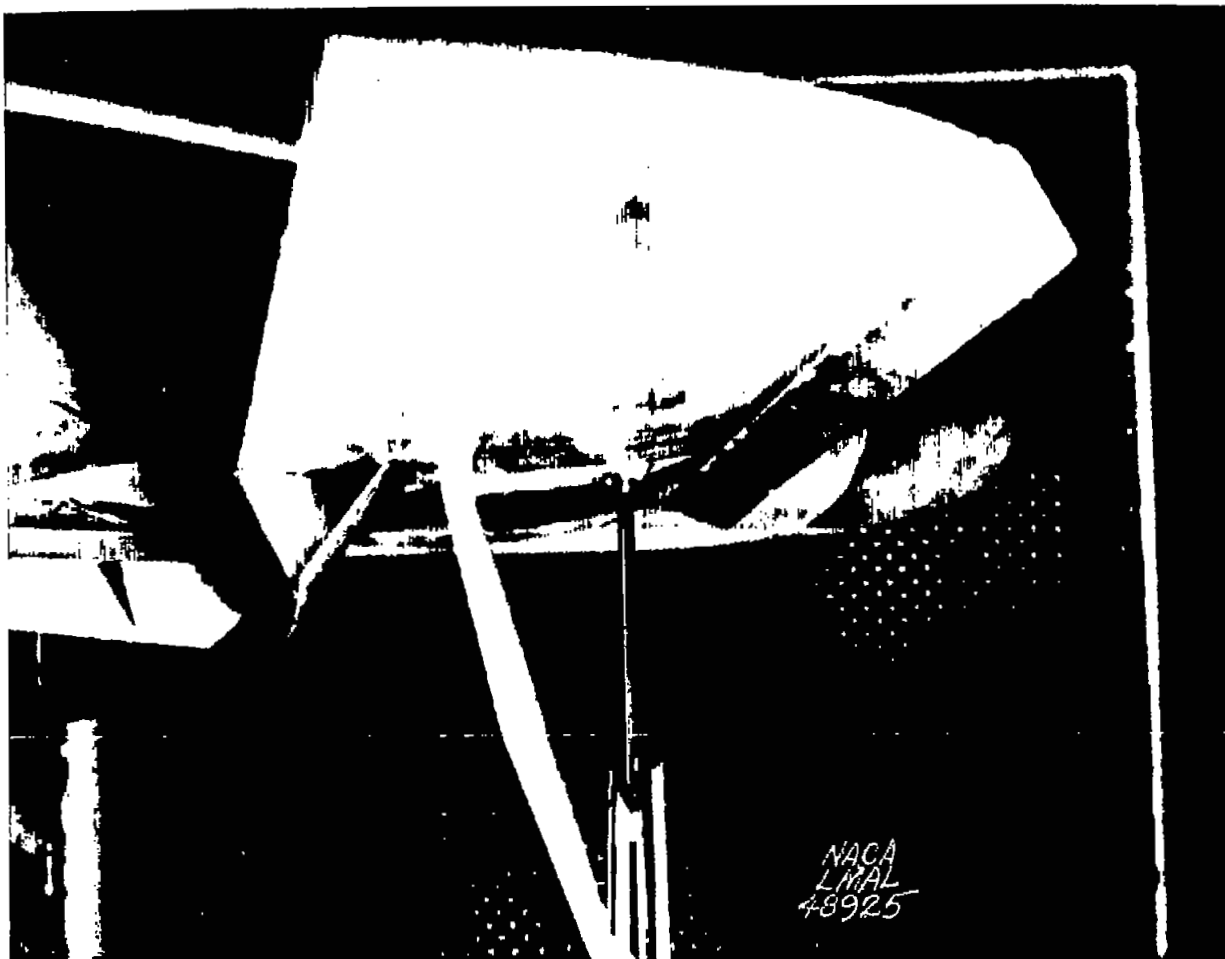
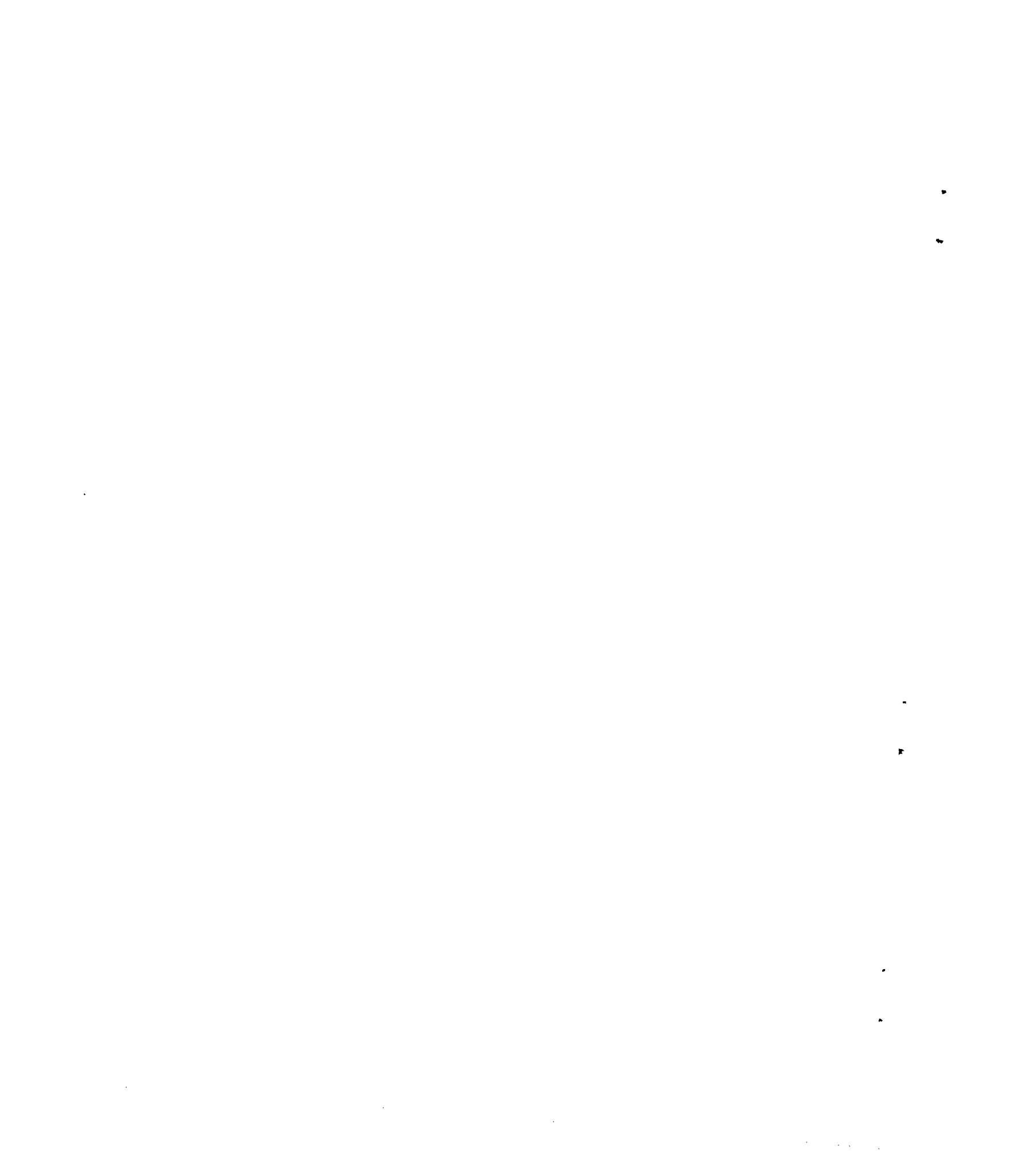


Figure 10.- The circular-arc wing showing the 0.20c split flap deflected  $55^\circ$  and the 0.15c nose flap deflected  $30^\circ$ .



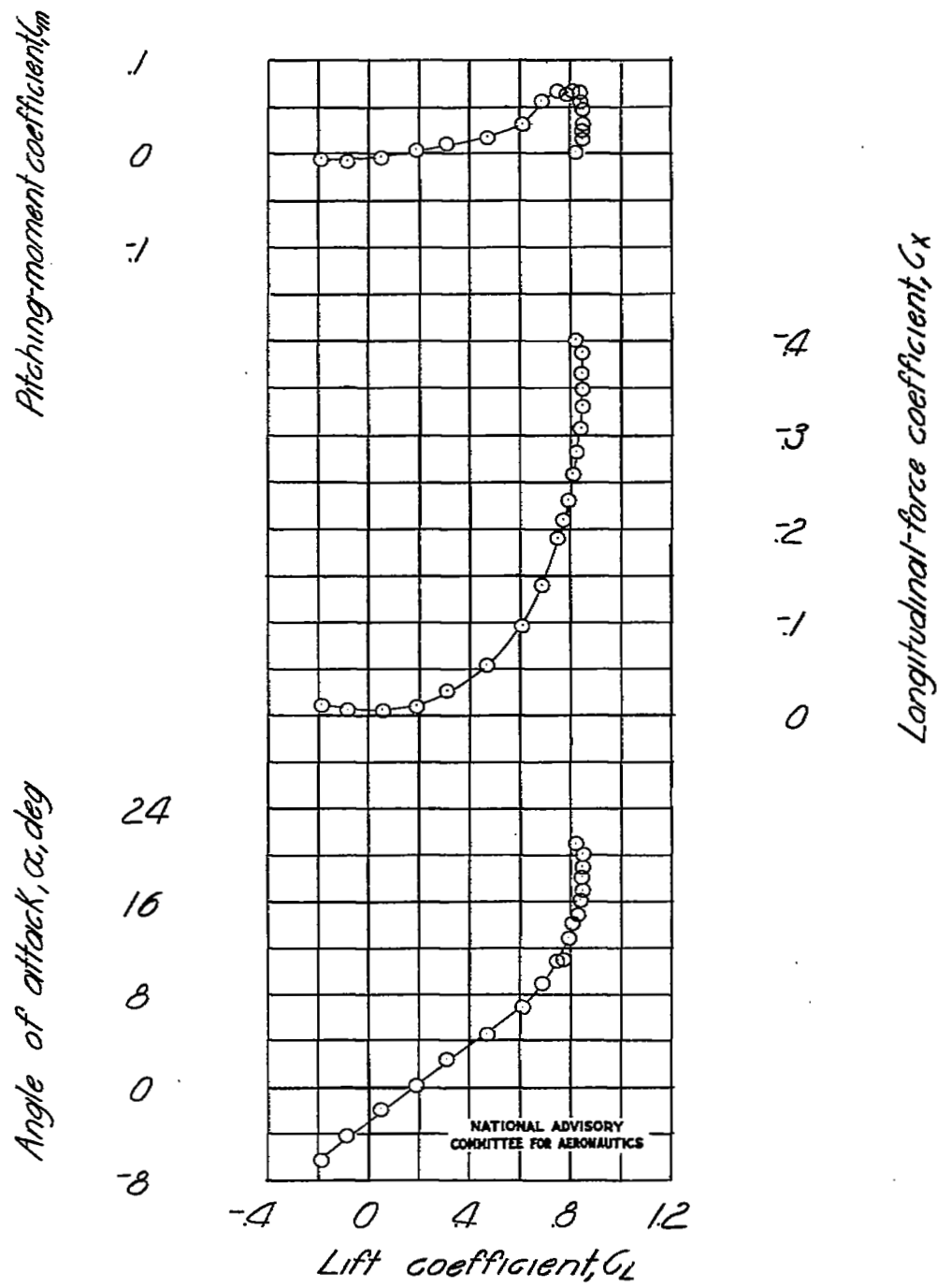


Figure 11.- Aerodynamic characteristics in pitch of a 42.8 - 4.00 - 0.50 wing;  $\delta_{fp} = 0^\circ$ ;  $\delta_{fn} = 0^\circ$ ;  $r = 3.5^\circ$ .

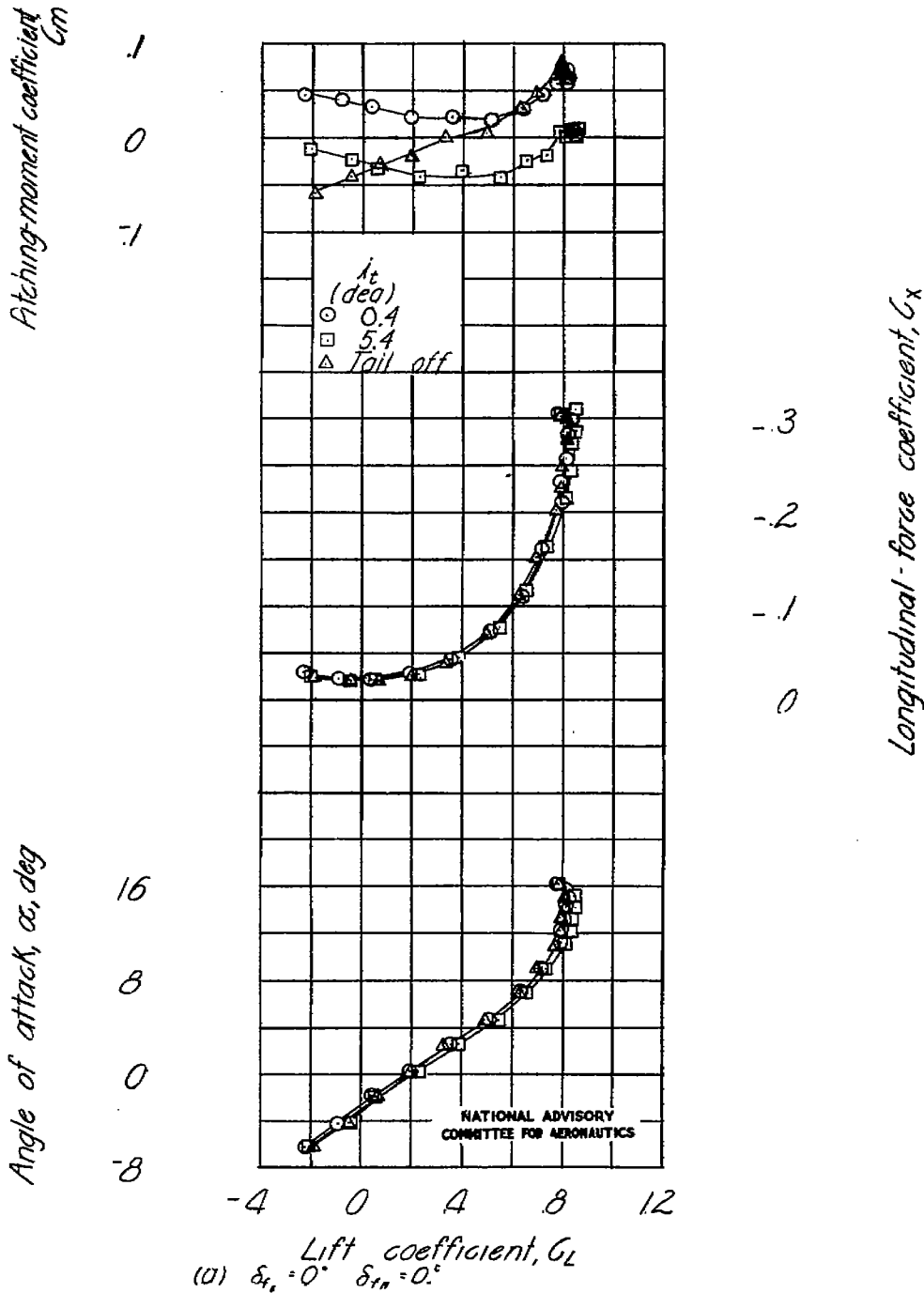
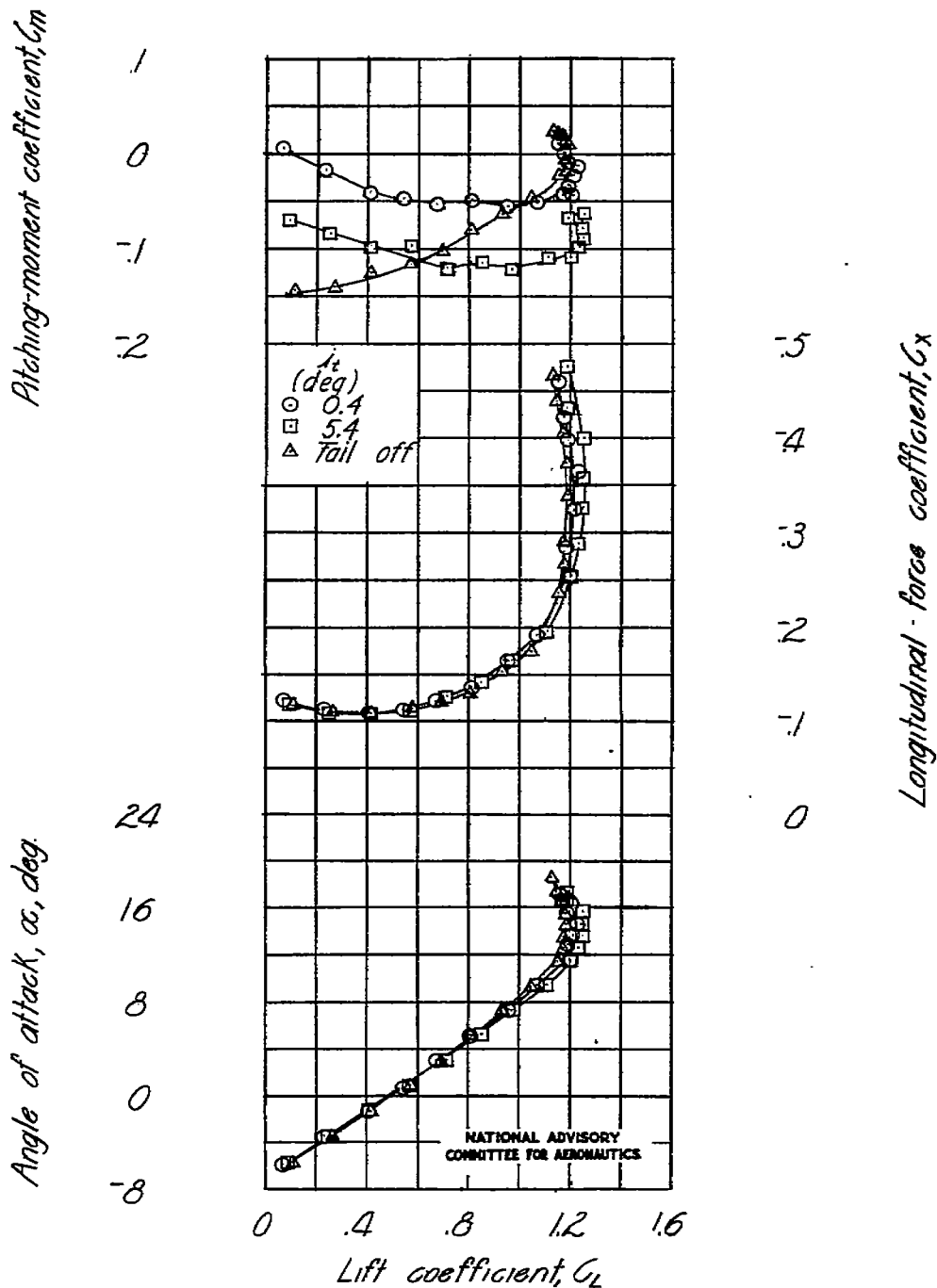


Figure 12.- Effect of stabilizer deflection on the aerodynamic characteristics in pitch of a model with a 42.8 - 4.00 - 0.50 wing; large fuselage; low wing;  $\Gamma = 5.7^\circ$ .



(b)  $\delta_{fs} = 55^\circ$ ,  $\delta_{fn} = 30^\circ$  (100% span)

Figure 12.- Concluded.

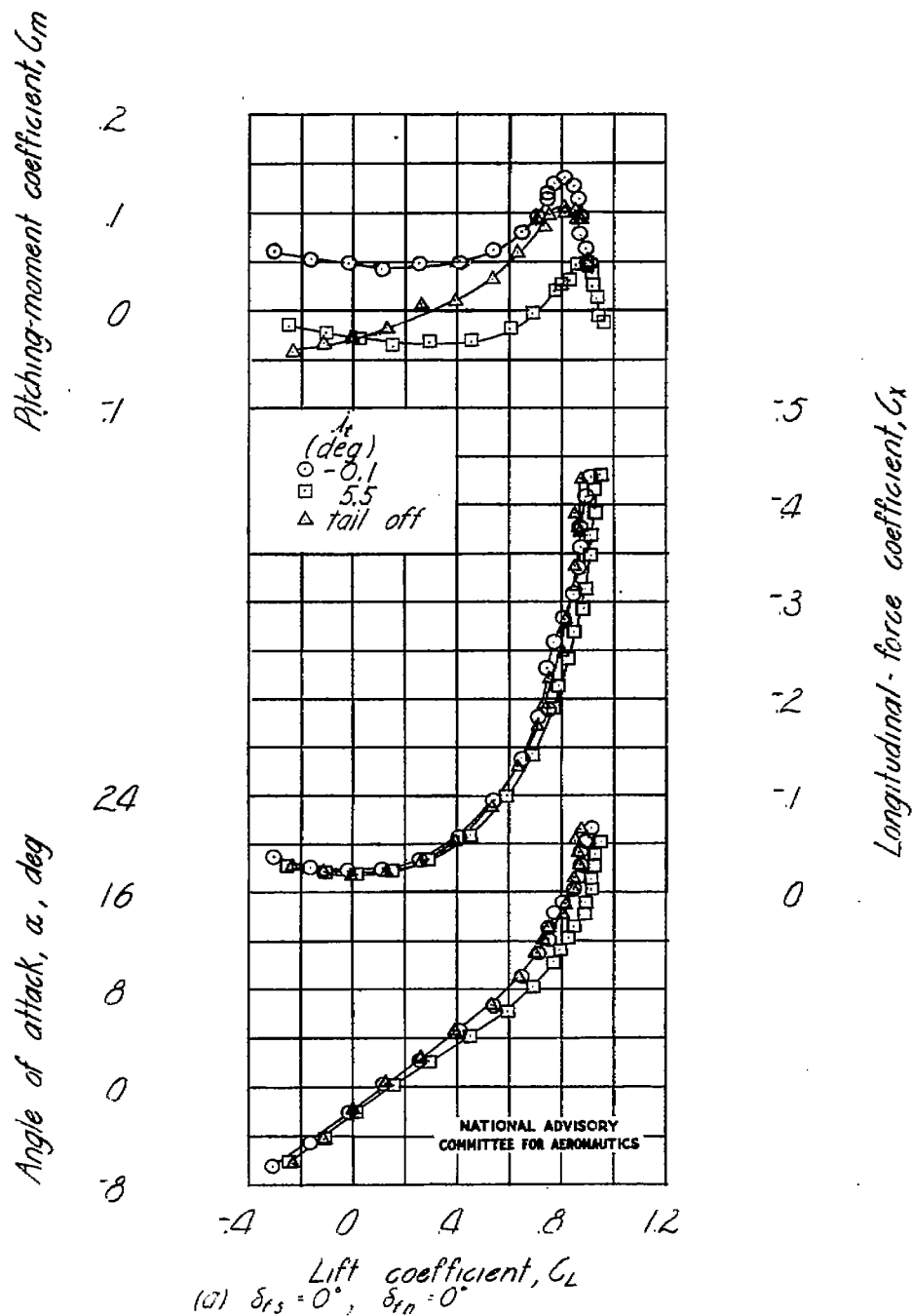


Figure 13.- Effect of stabilizer deflection on the aerodynamic characteristics in pitch of a model with a 42.8 - 4.00 - 0.50 wing; large fuselage; semihigh wing;  $\Gamma = 0^\circ$ .

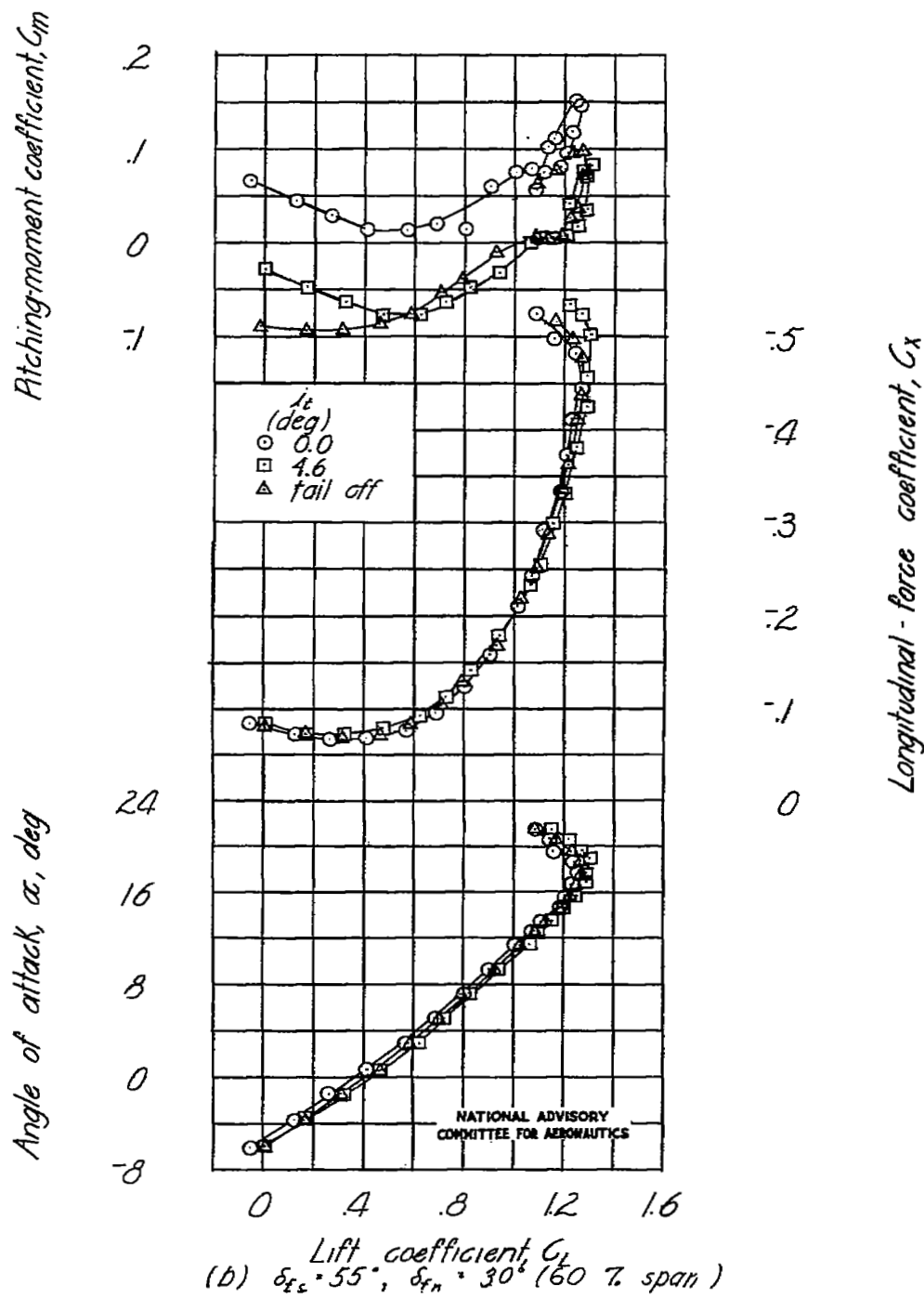


Figure 13.- Concluded.

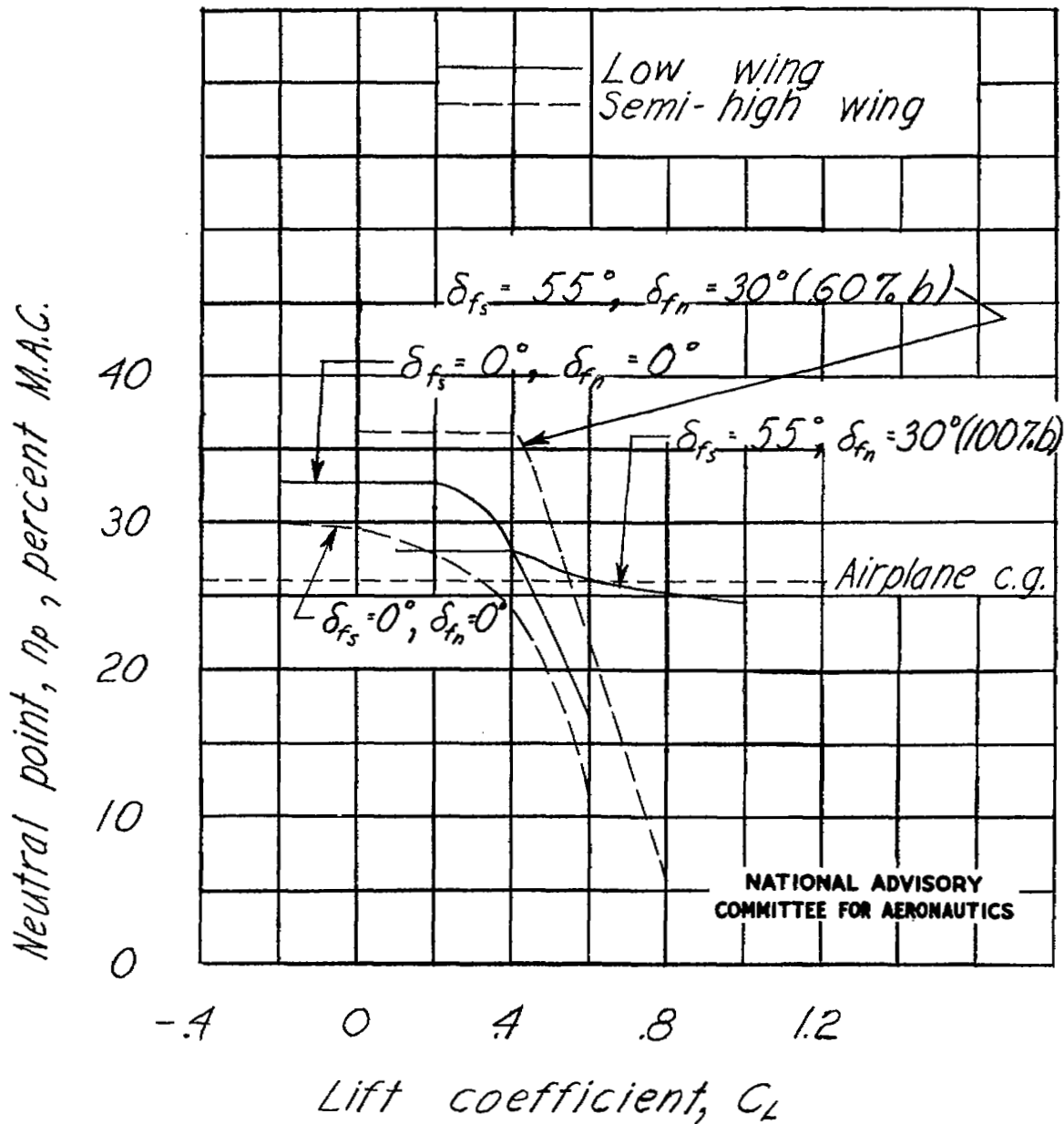
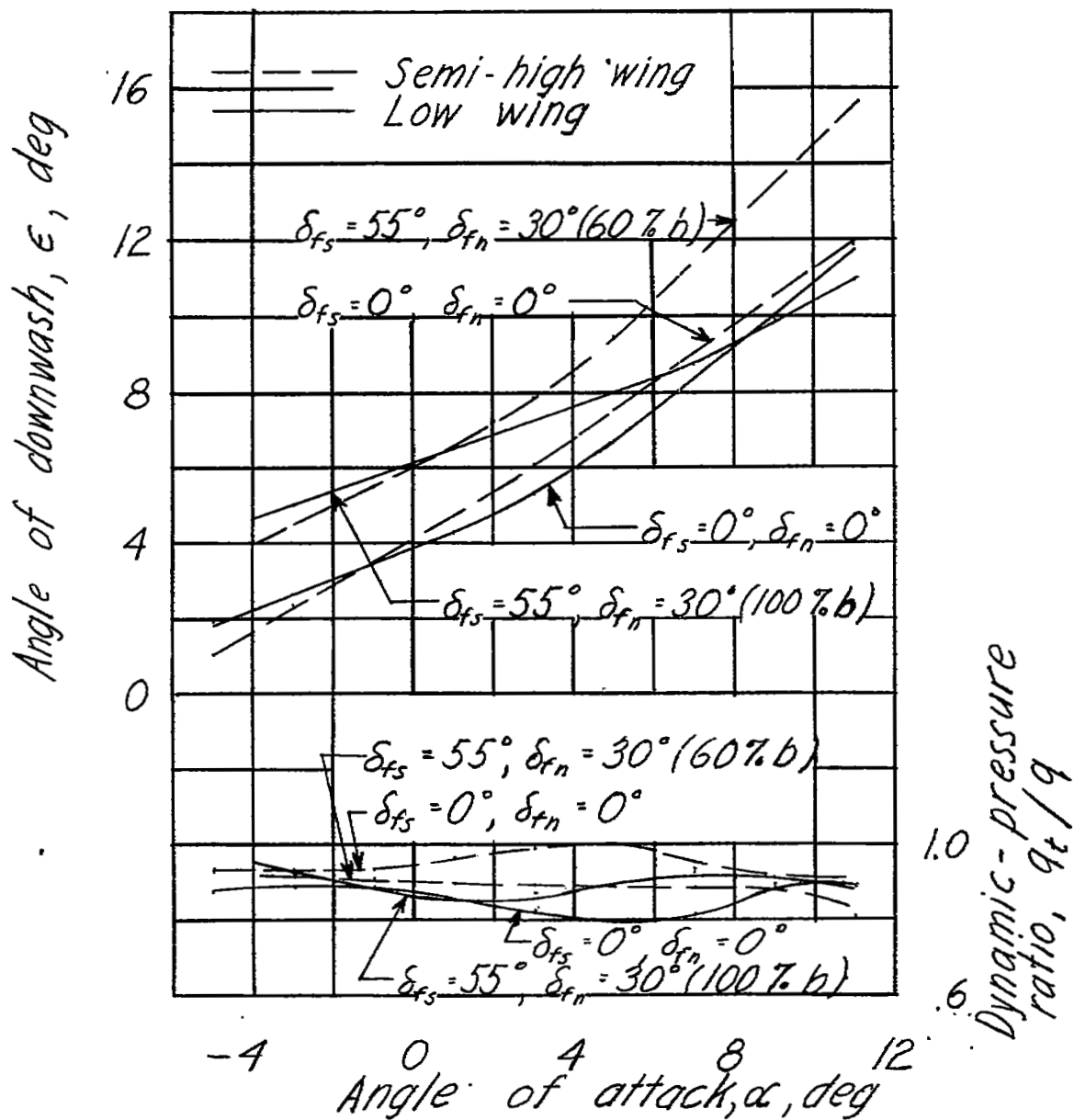


Figure 14.- The effect of wing position on the neutral points for a model with 42.8 - 4.00 - 0.50 wing; large fuselage.



NATIONAL ADVISORY  
COMMITTEE FOR AERONAUTICS

Figure 15.- The effect of wing position on the effective downwash angles and the dynamic-pressure ratios at the horizontal tail for a model with a 42.8 - 4.00 - 0.50 wing; large fuselage.

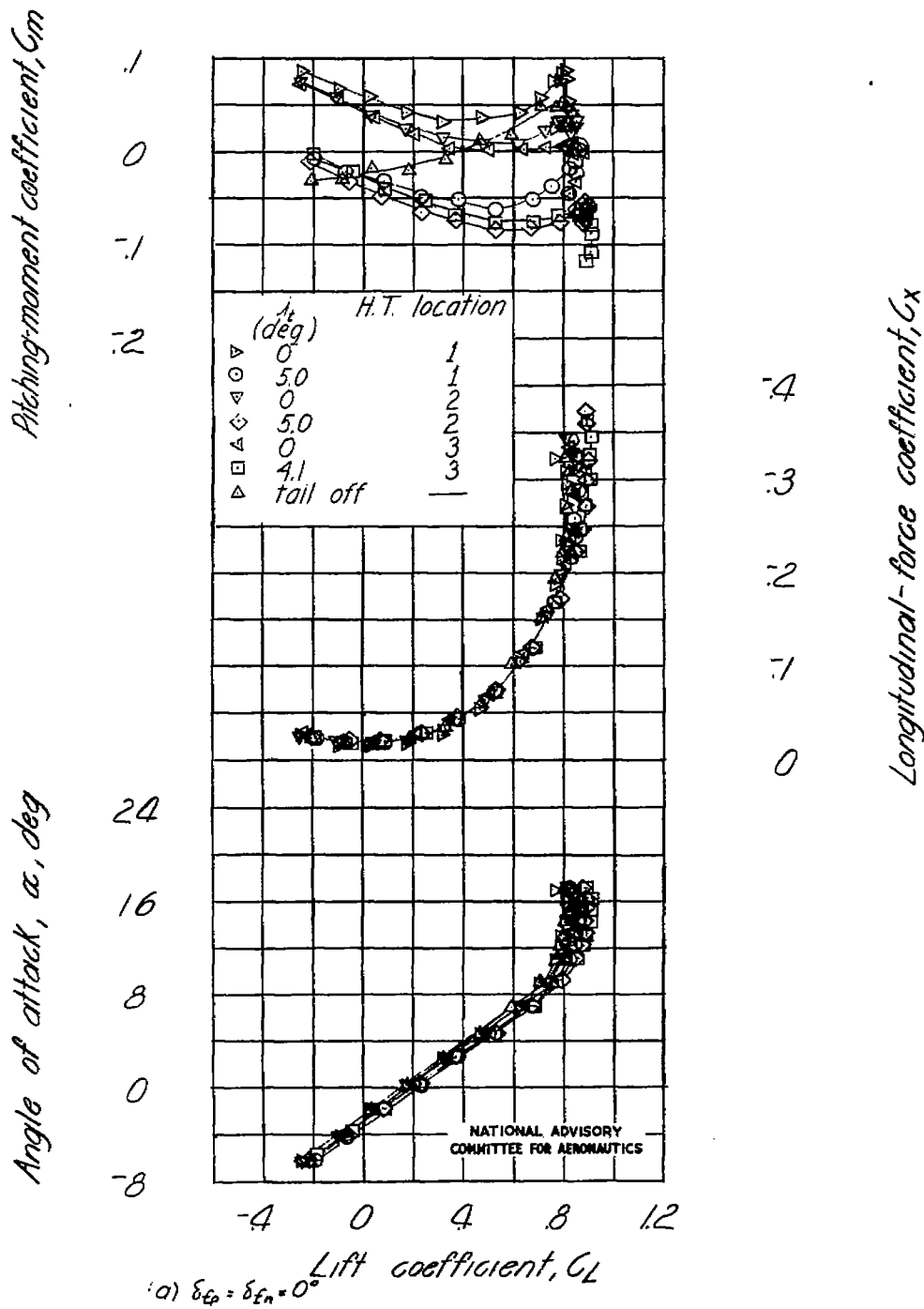
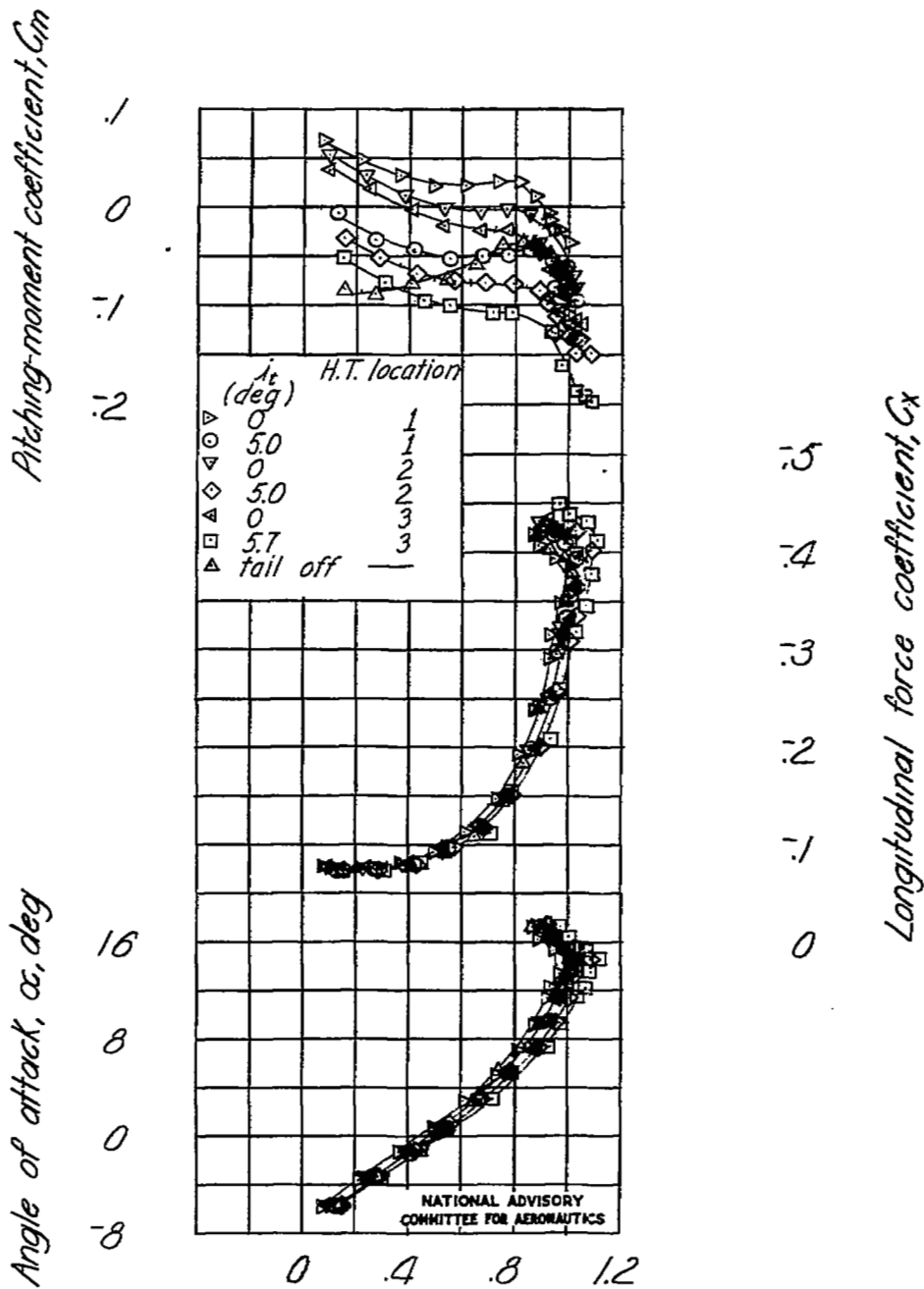


Figure 16.- Effect of stabilizer deflection and horizontal-tail location on the aerodynamic characteristics of a model with a 42.8 - 4.00 - 0.50 wing; small fuselage.



Lift coefficient,  $C_L$   
 (b)  $\delta_{fp} = 50^\circ$ ,  $\delta_{fn} = 15^\circ$  (40% span)

Figure 16.- Concluded.

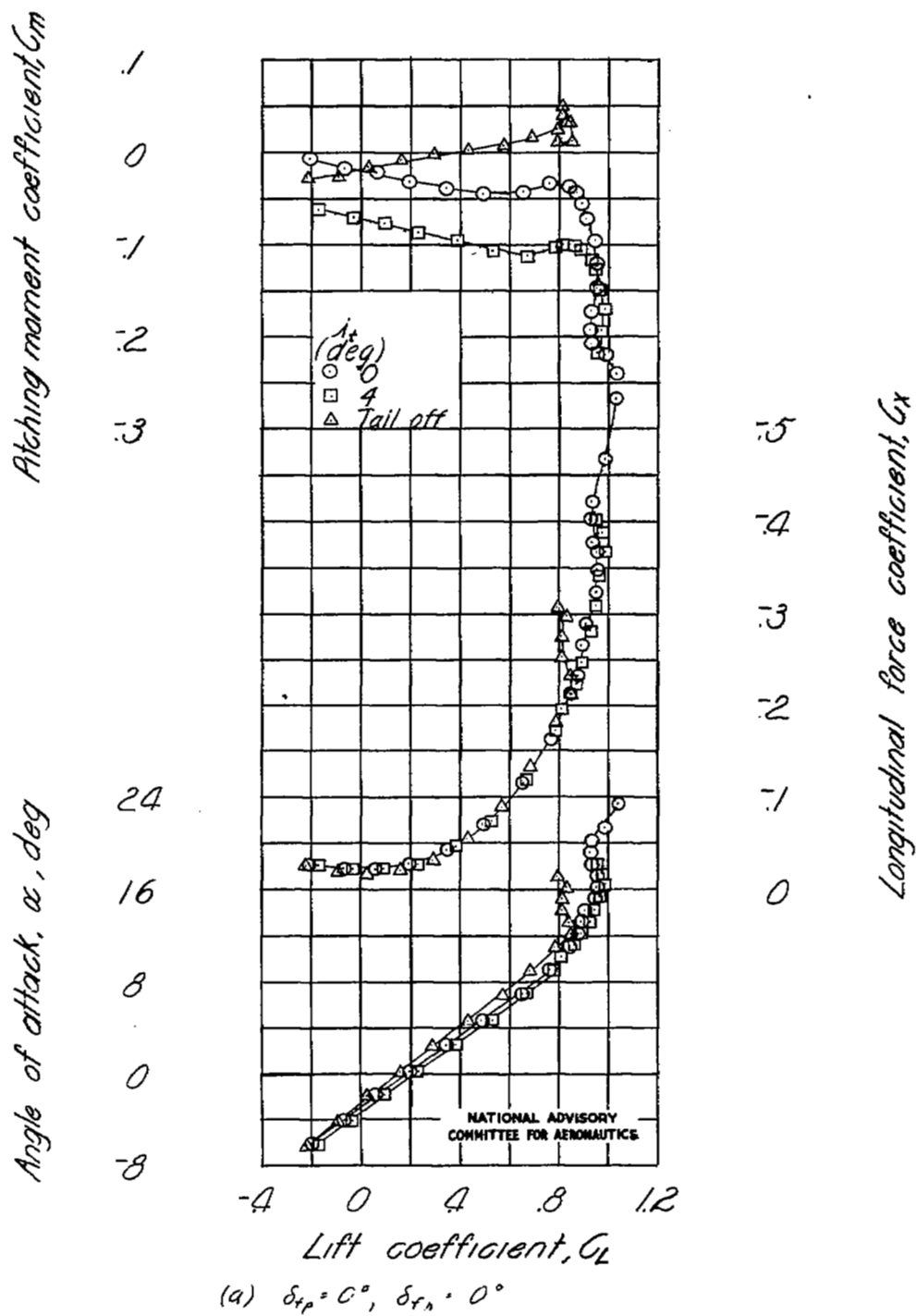
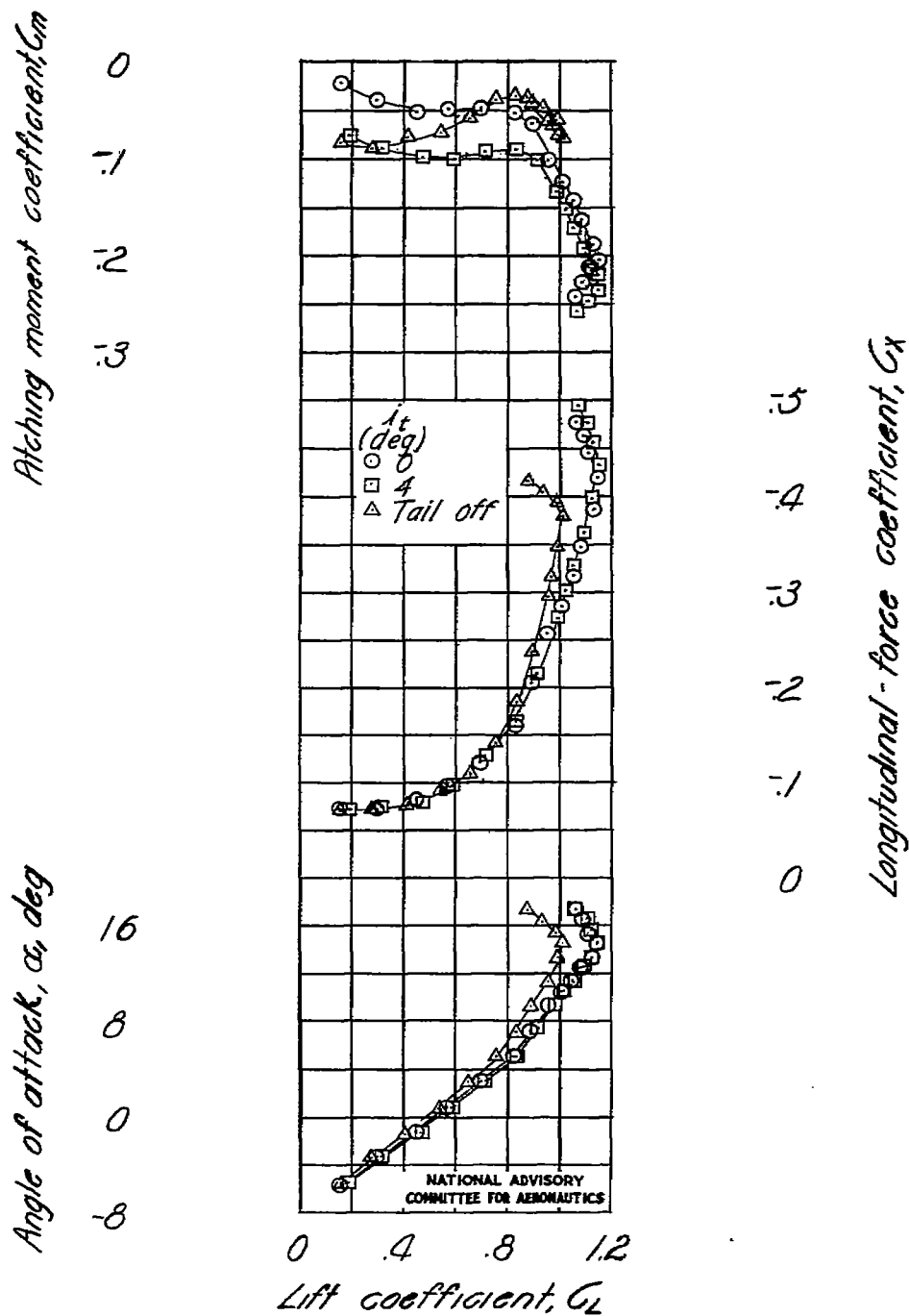


Figure 17.- Effect of stabilizer deflection at a low horizontal-tail location on the aerodynamic characteristics of a model with a 42.8 - 4.00 - 0.50 wing; small fuselage.



(b)  $\delta_{fp} = 50^\circ$ ,  $\delta_{fn} = 15^\circ$  (40% span)

Figure 17.- Concluded.

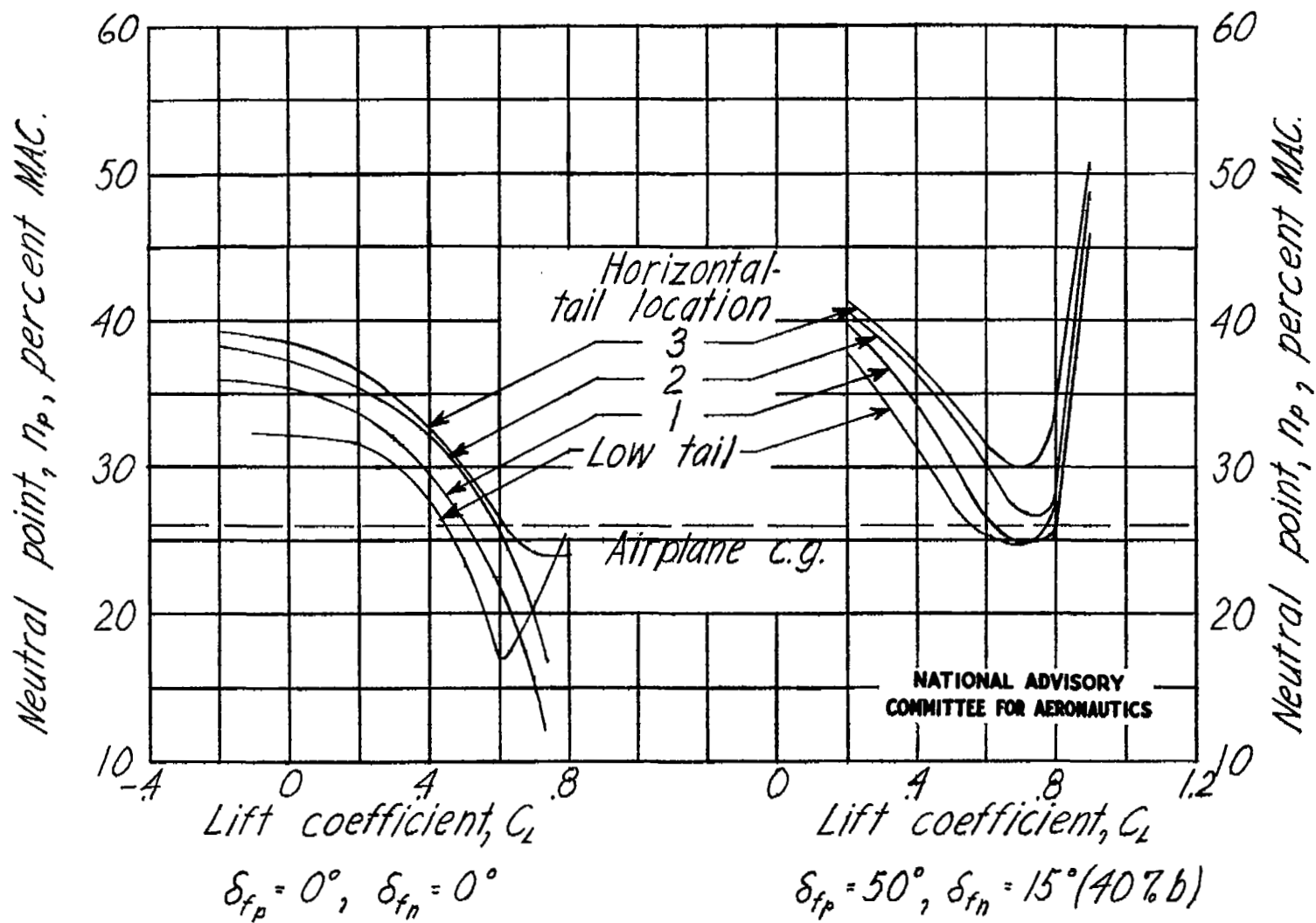
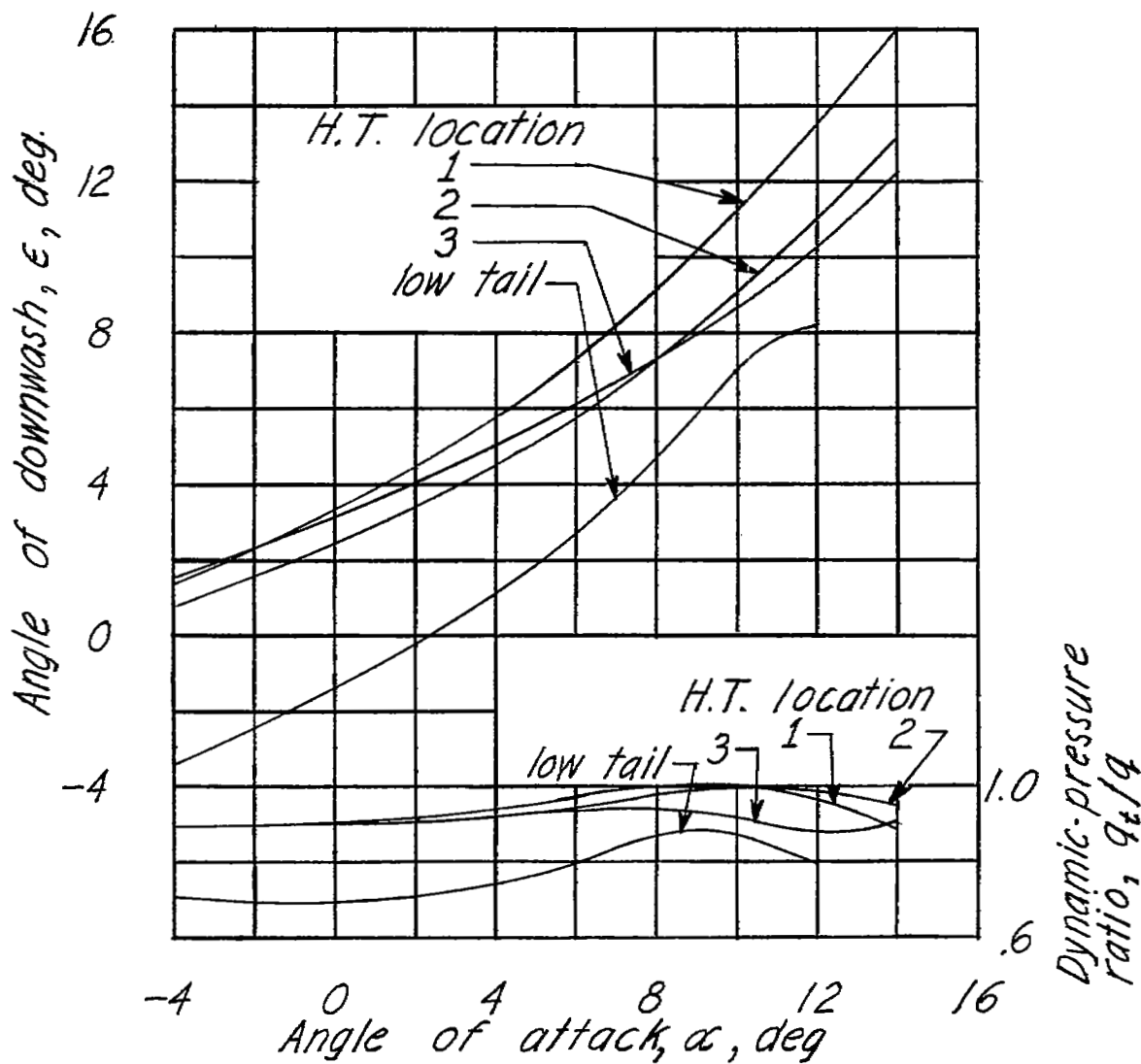


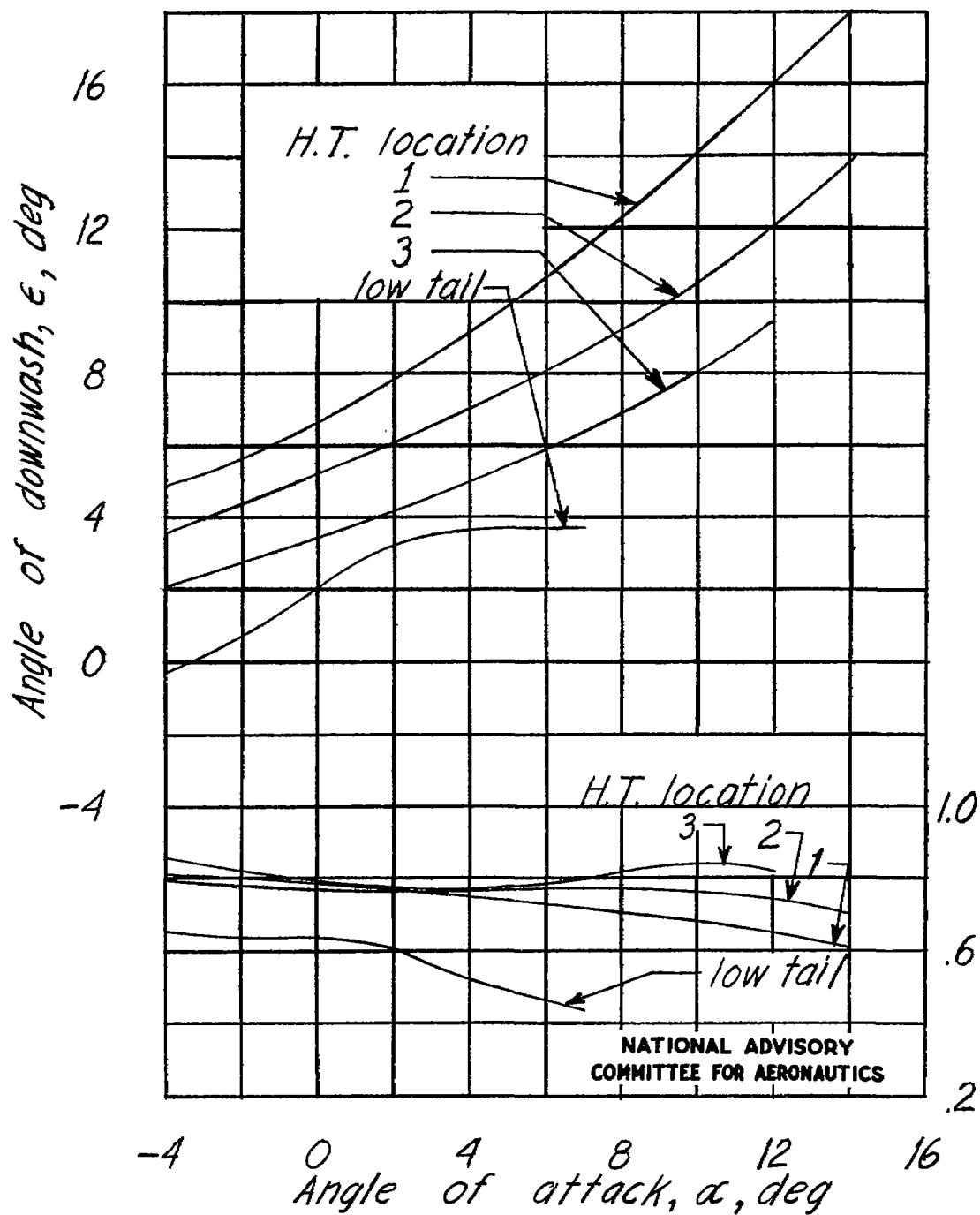
Figure 18.- Effect of horizontal-tail location on the neutral points for a model with a 42.8 - 4.00 - 0.50 wing; small fuselage.



(a)  $\delta_{fp} = 0^\circ$ ,  $\delta_{fn} = 0^\circ$

NATIONAL ADVISORY  
COMMITTEE FOR AERONAUTICS

Figure 19.- Effect of horizontal-tail location on the effective downwash angles and dynamic-pressure ratio at the horizontal tail for a model with a 42.8 - 4.00 - 0.50 wing; small fuselage.



(b)  $\delta_{fp} = 50^\circ$ ,  $\delta_{fn} = 15^\circ$  (40% span)

Figure 19.- Concluded.

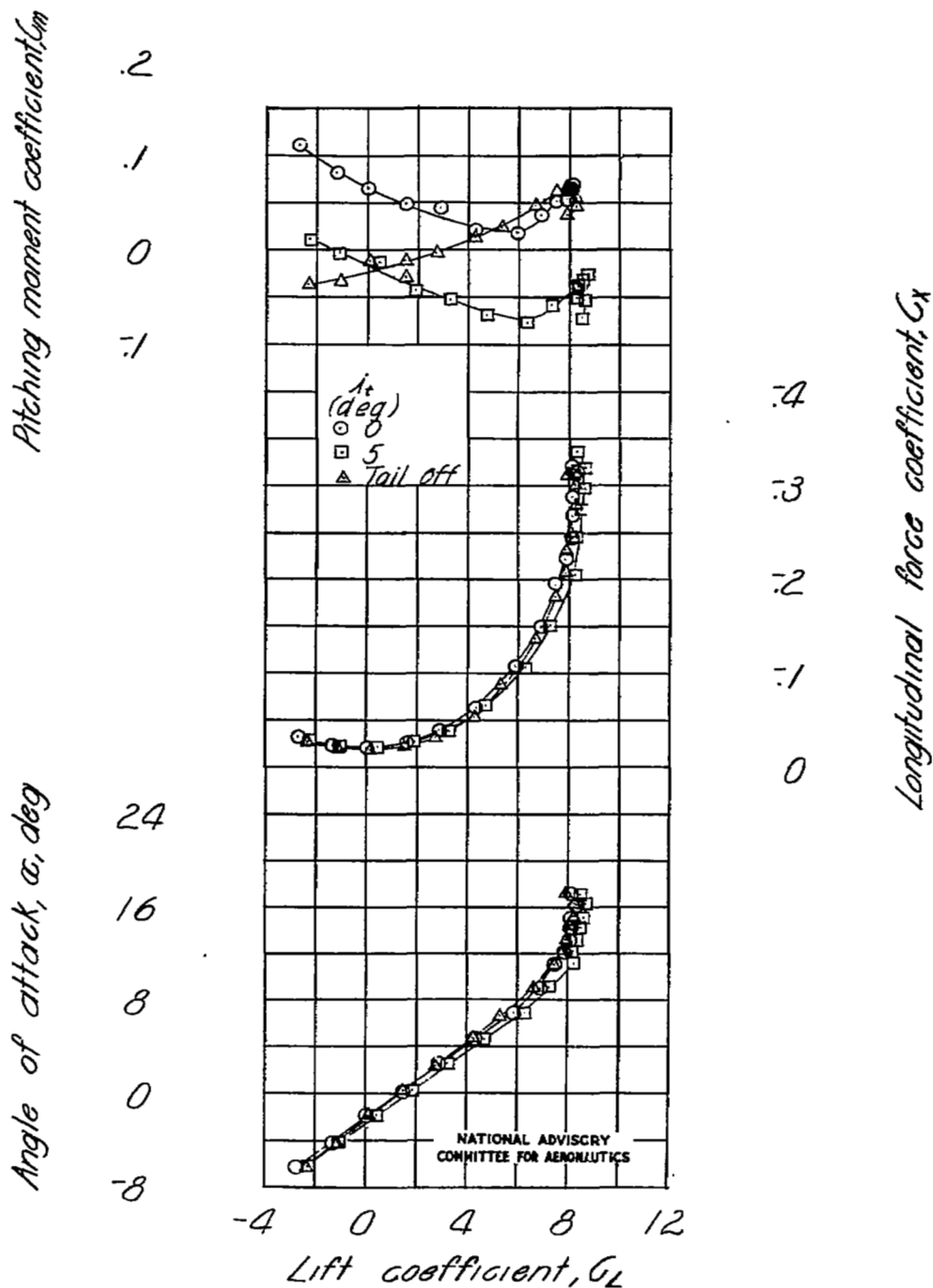


Figure 20.- Aerodynamic characteristics of a model with a 42.8 - 4.00 - 0.50 wing; extended small fuselage;  $\delta_{fp} = 0^\circ$ ;  $\delta_{fn} = 0^\circ$ .

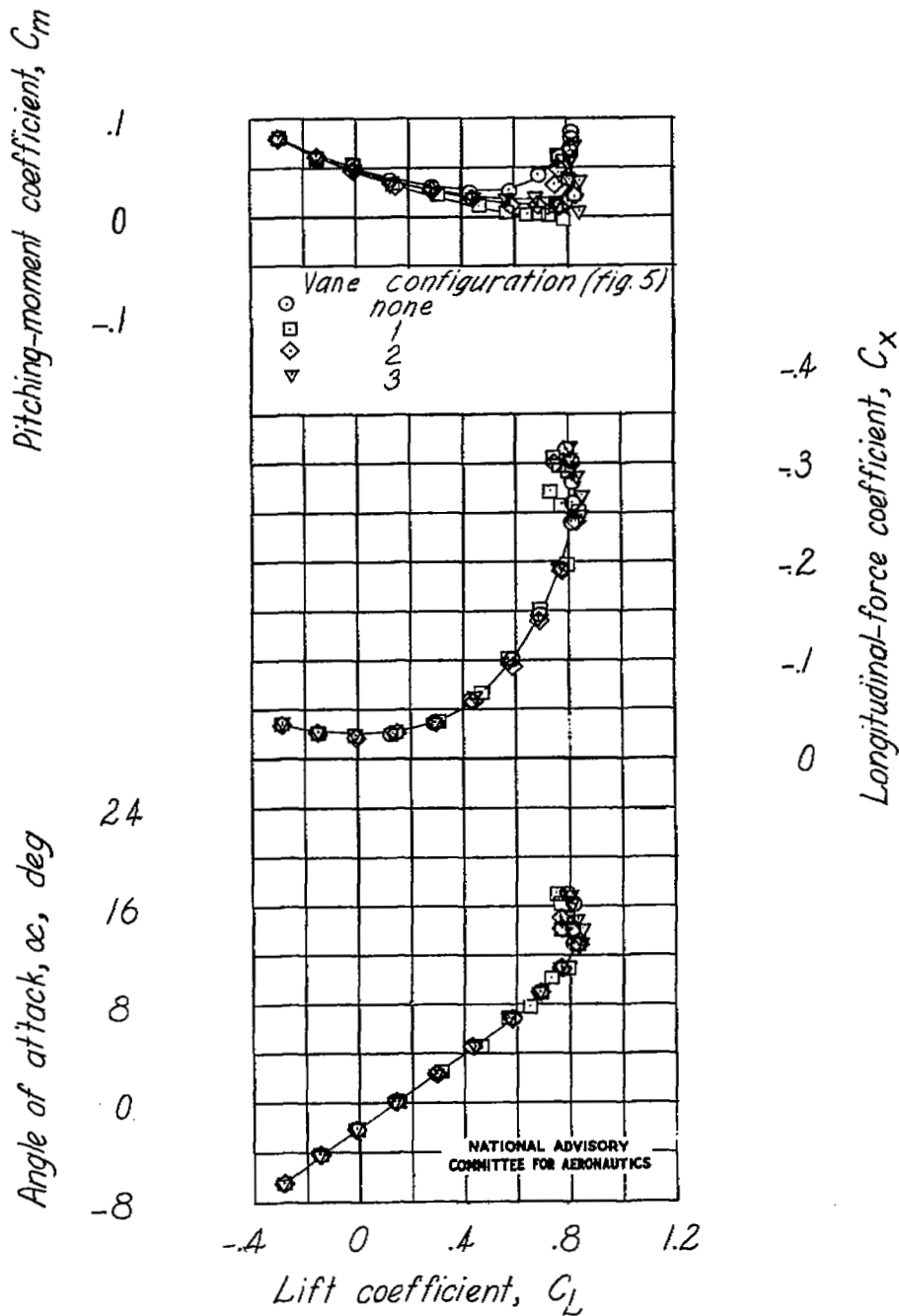


Figure 21.- Effect of spanwise location on stall-control vanes on the aerodynamic characteristics of a model with a 42.8 - 4.00 - 0.50 wing; small fuselage;  $\epsilon_{fp} = 0^\circ$ ;  $\epsilon_{fn} = 0^\circ$ ;  $i_t = 0^\circ$ .

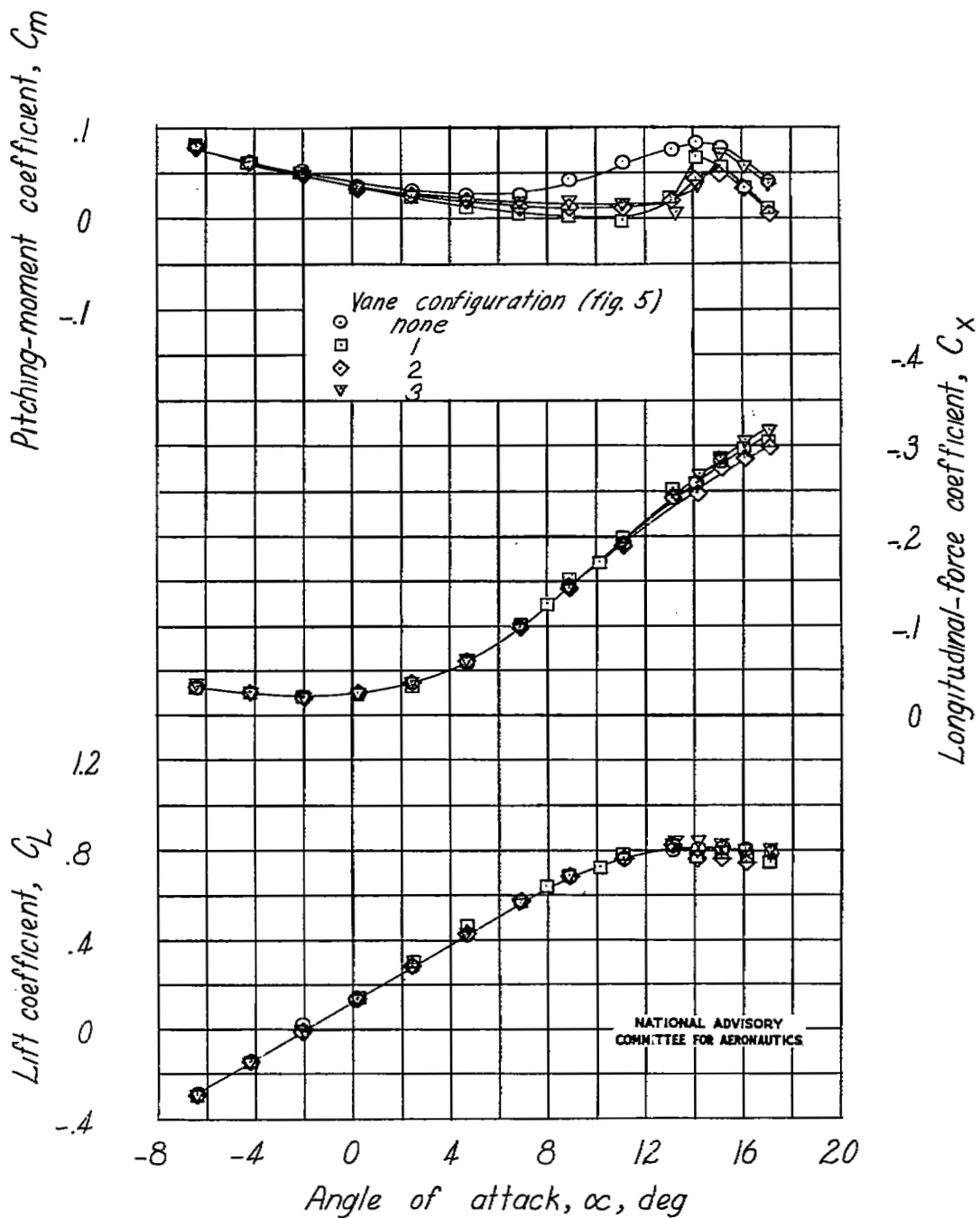


Figure 21.- Concluded.

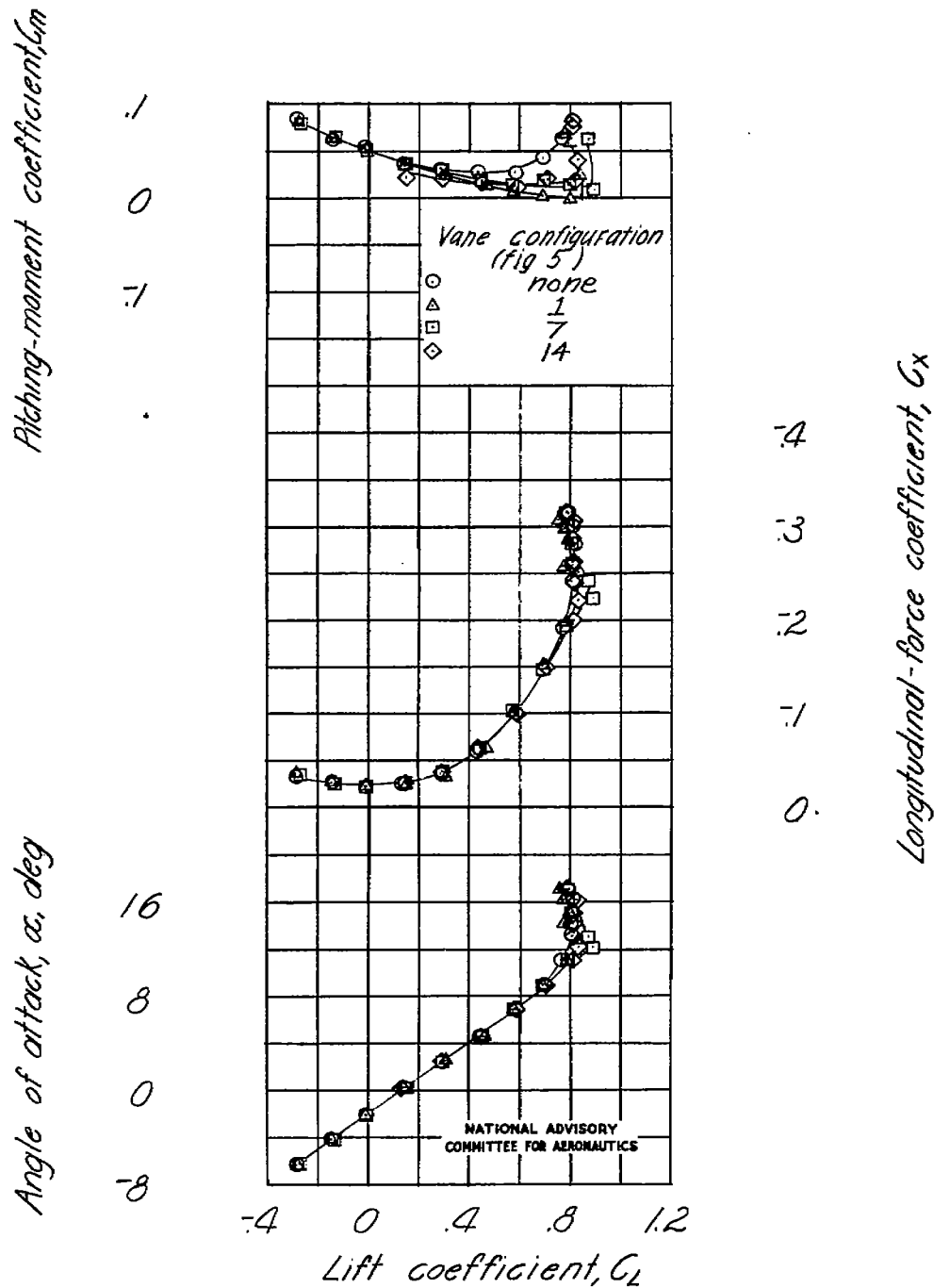


Figure 22.- Effect of chordwise geometry of stall-control vanes on the aerodynamic characteristics of a model with a 42.8 - 4.00 - 0.50 wing; small fuselage;  $\delta_{f_p} = 0^\circ$ ;  $\delta_{f_n} = 0^\circ$ ;  $i_t = 0^\circ$ .

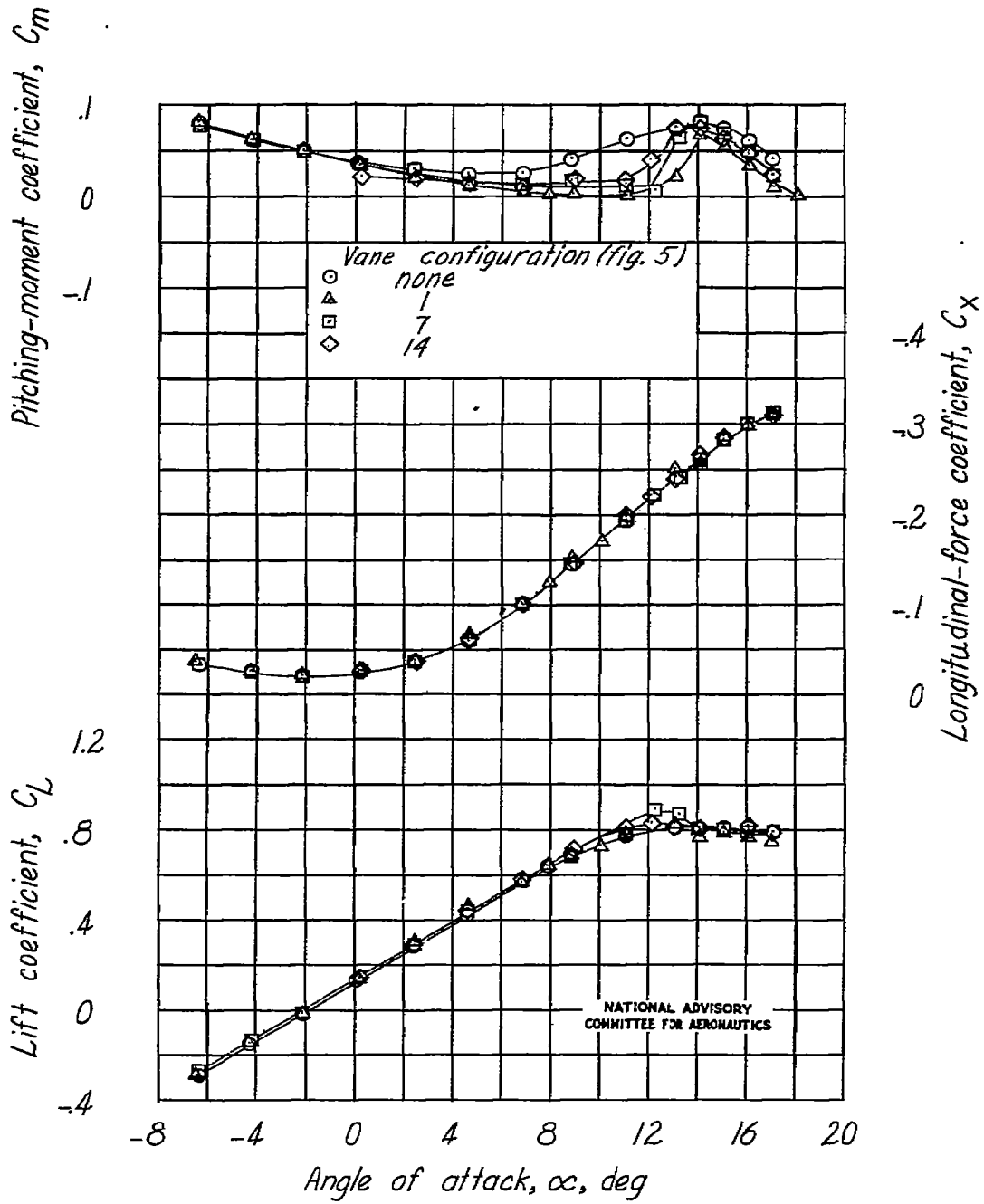


Figure 22.- Continued.

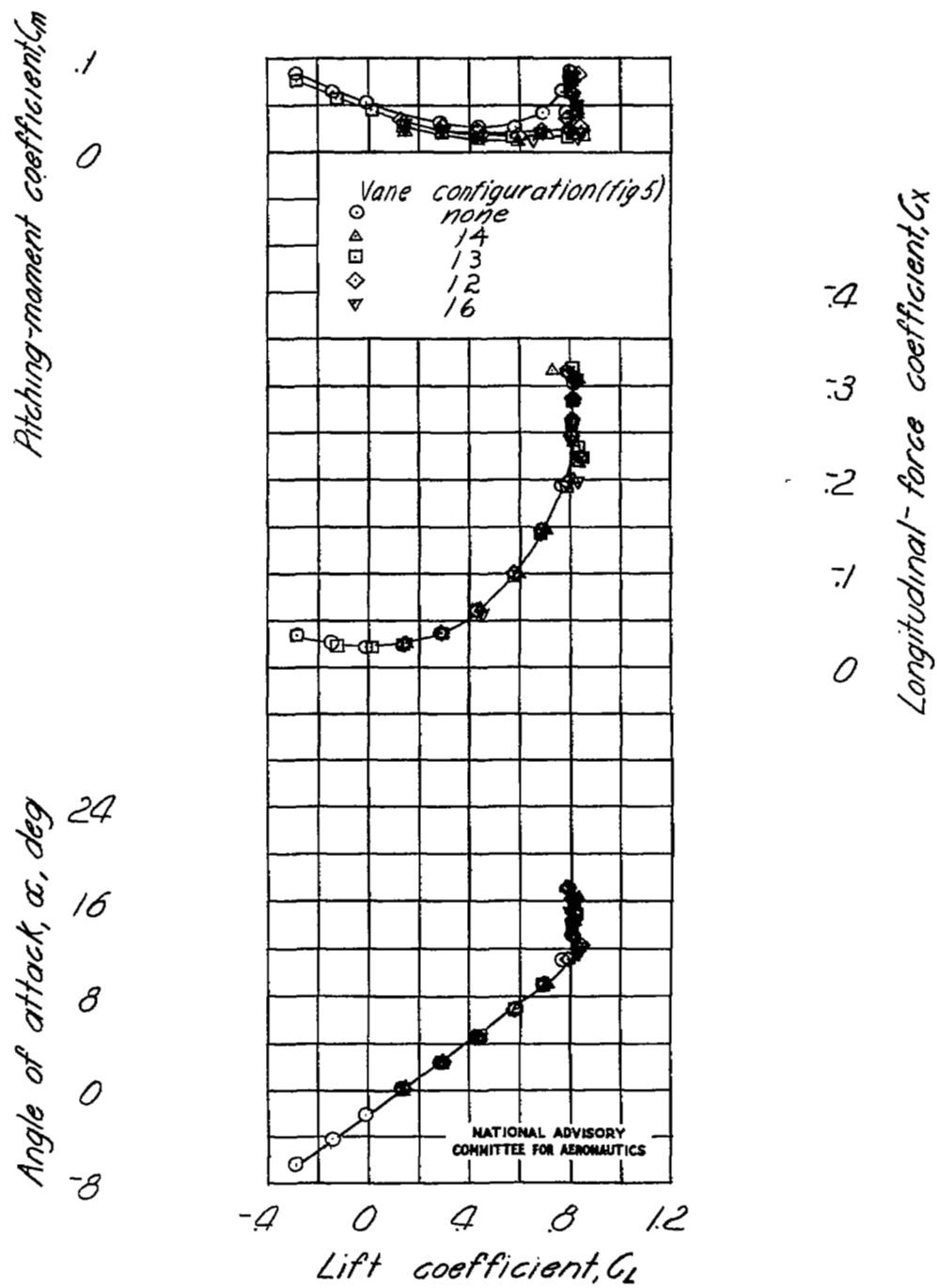


Figure 22.- Continued.

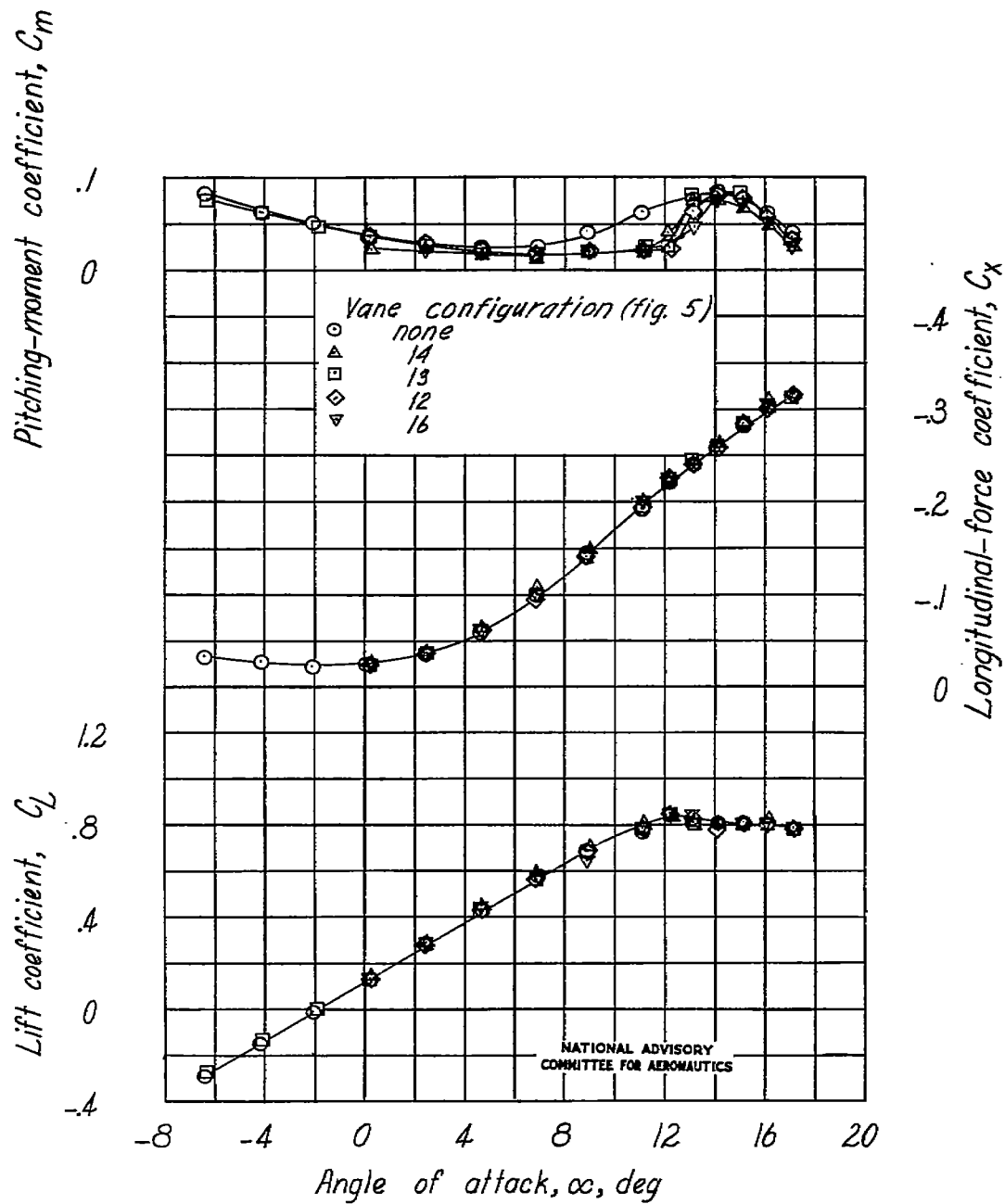


Figure 22.- Concluded.

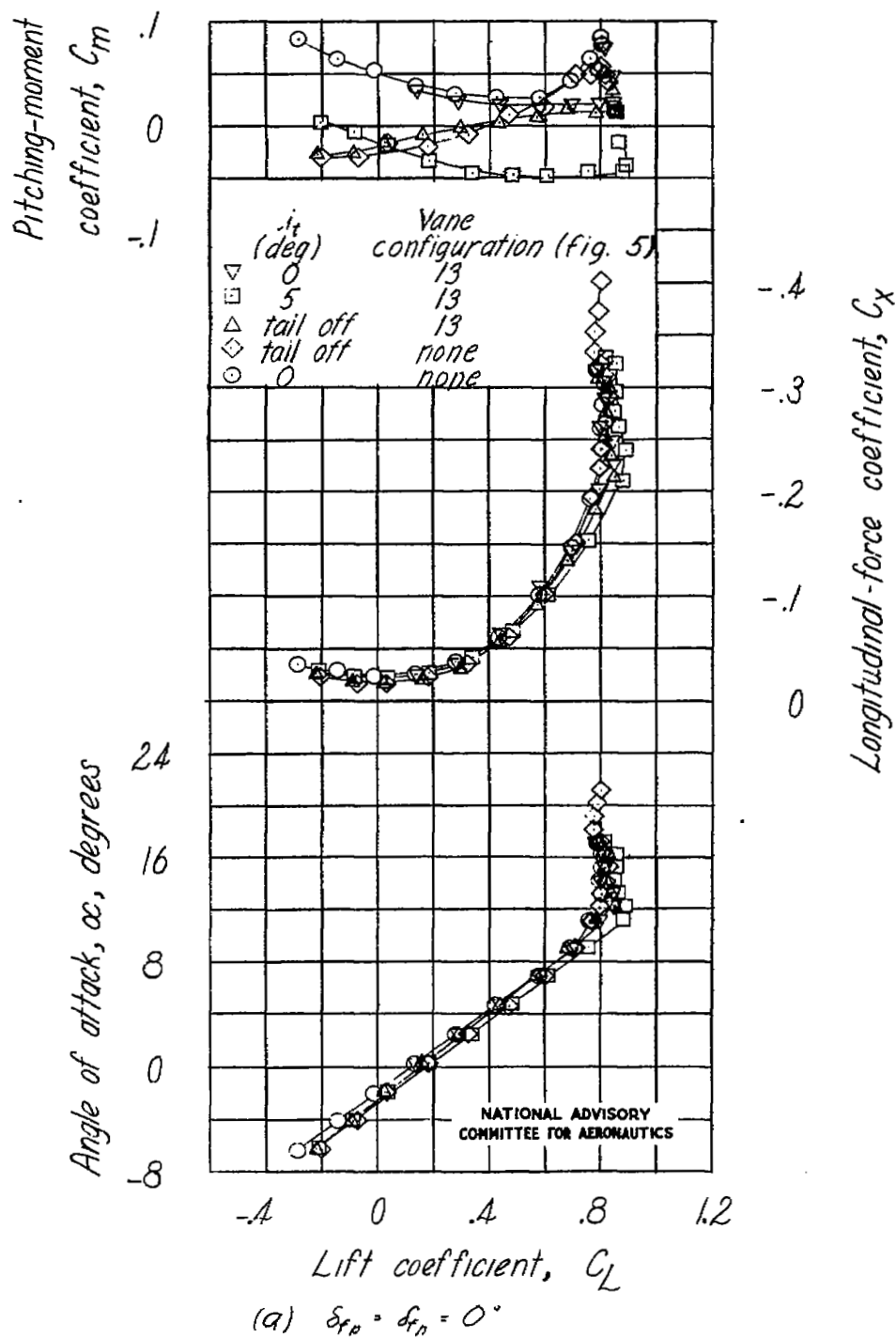
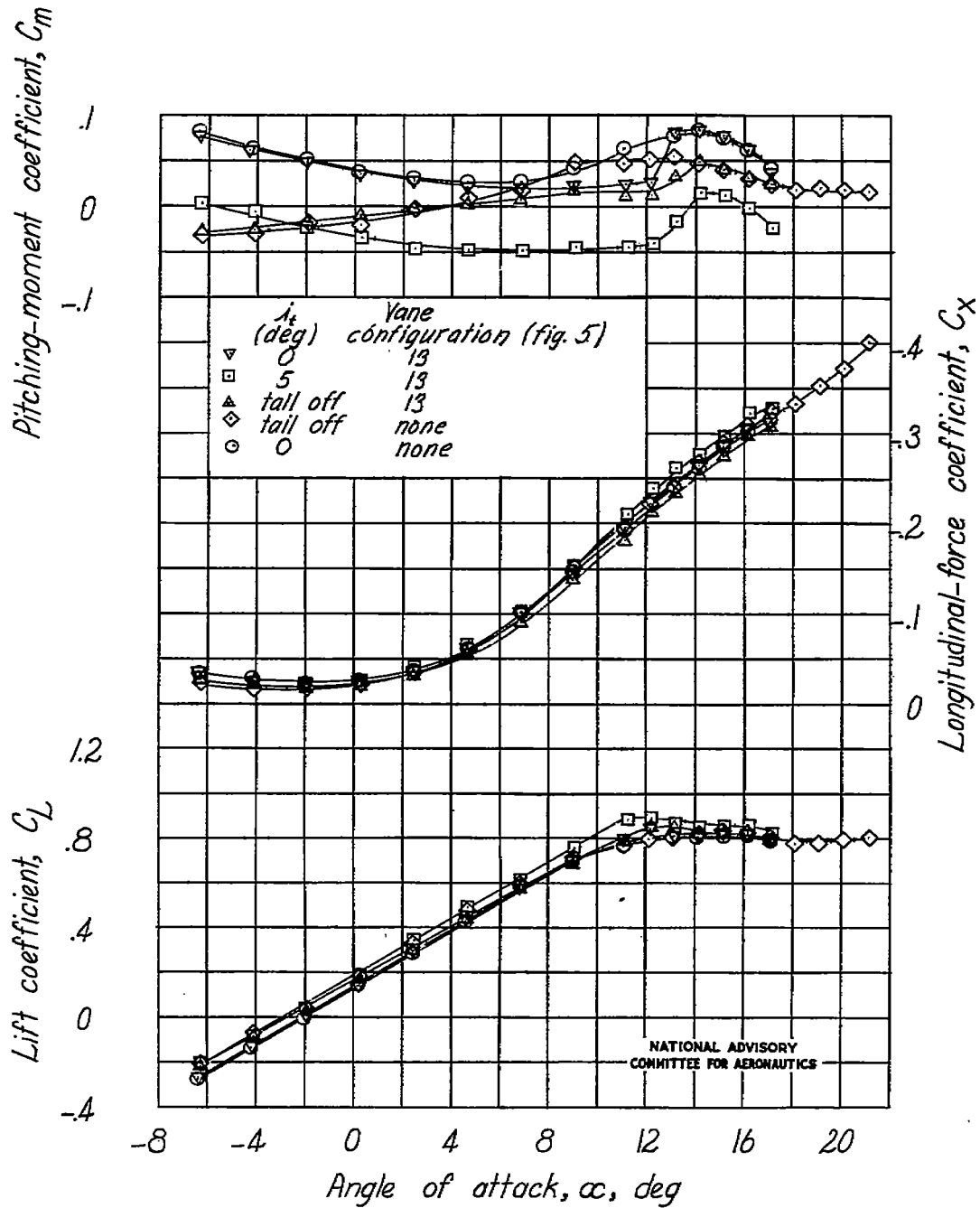
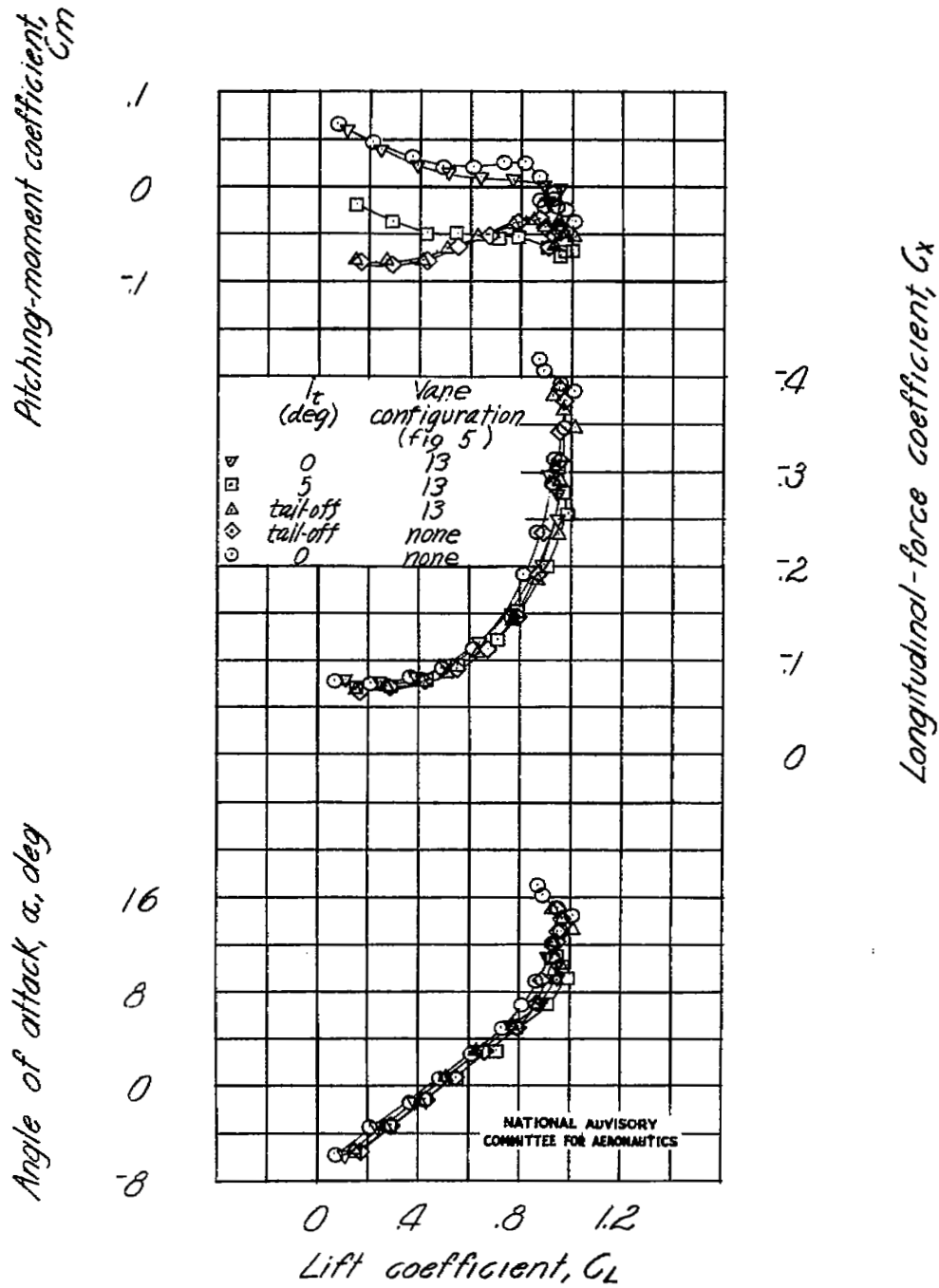


Figure 23.- Effect of stabilizer deflection and stall-control vane on the aerodynamic characteristics of a model with a 42.8 - 4.00 - 0.50 wing; small fuselage.



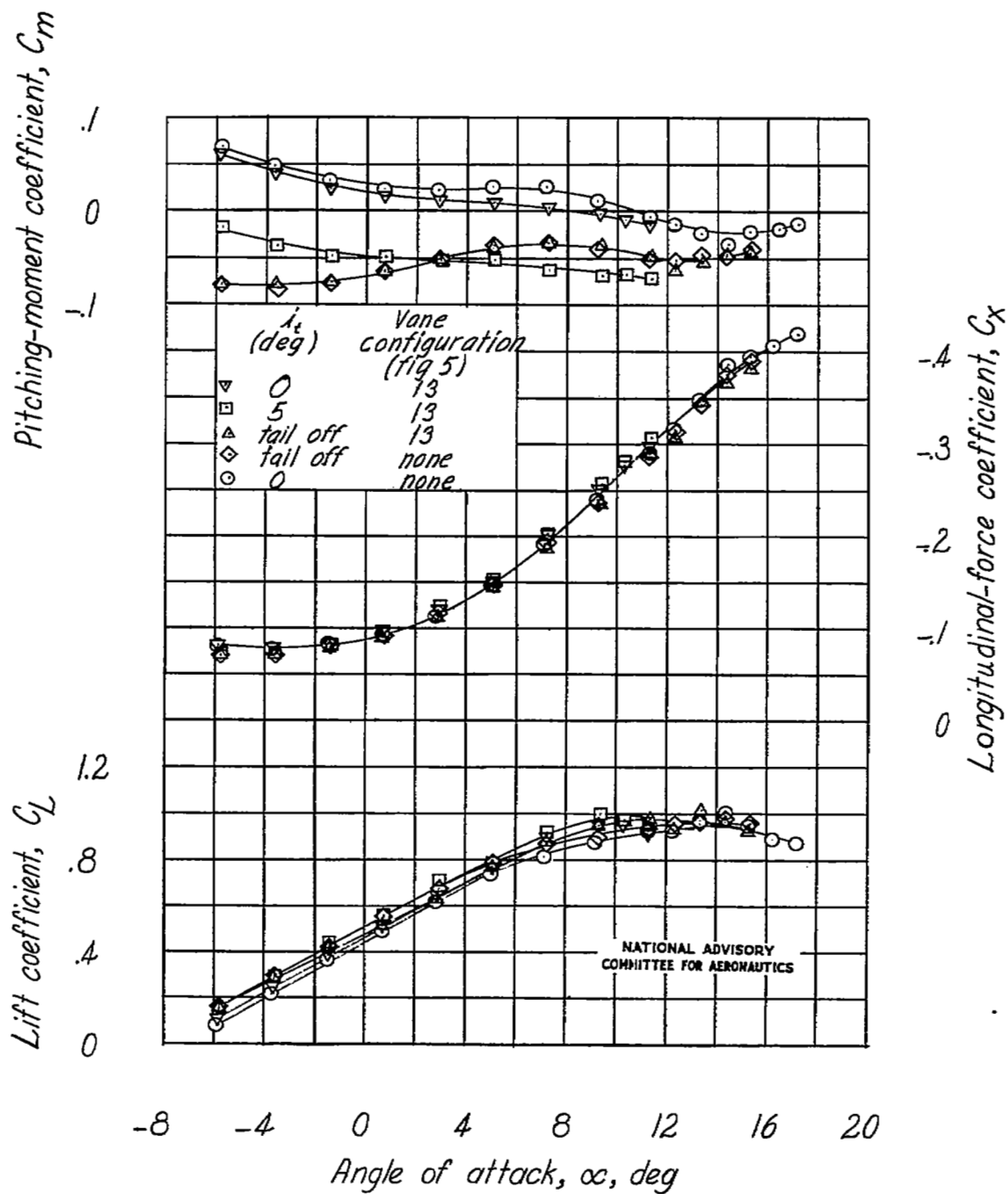
(a) Concluded

Figure 23.- Continued.



(b)  $\delta_{f_p} = 50^\circ$ ,  $\delta_{f_n} = 15^\circ$  (40% span).

Figure 23.- Continued.



(b) Concluded.

Figure 23.- Concluded.

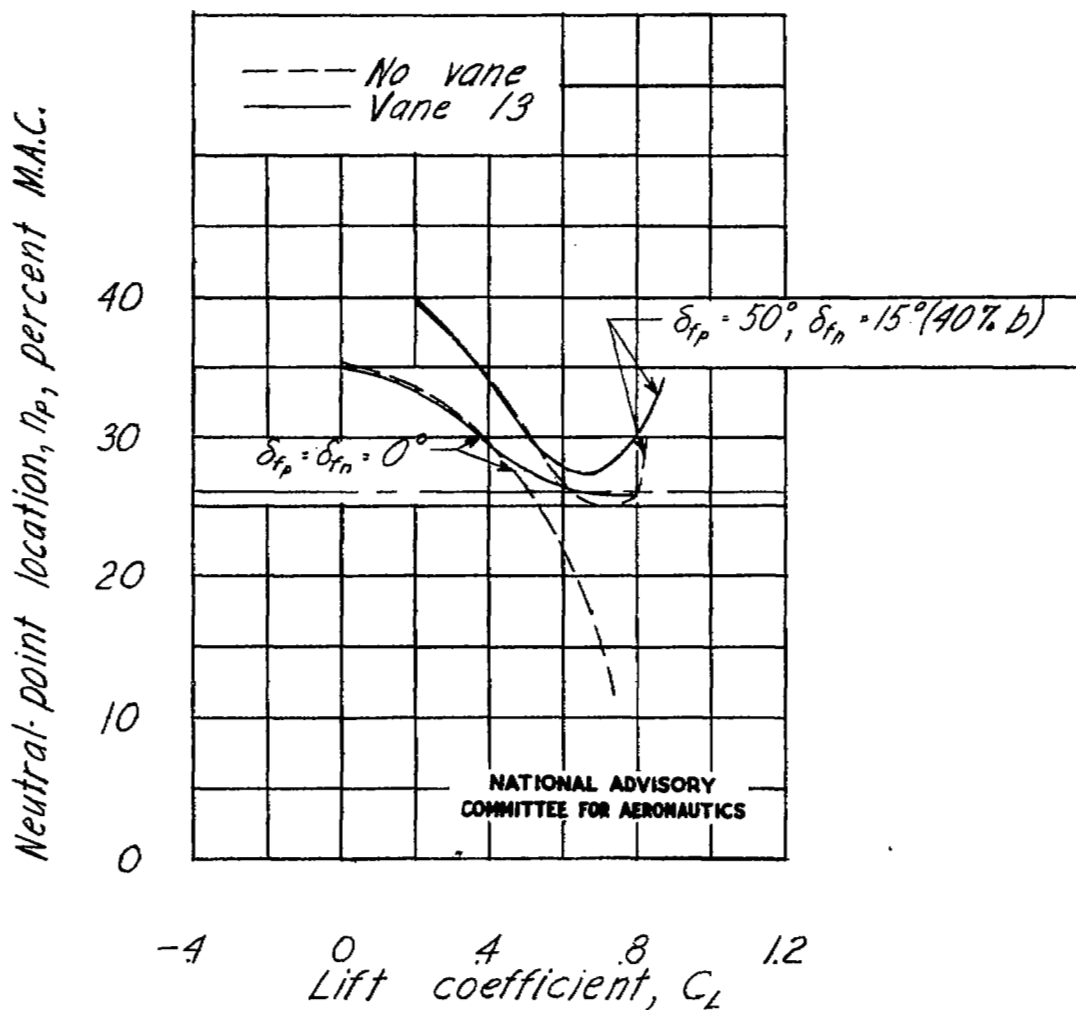


Figure 24.- Effect of stall-control vane 13 on the neutral-point location of a model with a 42.8 - 4.00 - 0.50 wing; small fuselage.

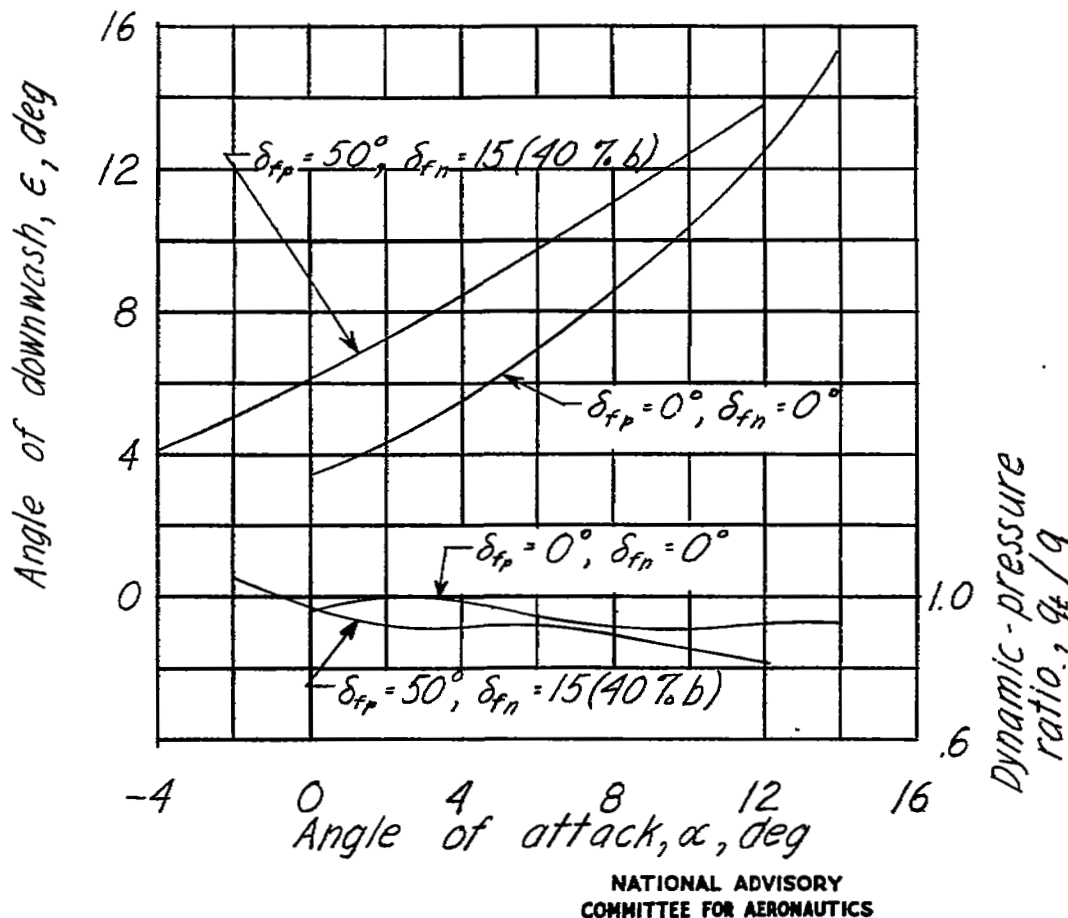


Figure 25.- Effective downwash angles and dynamic-pressure ratios at the horizontal tail with stall-control vane 13 on a model with a 42.8 - 4.00 - 0.50 wing; small fuselage.

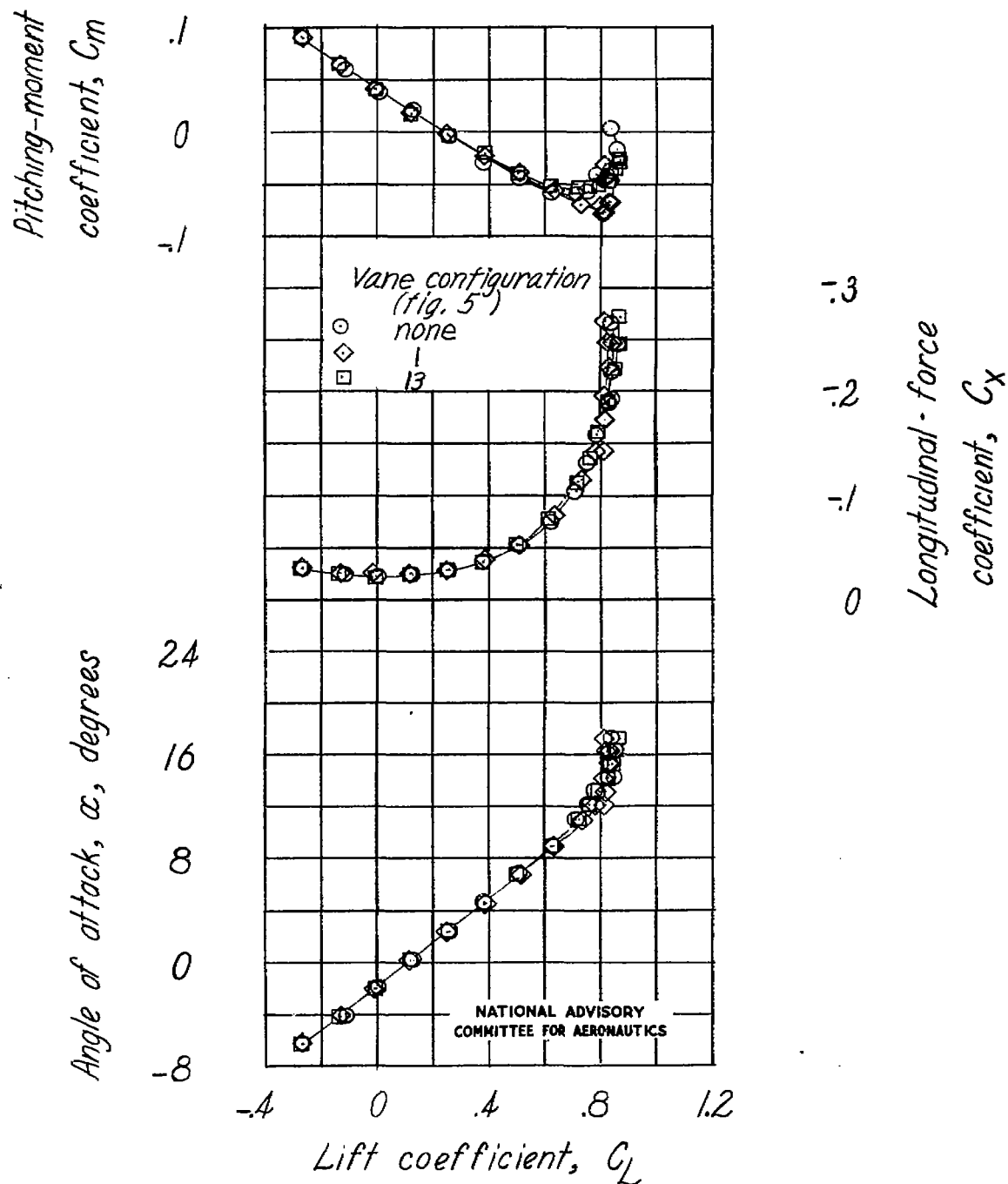


Figure 26.- Effect of stall-control vanes on the aerodynamic characteristics of a model with a 42.8 - 4.00 - 0.50 wing with a full-span round leading edge; small fuselage;  $\delta_{f_p} = 0^\circ$ ;  $\delta_{f_n} = 0^\circ$ ;  $i_t = 0^\circ$ .

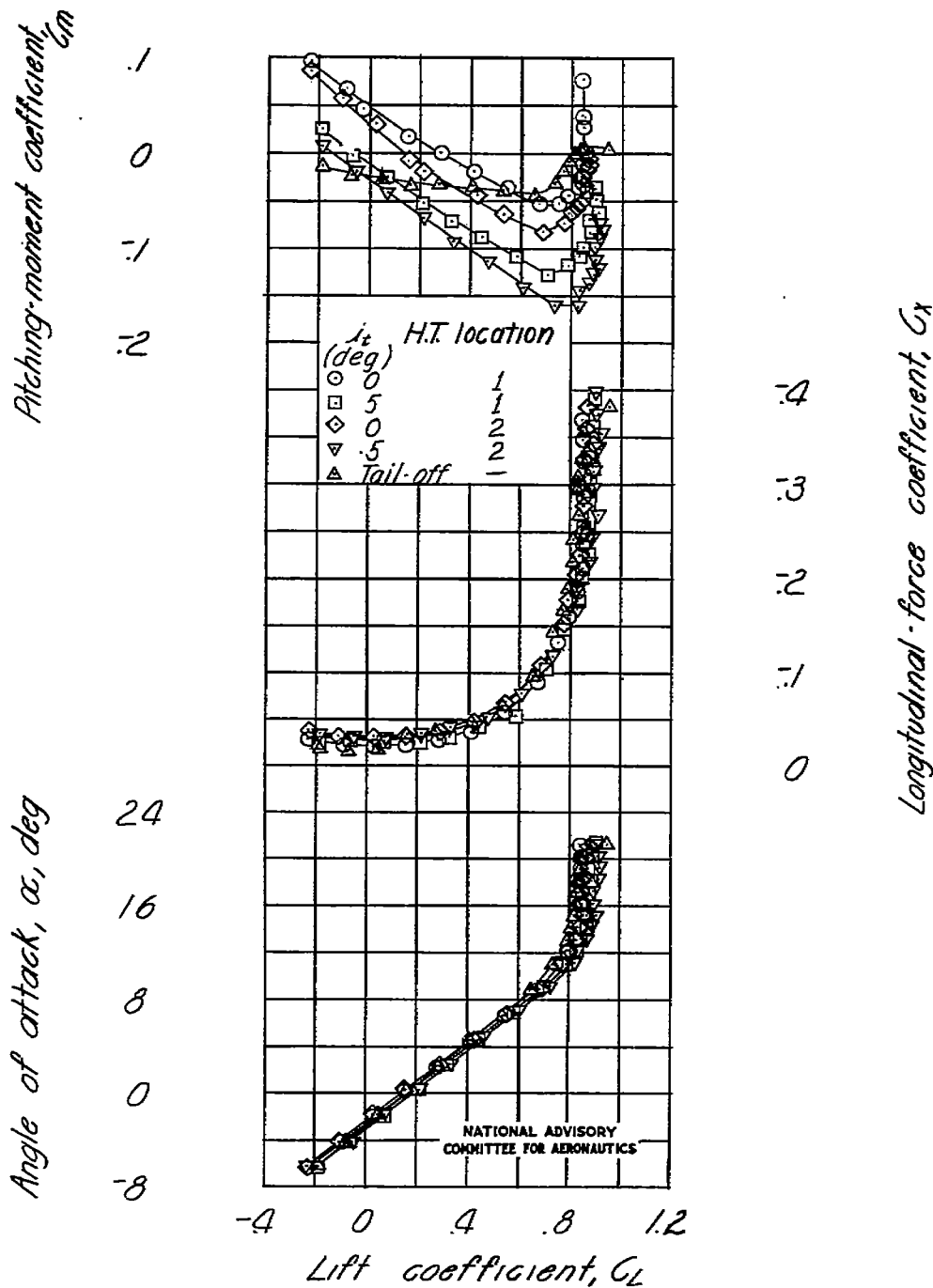


Figure 27.- Effect of stabilizer deflection and horizontal-tail location with a 100-percent-span round leading edge on the aerodynamic characteristics of a model with a 42.8 - 4.00 - 0.50 wing; small fuselage;  $\delta_{fp} = 0^\circ$ ;  $\delta_{fn} = 0^\circ$ .

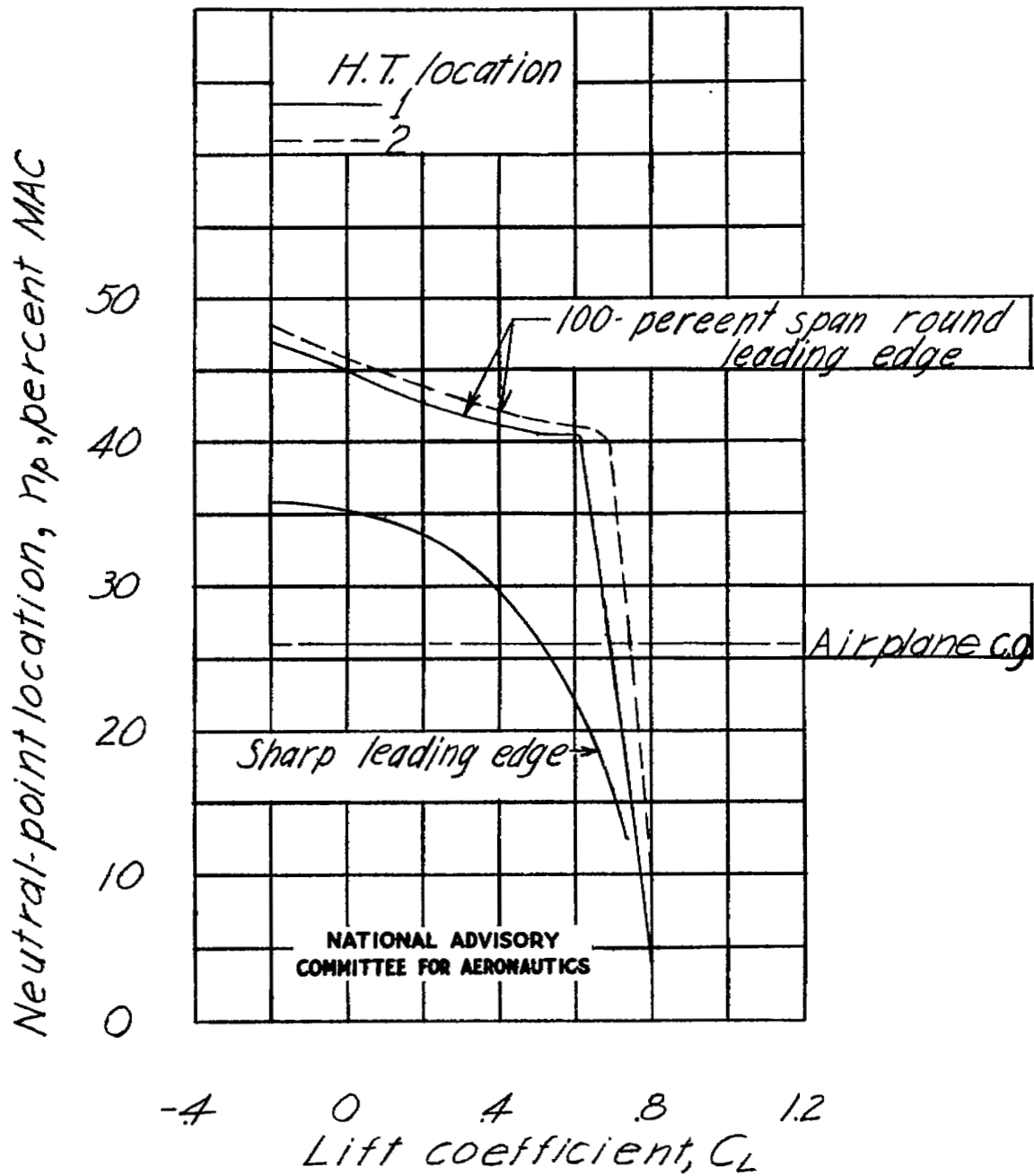


Figure 28.- Effect of 100-percent-span round leading edge on neutral points for a model with a 42.8 - 4.00 - 0.50 wing;  $\delta_{f_s} = 0^\circ$ ;

$$\delta_{f_n} = 0^\circ.$$

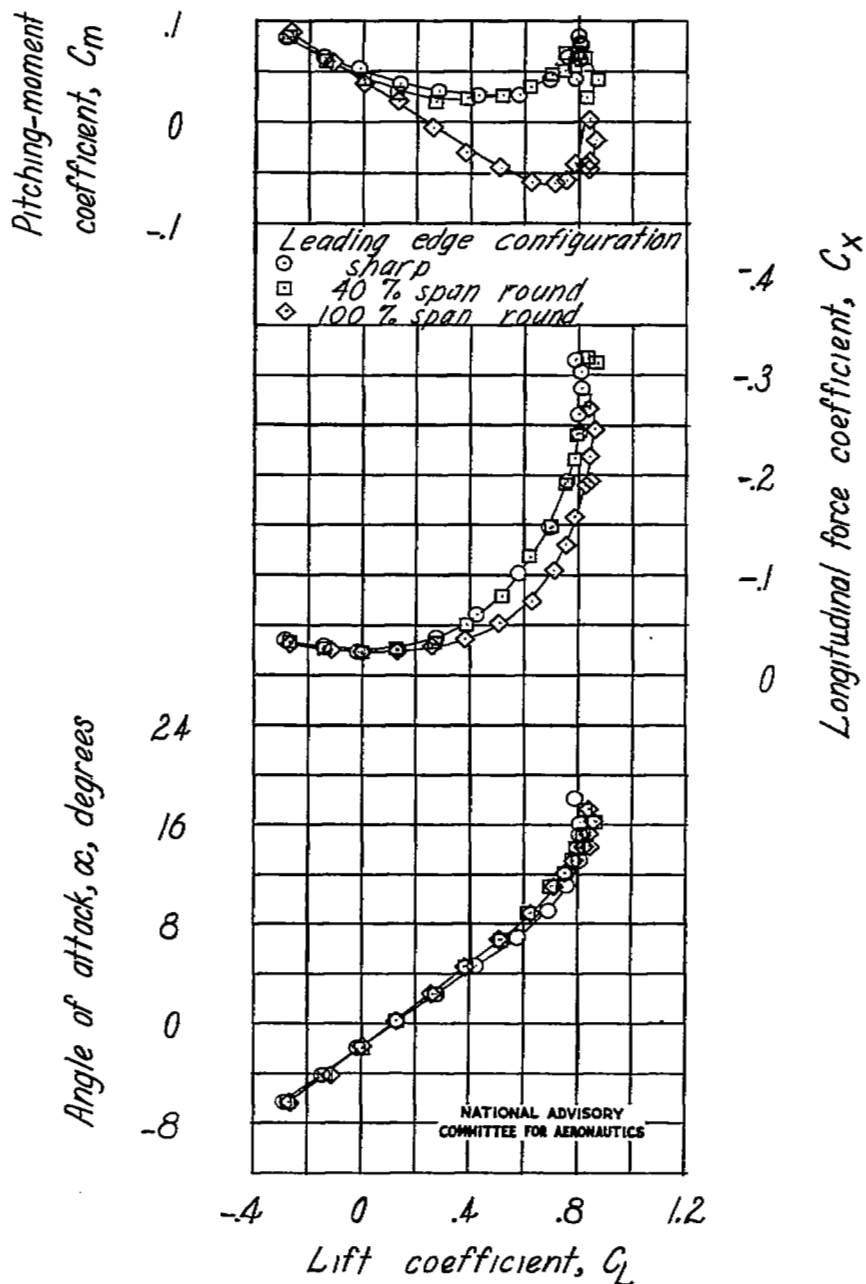


Figure 29.- Effect of various leading-edge configurations on the aerodynamic characteristics of a model with a 42.8 - 4.00 - 0.50 wing; small fuselage;  $\delta_{fp} = 0^\circ$ ;  $\delta_{fn} = 0^\circ$ ;  $i_t = 0^\circ$ .

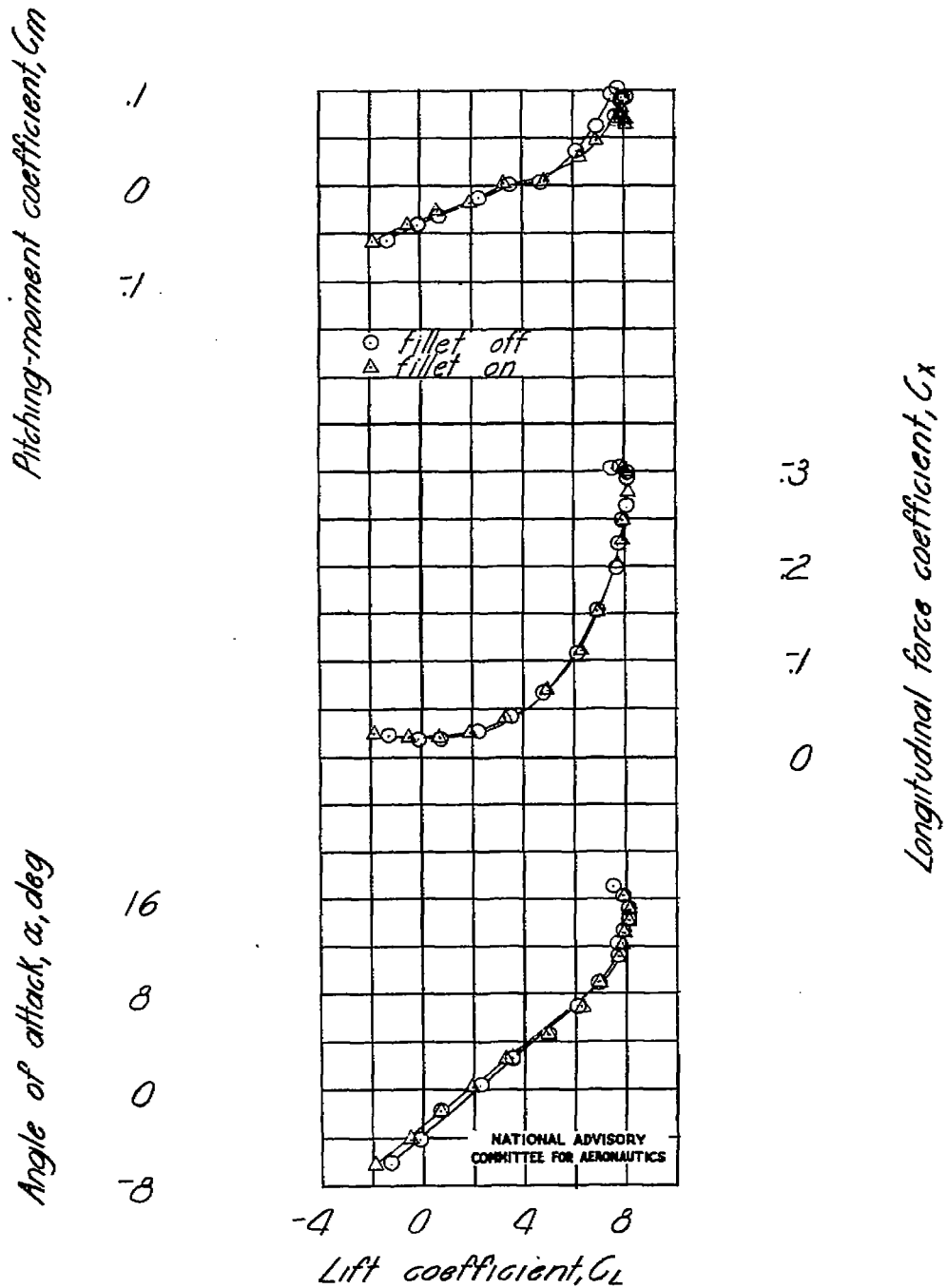


Figure 30.- Effect of wing fillet on the aerodynamic characteristics of a model with a 42.8 - 4.00 - 0.50 wing; large fuselage;  $\delta_{f_s} = 0^\circ$ ;  $\delta_{f_n} = 0^\circ$ .

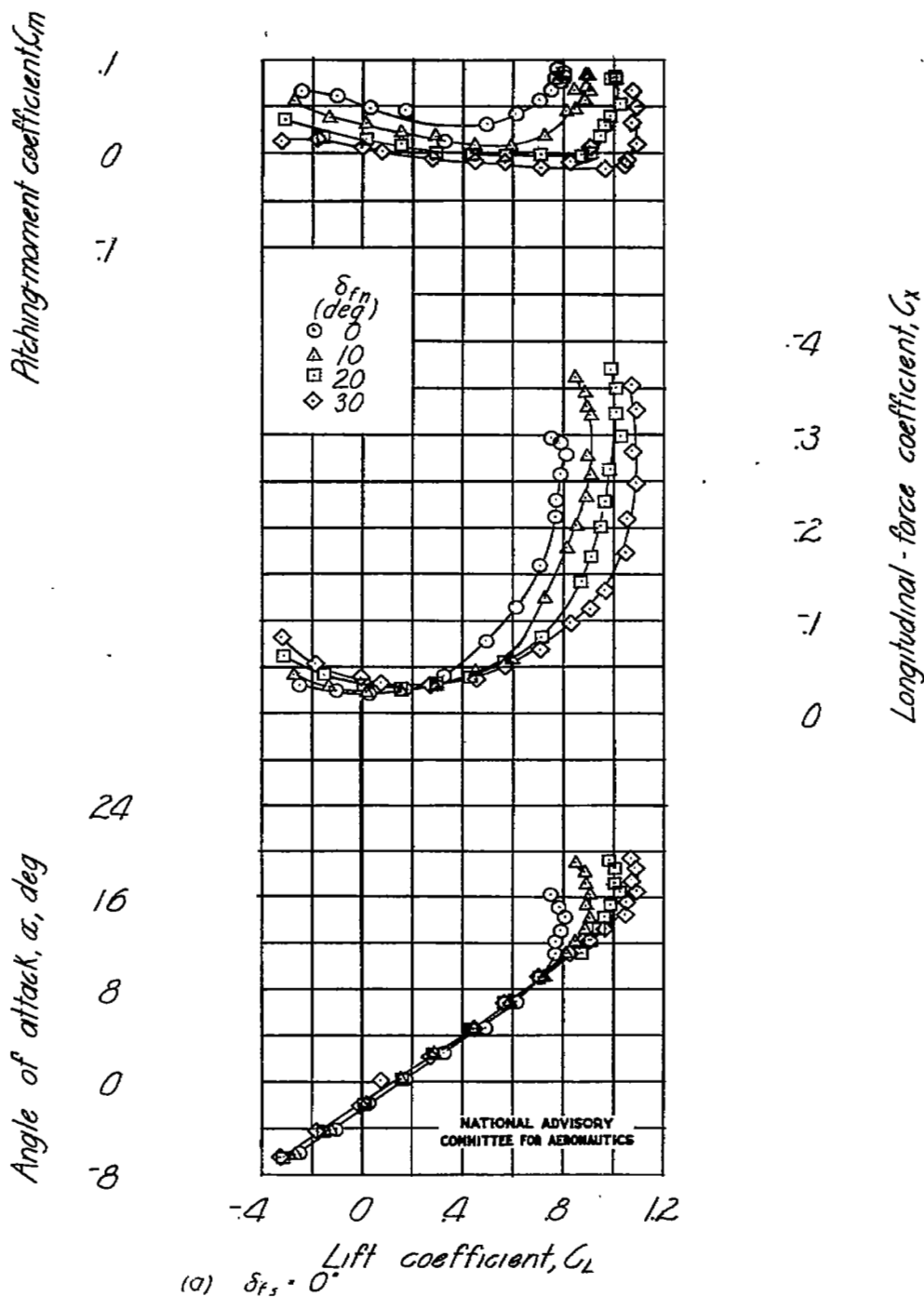
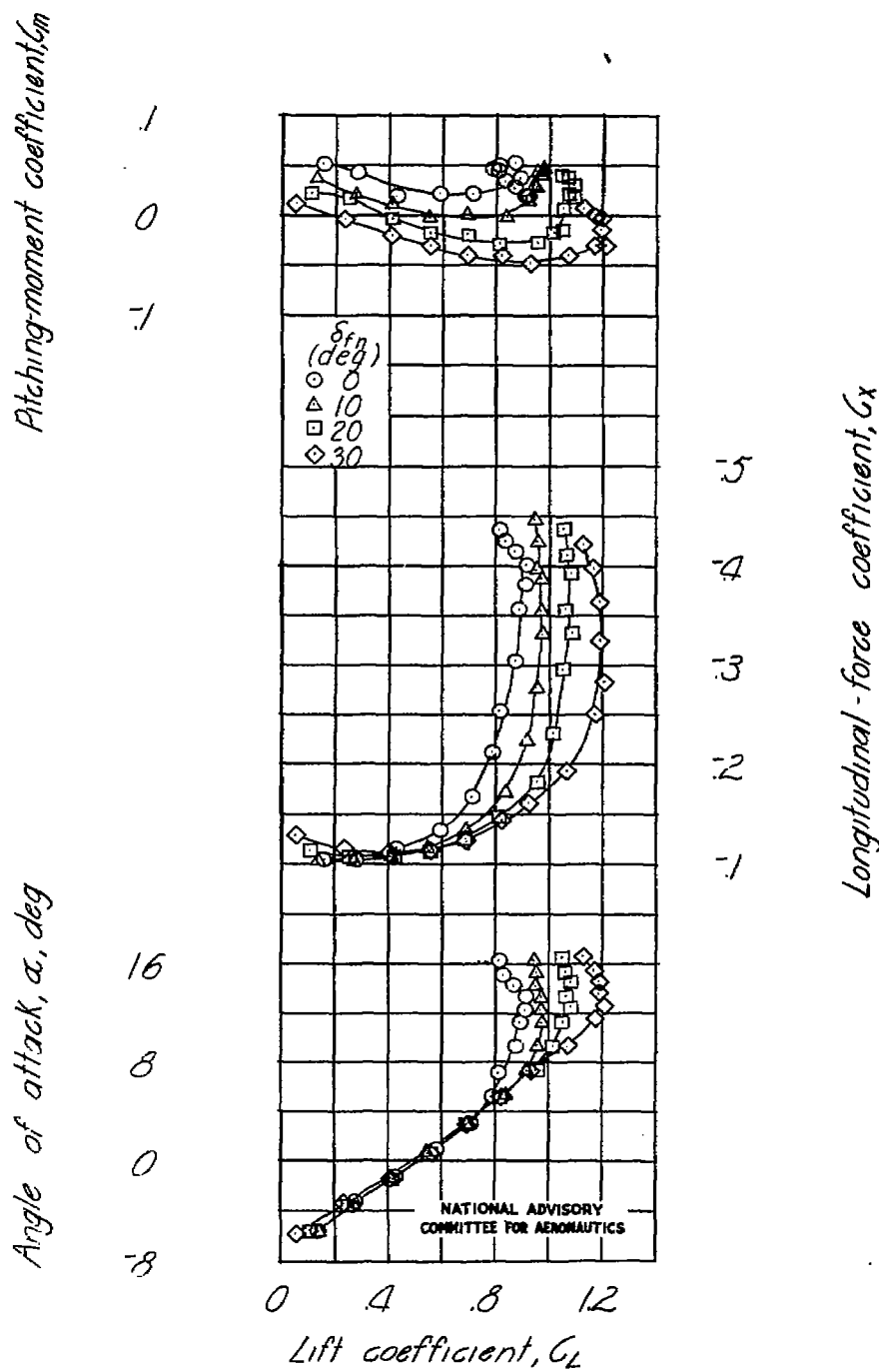


Figure 31.- Effect of 100-percent-span nose-flap deflections of the wing leading edge on the aerodynamic characteristics in pitch of a model with a 42.8 - 4.00 - 0.50 wing; large fuselage;  $i_t = 0^\circ$ .



(b)  $\delta_{f_s} = 55^\circ$

Figure 31.- Concluded.

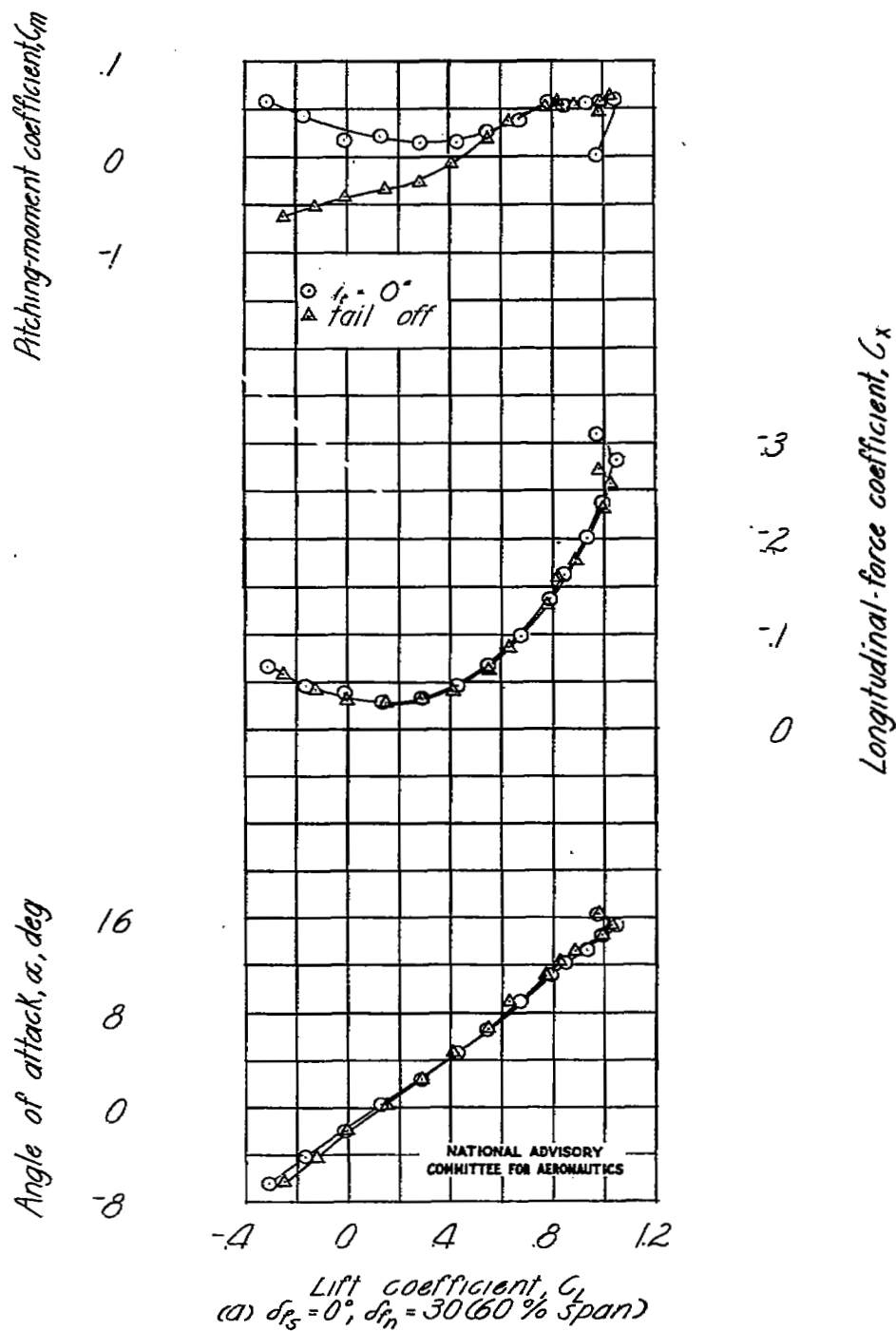


Figure 32.- Effect of various split-flap and nose-flap combinations on the aerodynamic characteristics of a model with a 42.8 - 4.00 - 0.50 wing; large fuselage.

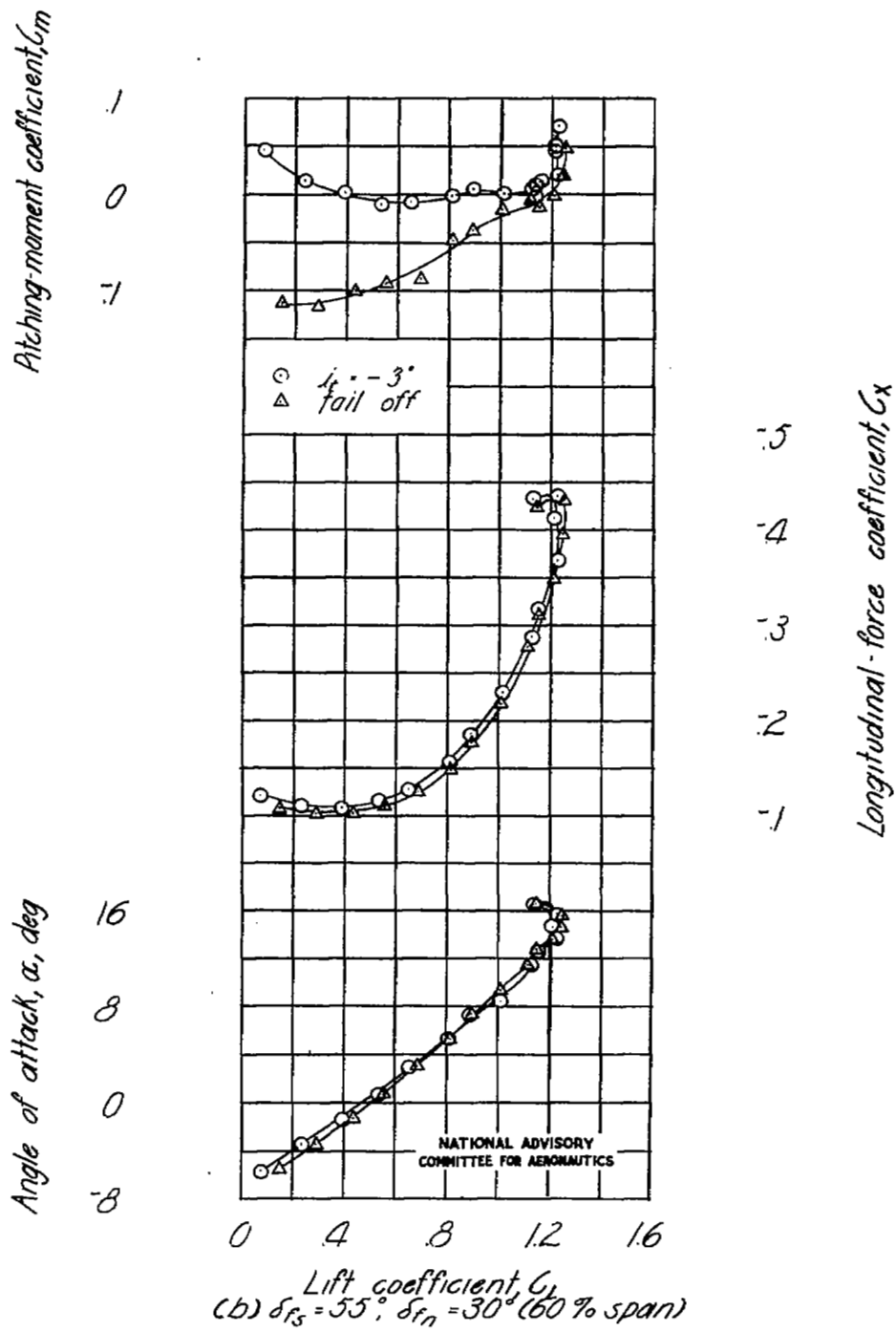


Figure 32.- Continued.

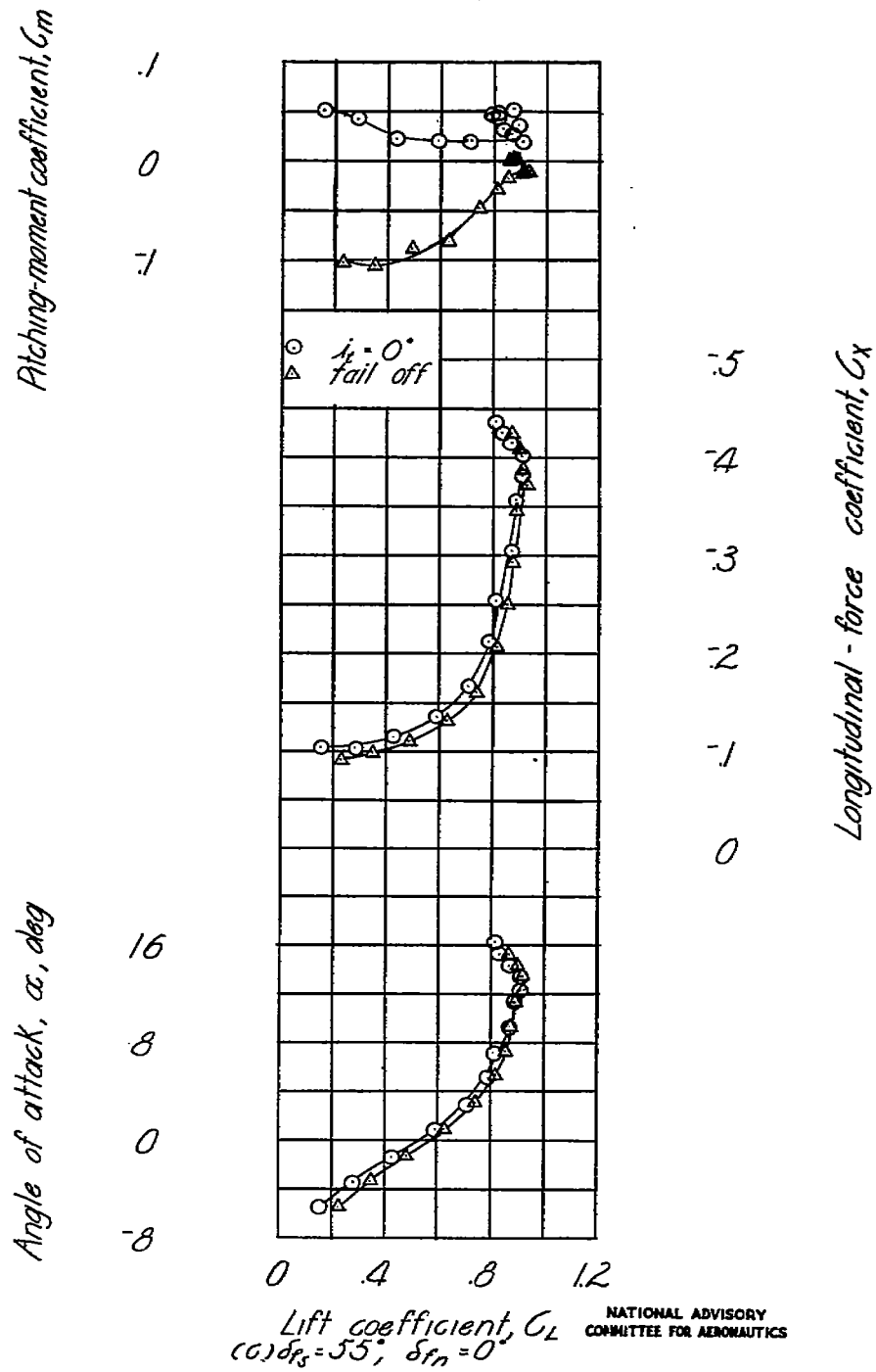


Figure 32.- Concluded.

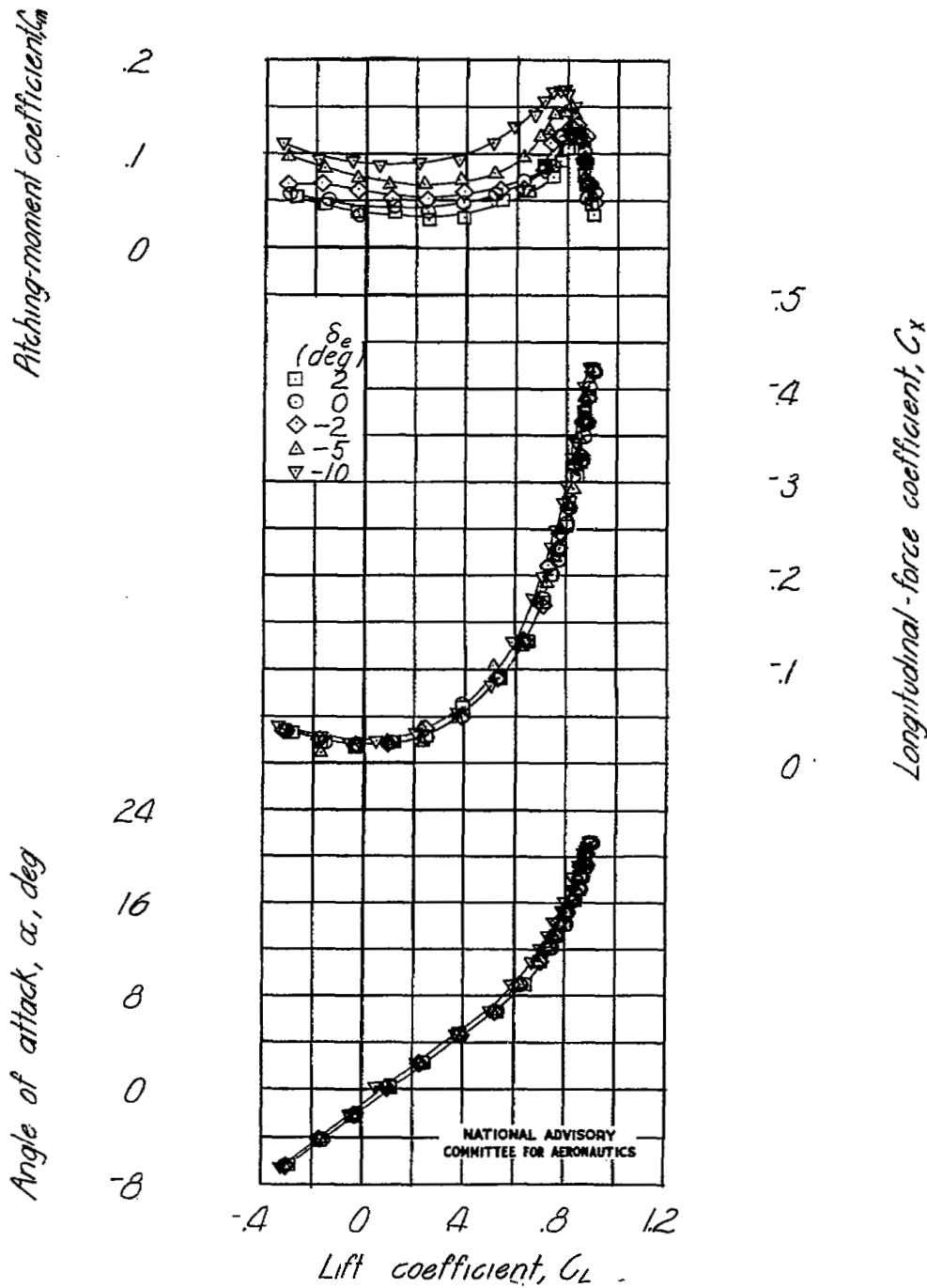
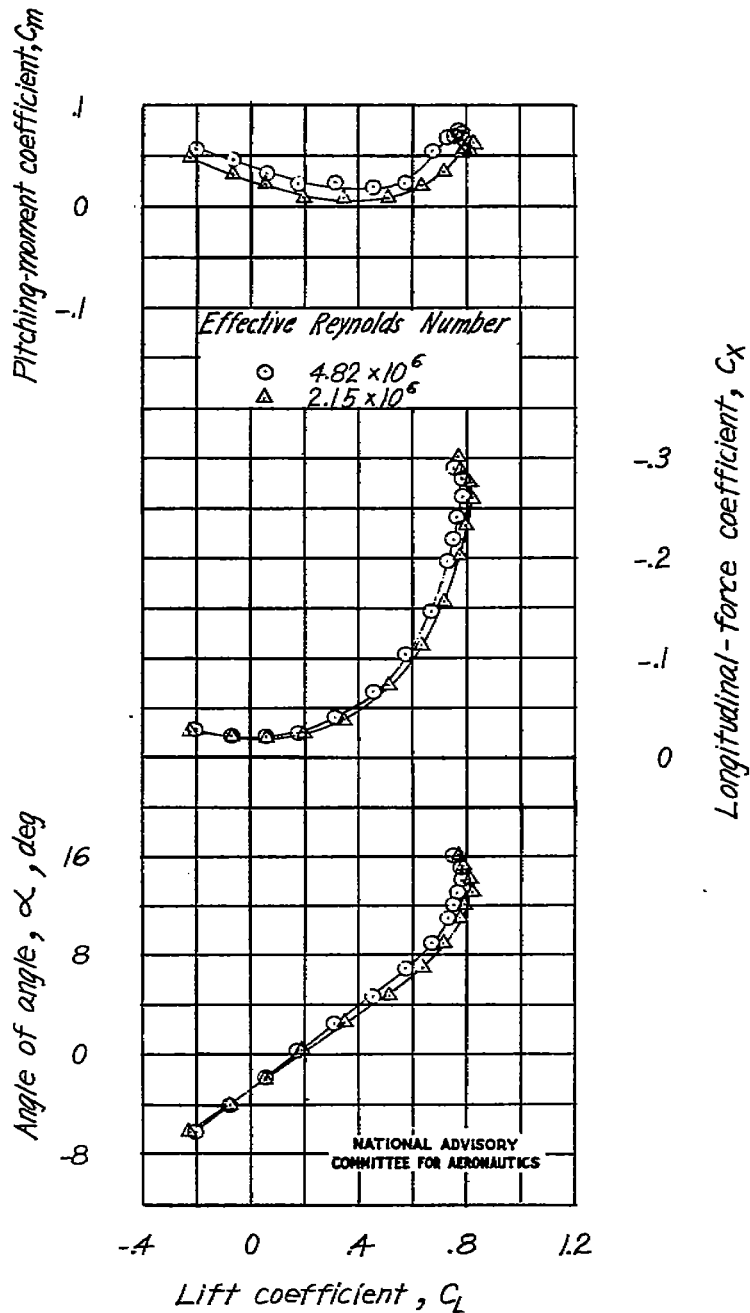
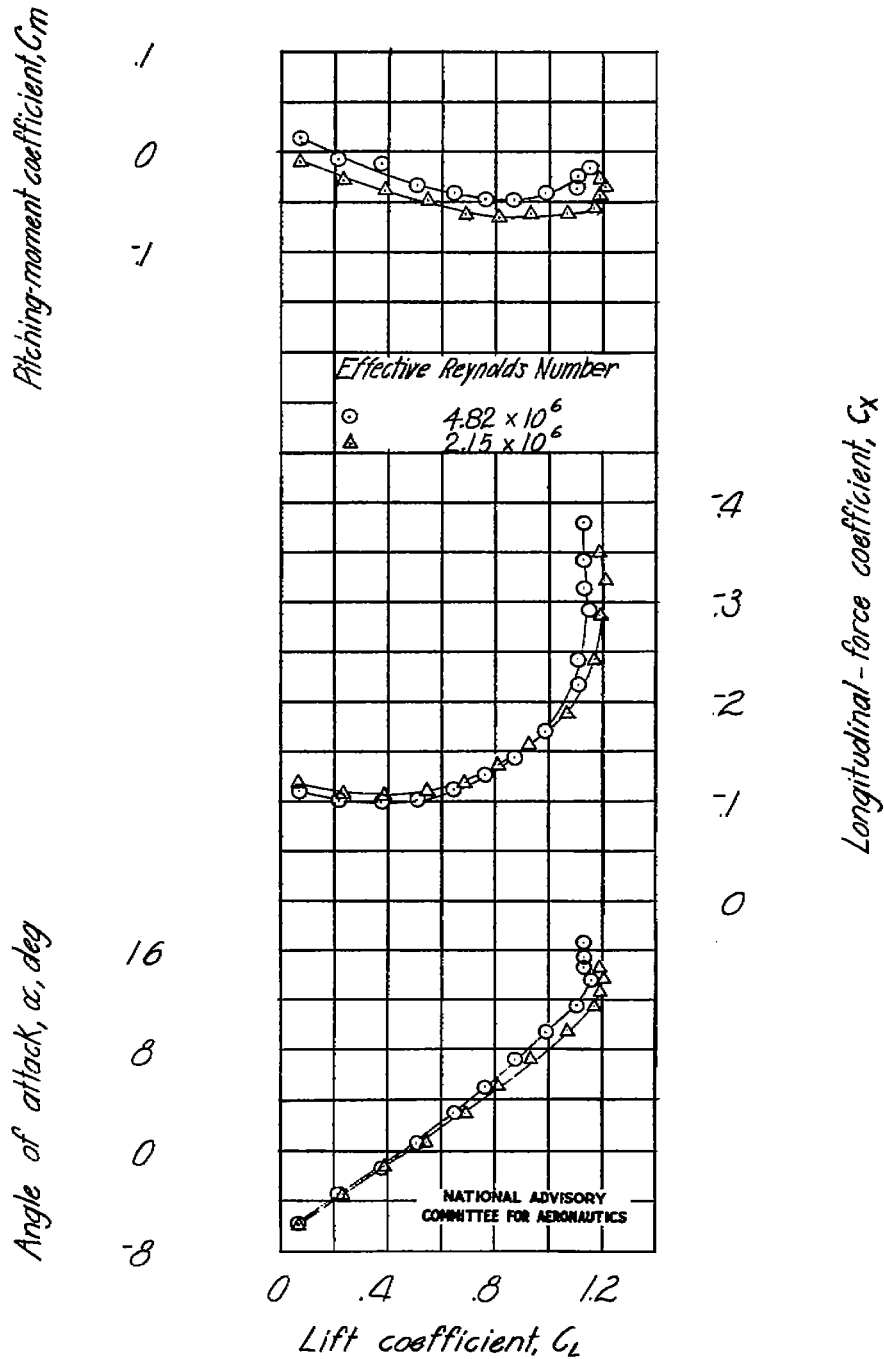


Figure 33.- Effect of elevator deflection on the aerodynamic characteristics of a model with a 42.8 - 4.00 - 0.50 wing; large fuselage; semihigh wing;  $\delta_{f_s} = 0^\circ$ ;  $\delta_{f_n} = 0^\circ$ ;  $i_t = 0^\circ$ .



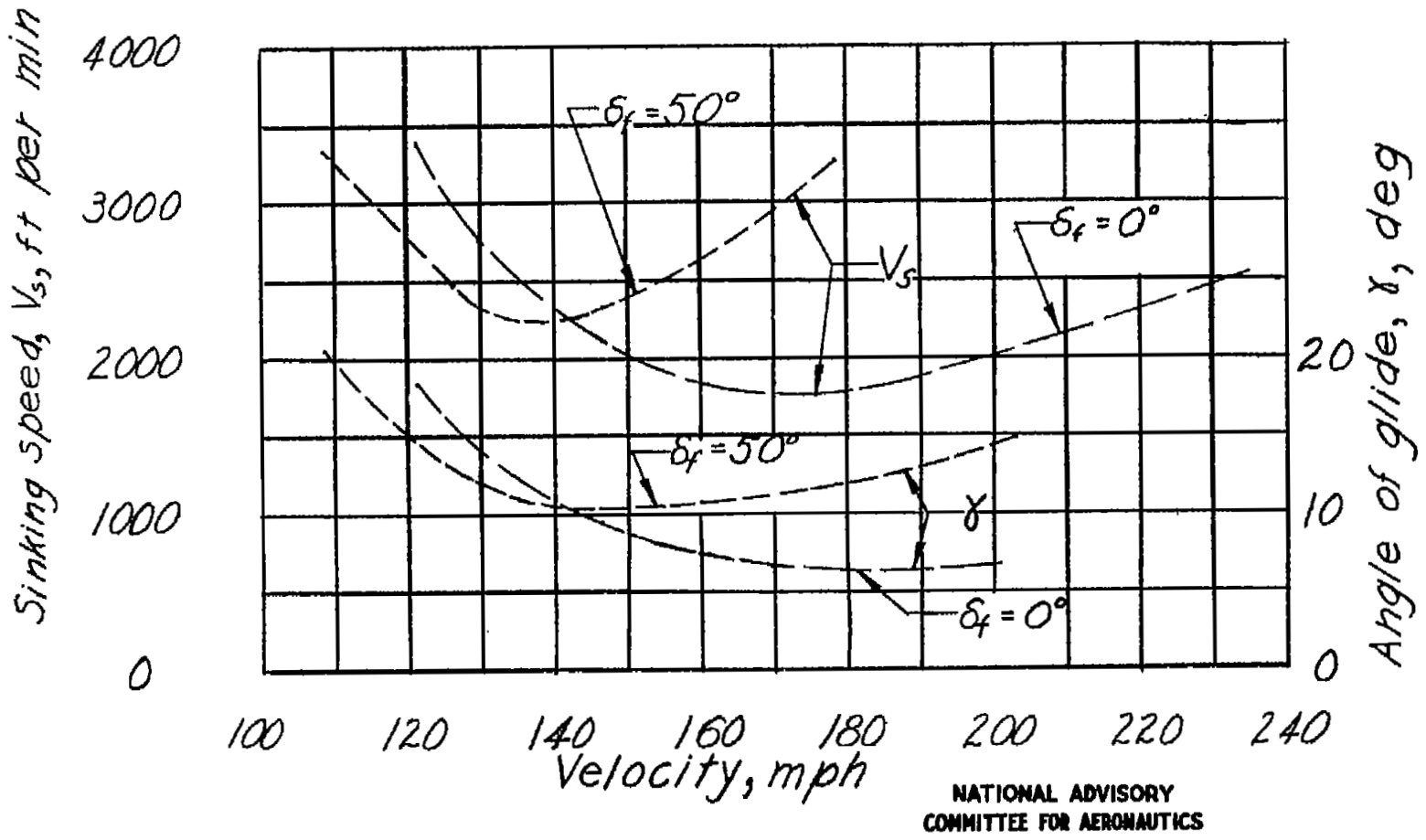
(a)  $\delta_{f_s} = 0^\circ$ ;  $\delta_{f_n} = 0^\circ$ .

Figure 34.- Effect of Reynolds number on the aerodynamic characteristics in pitch of a model with a 42.8 - 4.00 - 0.50 wing; large fuselage;  $i_t = 0^\circ$ ;  $\psi = 5^\circ$ .



(b)  $\delta_{fs} = 55^\circ$  ;  $\delta_{fn} = 30^\circ$  (100% span).

Figure 34.- Concluded.



NATIONAL ADVISORY  
COMMITTEE FOR AERONAUTICS

Figure 35.- Effect of flap deflection on the estimated sinking speed and glide-path angle for a model with a 42.8 - 4.00 - 0.50 wing; small fuselage;  $W/S = 33.3$  at sea level.

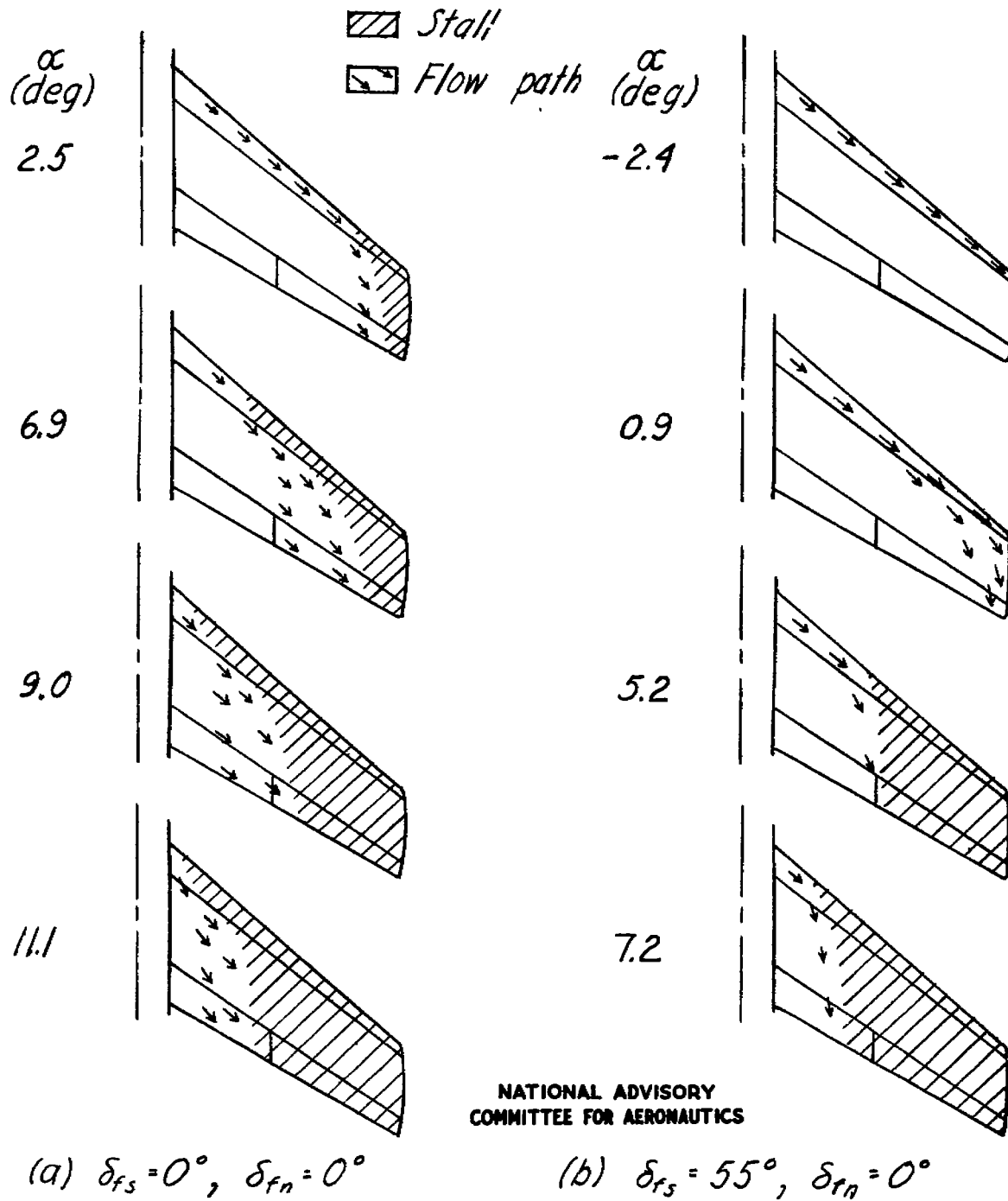
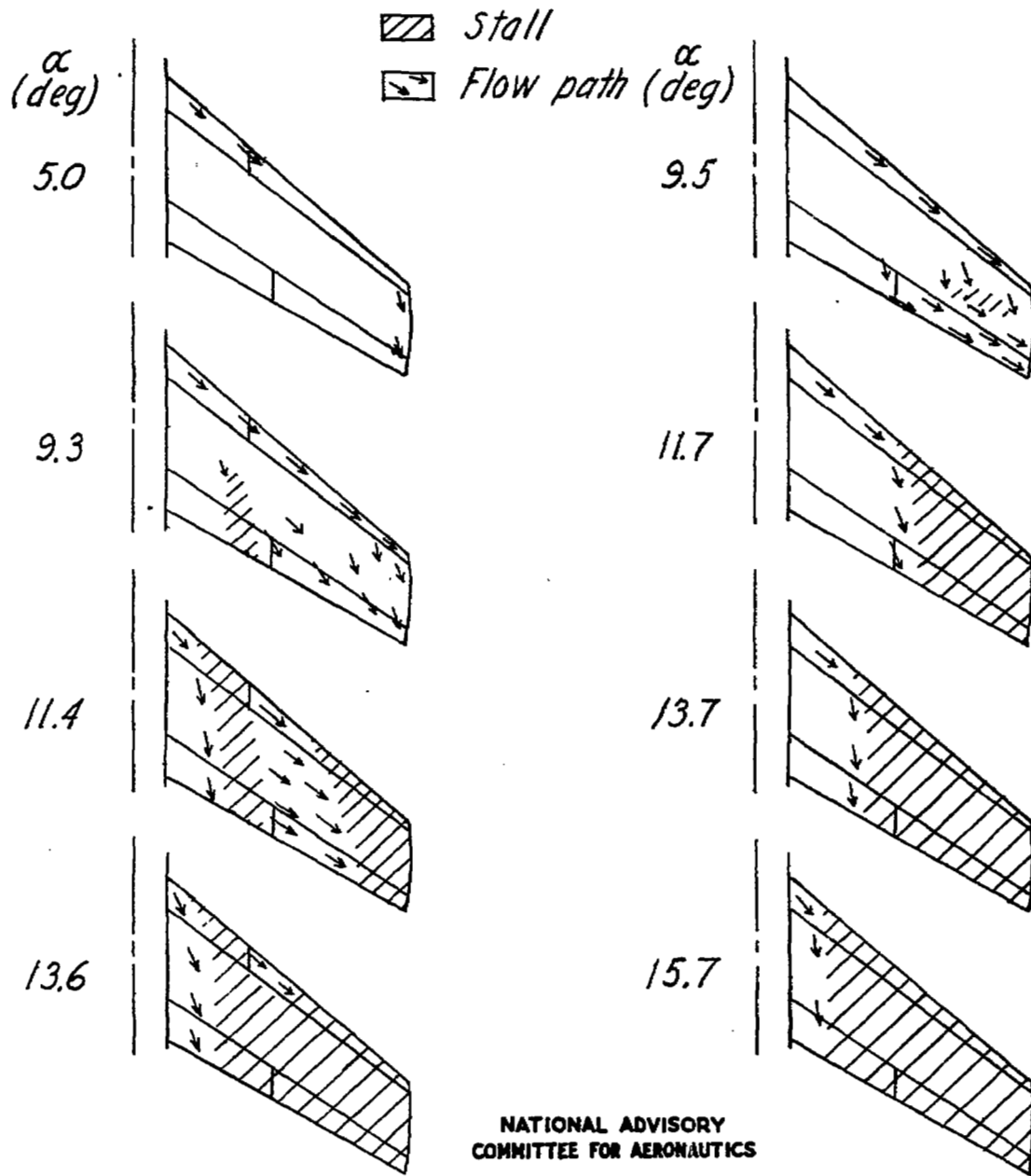


Figure 36.- Stalling characteristics shown on right wing of a model with a 42.8 - 4.00 - 0.50 wing.



(c)  $\delta_{fs} = 55^\circ$ ,  $\delta_{rn} = 30^\circ (60\% \frac{b}{2})$  (d)  $\delta_{fs} = 55^\circ$ ,  $\delta_{rn} = 30^\circ (100\% \frac{b}{2})$

Figure 36.- Concluded.

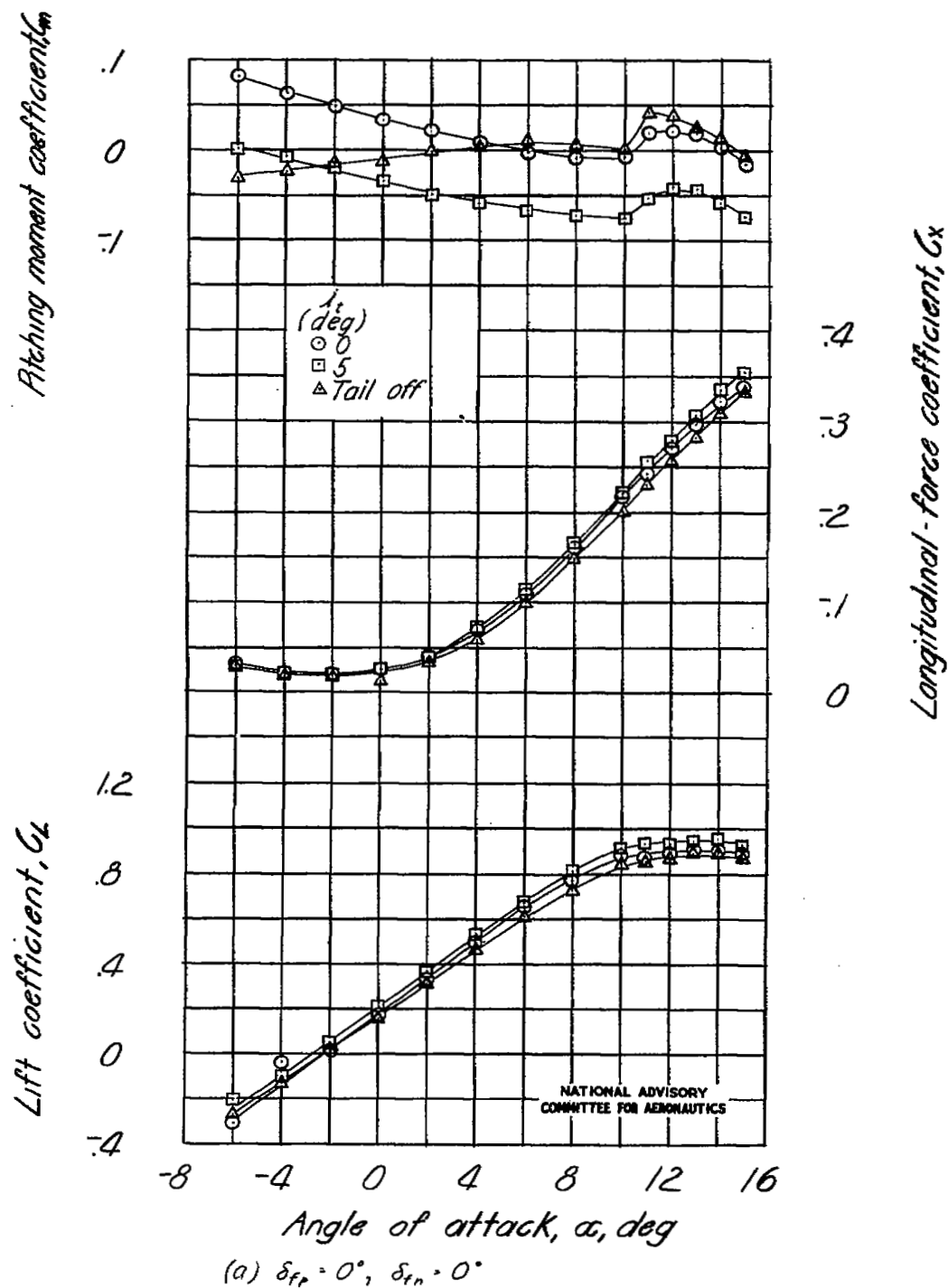
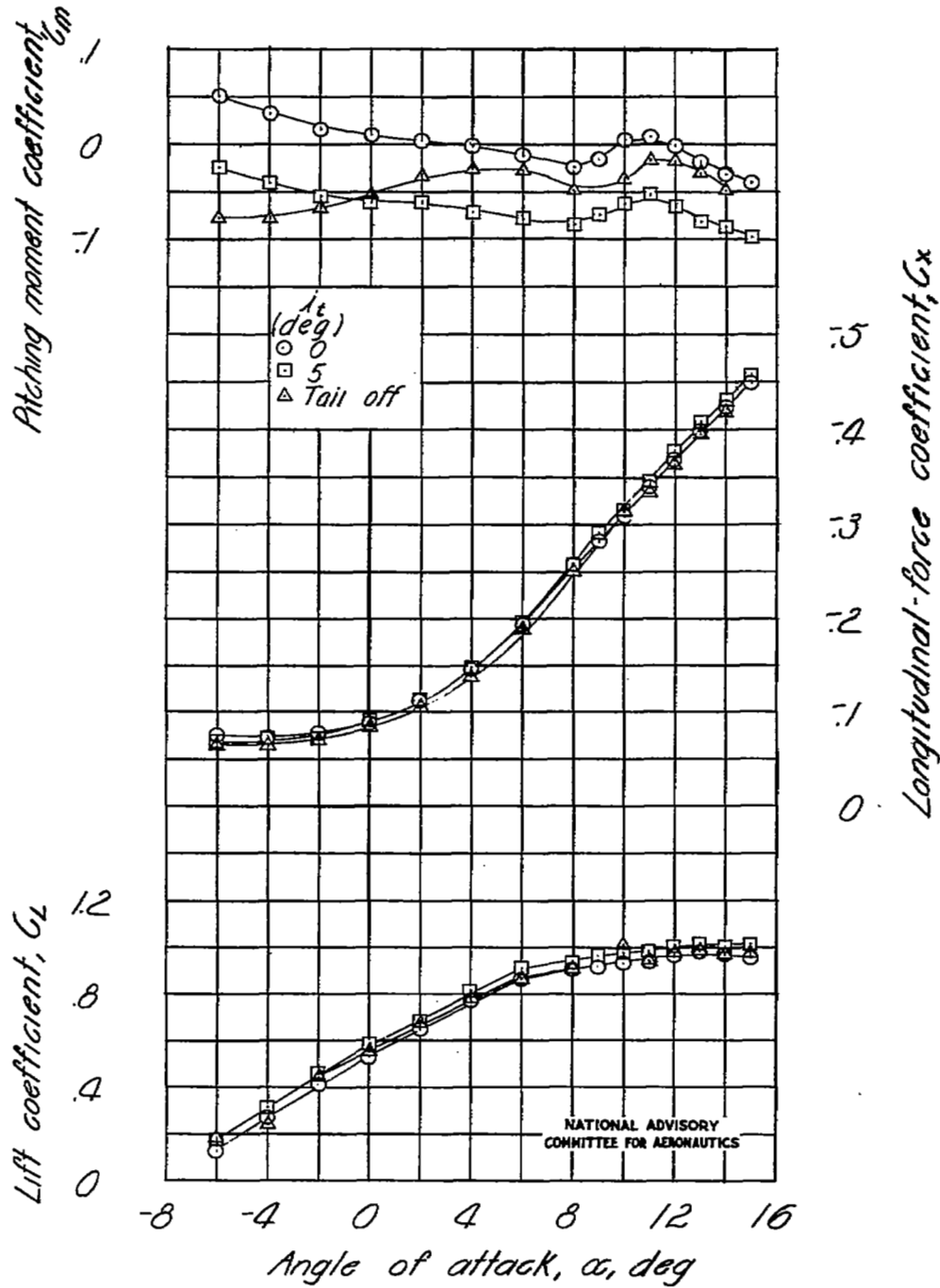


Figure 37.- Effect of stabilizer deflection on the aerodynamic characteristics of a model with a 42.8 - 4.00 - 0.50 wing in the presence of a ground board 14.1 inches below center of gravity; small fuselage.



(b)  $\delta_{rp} = 50^\circ$ ,  $\delta_{rn} = 15^\circ$  (40% span)

Figure 37.- Concluded.

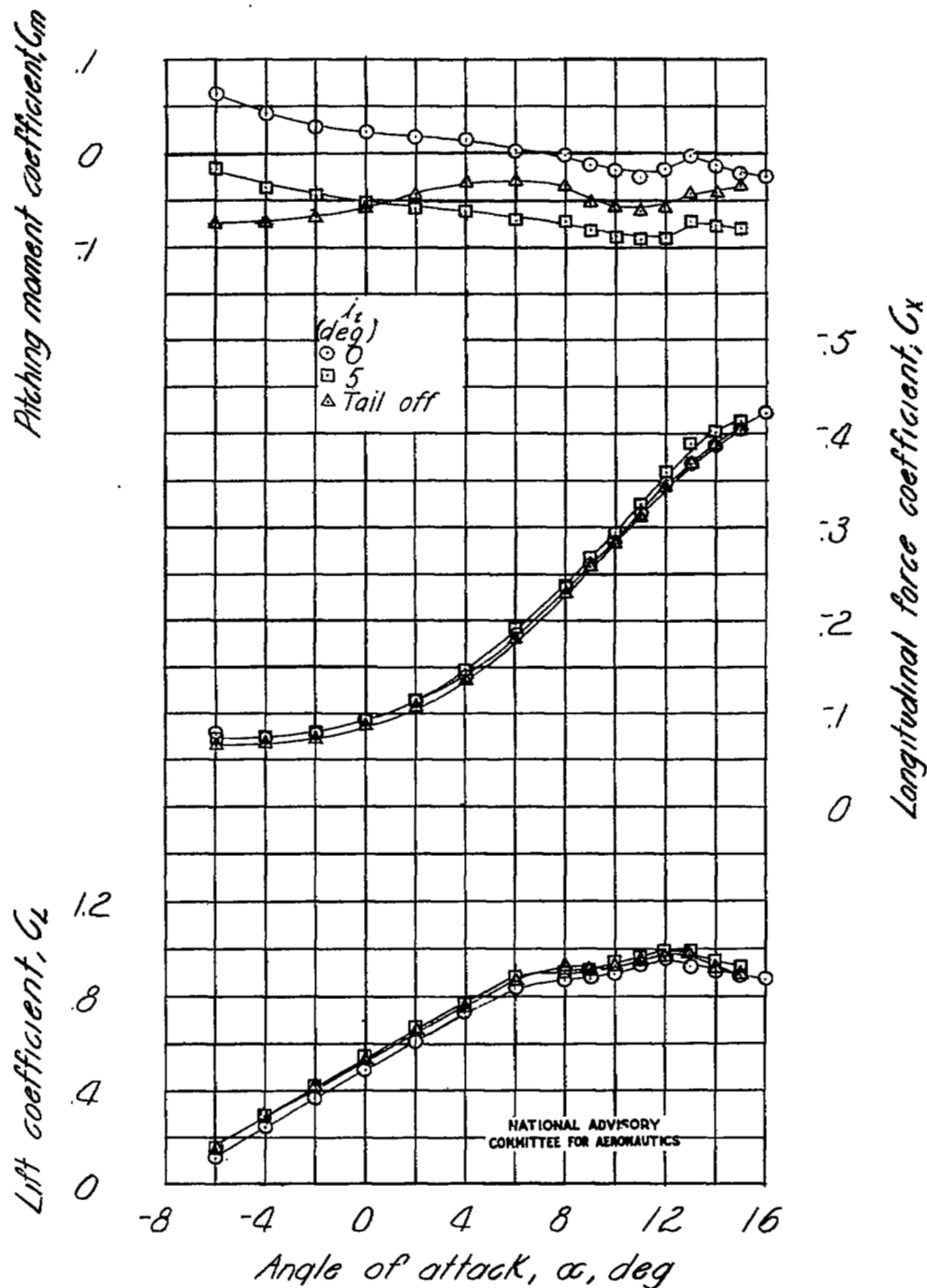


Figure 38.- Effect of stabilizer deflection on the aerodynamic characteristics of a model with a 42.8 - 4.00 - 0.50 wing in the presence of a ground board 24.1 inches below center of gravity; small fuselage;  $\delta_{fp} = 50^\circ$ ;  $\delta_{fn} = 15^\circ$  (40-percent span).

NASA Technical Library



3 1176 01436 7776